Structural and Functional Asymmetries Underlying Intrinsic Brain Dynamics

Atharva Ashutosh Parolekar

A dissertation submitted to the faculty of
the **National Brain Research Centre** in
partial fulfilment of the requirements for a
Master of Science in Neuroscience

June, 2025

National Brain Research Centre
(Deemed University)
Manesar, Haryana – 122052, India

ब्रिक – राष्ट्रीय मस्तिष्क अनुसंधान केंद्र
BRIC – National Brain Research Centre
(जैव प्रौद्योगिकी अनुसंधान एवं नवाचार परिषद, भारत सरकार)
एन० एच०–08, मानेसर-122 052 (हरियाणा), भारत
(An Institute of the Biotechnology Research and Innovation Council, Govt. of India)
NH-08, Manesar - 122 052 (Haryana), INDIA

CERTIFICATE

This is to certify that the dissertation report entitled '**Structural and Functional Asymmetries Underlying Intrinsic Brain Dynamics**' is the result of work carried out by **Atharva Parolekar** in the Division of **Cognitive Brain Dynamics**, National Brain Research Centre, Manesar, Haryana, India, for partial fulfilment of the requirements for the M.Sc. in Neuroscience's degree.

The work presented herein is original and has not been submitted previously for the award of any degree or diploma to **National Brain Research Centre (Deemed to be University)** or to any other University. This work is based on the guidelines of **National Brain Research Centre (Deemed to be University)** and is a record of the candidate's own efforts.

Dr. Arpan Banerjee
(Supervisor)

(Director, NBRC)

Place: Manesar
Date: 02/06/2025

दूरभाष / Telephone : +91-124-2845200 फैक्स / Fax : +91-124-2338910
ई-मेल / E-mail : info.nbrc@nbrc.ac.in Website : www.nbrc.ac.in

DECLARATION BY CANDIDATE

I, **Atharva Parolekar**, hereby declare that the work presented in the dissertation report entitled '**Structural and Functional Asymmetries Underlying Intrinsic Brain Dynamics**' was carried out by me under the guidance of **Prof. Arpan Banerjee**, Division of **Cognitive Brain Dynamics**, National Brain Research Centre (Deemed to be University), Manesar, Haryana, India.

I declare that no part of the thesis contains any plagiarised material. Any previously published or other material sourced from elsewhere has been appropriately attributed to the source.

I also declare that no part of this thesis has been previously submitted for the award of any degree or diploma to the National Brain Research Centre (Deemed to be University) or to any other university.

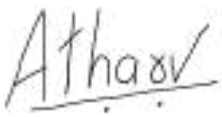

Place: Manesar
Date: June 25, 2025

Atharva Parolekar

Dedicated to the never-ending quest for knowledge,
and to those who dare to seek it.

GREAT GURU, WHAT IS THE MEANING OF LIFE?
TOONHOLE.com
Life, [noun.] ; pl. LIVES.
[/lIf/ ; See LIVE.]
1. That state of an animal or plant in which its organs are capable of performing their functions; animate existence ; vitality ; also, the time during which this state continues, either in general, or in an individual instance; as, the life of a tree, or a horse.
2. The time during which the human soul and body are united ; the period
birth and death; the present sta
sometimes, the perpetual existen
the present and future state.
Shak.
3. External
condition
circumstances,
living, as moral
ment; as, to

Acknowledgments

I have been very lucky to be able to work on what I love. Numerous pillars of support latently uphold this reality. I am earnestly grateful to my Ajji, Mummy, and Baba, who, despite their many hardships, have always been there for me. They actively push me to seek a life path that speaks to me.

Freedom to explore is found in abundance also at the Cognitive Brain Dynamics Lab, stemming from the liberal guidance of Prof. Arpan Banerjee. I thank him for accepting me on his team, his timely support, and his masterly counsel that braces this expedition.

This turbulent journey has indebted me to a great many folks for aiding me to tame its chaos. Insightful comments from Rishabh helped turn some scrambled ideas into bulleted actionables. Processing of large-scale structural data by Pratika blitzed the pace of my workflow. The computational resources of Neuroscience Gateway made possible the rapid analysis of the expansive functional data. Wisdom from Azman promoted the implementation of some nonclassical statistical methods. The works of Dr. Neeraj and Dr. Anagh corresponded to a conceptual and methodological scaffold, respectively, for some of the questions addressed in this dissertation. I sincerely thank them all for their contributions to this study.

Besides this, I could recall being on the receiving end of random kindness and miscellaneous learnings from each member of CBDL. I have been promptly saved from trouble multiple times by Shashwati, for instance. The people who constitute this lab have fostered a healthy work environment, and I am glad to have been a part of it. Shoutout to Austin and Vibha—while the cursed conversations that we have might have vanquished millions of my neurons, their friendship is compensation enough. I also (hesitantly) thank Dr. Dhrubajyoti for his suggestion to write this dissertation in LaTeX.

The coursework was an instrumental part of the holistic development of my academic and research fundamentals. I express my gratitude to all the faculty and peers who helped me grow during this time. I was also fortunate to have met and worked with many bright researchers at BCW 6, BrainDy '24, CAMP 9, and Neuromatch CN. I thank them all for their many teachings in the areas of cognitive, computational, network, and systems neuroscience.

Life at NBRC felt safe and convenient, and I am grateful to all the staff who work towards making it so. It also felt exciting, partly because of the initiatives I could be a part of through the Journal Club and Newsletter committees. I thank Dr. Vidhya for her constant motivation and all the volunteers who dared to venture beyond their comfort for communal benefit. Running a monthly mess was sort of fun too! Weightlifting and playing badminton were two other activities that made my time at NBRC quite enjoyable. Thanks to the many who patiently taught and encouraged me and continue to do so.

With gratitude,
Atharva Parolekar

Structural and Functional Asymmetries Underlying Intrinsic Brain Dynamics

by

Atharva Parolekar

Submitted to the National Brain Research Centre

on June, 2025 in partial fulfillment of the requirements for the degree of

MASTER OF SCIENCE IN NEUROSCIENCE

ABSTRACT

Cognitive functions spanning domains are known to specialize across the hemispheres. Many structural differences among hemispheric homologous components are known of and have been speculated to connect with the lateralized capabilities of the brain. There has been, however, a notable lack of empirical mechanistic explanations of how the structure shapes the function. To this end, here we argue that the differential communication latencies among the hemispheres drive their intrinsic dynamics. In this work, we make advancements to a delay estimation algorithm and see that the small-band delays and large-band delays are significantly related to the underlying white-matter architecture. However, large-band delays consistently have a weaker relationship to the tracts, remarking on their sensitivity to capture the latent processes that shape communication on a higher order. When hemispheric differences of

delays and tracts were assessed, the tracts and the small-band delays were largely symmetric; however, large-band delays showed significant lateralization between the hemispheres. Moreover, laterality of the large-band delays was significantly correlated to laterality of the MEG amplitude envelopes. Collectively, these results suggest that the large-band delays, as computed with this method, are set by factors beyond just the connectome, and they are the primary drivers of the differential emergent properties of the brain.

Thesis supervisor: Prof. Arpan Banerjee

Title: Scientist VI

Contents

List of Figures xvii

List of Tables xix

1 Introduction **1**

1.1 Hemispheric Specialization 1

1.2 Structural Heterogeneity 2

1.3 Tuning by Delay 3

1.4 Goals 3

2 Using Criticality to Decipher Time Delays **5**

2.1 Introduction 5

2.2 Methods 6

2.2.1 Data Description 6

2.2.2 Volumetric Processing and Parcellation 6

2.2.3 Tractography Processing and Connectome 7

2.2.4 rs-MEG Preprocessing and Source Reconstruction 7

2.2.5 Neuronal Avalanches 7

2.2.6 Branching Parameter Estimation 8

2.2.7 Power Law Analysis 9

2.3 Results 9
2.4 Discussion 12

3 Structural Architecture Directs Functional Cascades 13

3.1 Introduction 13
3.2 Methods 13
3.2.1 Delay Estimation 14
3.2.2 Connectome Rearrangement and Velocity Estimation . . . 15
3.2.3 Statistical Analysis 17
3.3 Results 18
3.3.1 Correlational Analysis 18
3.3.2 Regressional Analysis 19
3.3.3 Representational Similarity Analysis 21
3.4 Discussion 23

4 Delays in Hemispheric Specialization 25

4.1 Introduction 25
4.2 Methods 25
4.2.1 Participant Selection and Metric Laterlization Assessment 25
4.2.2 Computing amplitude envelopes and their laterality 26
4.2.3 Statistical Analysis 27
4.3 Results 27
4.3.1 Distributional Analysis 27
4.3.2 Laterality Analysis 29
4.4 Discussion 30

5 Conclusion **31**

5.1 Summary 31

5.2 Future Directions 31

A Statistical Table **33**

B Parcellation Lookup Table **35**

C Code Listings **37**

C.1 MATLAB Script for Functional Data Processing 37

C.2 MATLAB Script for Statistical Analysis and Figures 44

References 57

List of Figures

1.1 Reductionist views of hemispheric specialization. 1

2.1 Methodological pipeline for combined structural and functional analysis. 8

2.2 Avalanche distributions follow the power law. 10

2.3 Distributions of branching and avalanche quantity. 10

2.4 Variance of averaged parameters across initial avalanche conditions. 11

2.5 Power law fitted parameters across initial avalanche conditions. . . 12

3.1 Estimating delays in functional cascades. 14

3.2 Delay distributions. 15

3.3 Structural distributions. 16

3.4 Velocity distributions. 17

3.5 Delays are related to tract lengths. 18

3.6 Delays are related to tract widths. 19

3.7 However lengths and widths are interrelated. 19

3.8 Delays can be accurately predicted from structure. 20

3.9 Partial regression retains effects of widths and lengths on delays. . 21

3.10 Patterns of dissimilarity across pairs of regions. 22

3.11 Structural-functional similarity of pairwise dissimilarity. 22

4.1 Laterality maps of tract lengths, widths, functional delays, and amplitude envelopes. 26

4.2 Tract lengths and widths are mostly symmetric between the hemispheres. 27

4.3 Large-band delays, but not small-band delays, are hemispherically asymmetric. 28

4.4 Large-band delays show asymmetry across more pairs of regions. . 28

4.6 Afferent delay laterality is significantly correlated to that of source amplitudes. 29

List of Tables

A.1 Statistical parameters of structural-functional regression models . . 34

B.1 Hemisphere aggregated parcellation scheme. 35

Chapter 1

Introduction

1.1 Hemispheric Specialization

The intricate blob of mass known as the human brain takes its form through multitudes of developmental processes. Early on in its becoming, it molds into a bipartite frame that becomes its two hemispheres. The hemispheres are largely similar to one another, with the presence of identical cortical and subcortical modules spread through their respective topographies. However, they are not exactly destined for the same fates.

It is often observed that homologous hemispheric modules, despite their morphological similarities, partake in cognition differentially. A century after Broca's discovery of the modular substrate of speech[1,2], the seminal work of Roger Sperry on split-brain patients who had undergone a callosotomy discovered that language comprehension and production were impaired if the right hemisphere attempted their information processing but remained intact with the left hemisphere[3]. Contrarily, it was the left hemisphere that had an impediment in visuospatial abilities, while the right hemisphere performed well[4].

Figure 1.1: **Reductionist views of hemispheric specialization.** While such figures are visually intriguing, it is crucial to consider the nuances of the brain and avoid drawing simplistic inferences.

In the decades following these findings, various lesion-based, electrophysiological, and neuroimaging studies have confirmed the specialization of functions across hemispheres. For the majority of the population, auditory cognition lateralizes with speech and semantics to the left and emotional prosody and music to the right[5].

More fundamentally with acoustics, sequential timing is better assessed by the left, and spectral differentiation is performed better by the right homologs[6]. Similarly, visual processes lateralize to better represent local features to the left and global features to the right[7]. With sensory processes being implicily involved in complex higher-order operations, functional lateralization is observable athwart cognitive modes like perception[8], attention[9,10], reasoning[11], and motor control[12–14].

The brain is a system laden with complexity that spans scales as a result of its dynamic organization under the influence of genetic instructions, environmental interactions, and considerable stochasticity. A characteristic feature of complex systems like the brain is that their modules carry out independent tasks, but they also coordinate to perform duties distributively. In this light, the differential recruitment of hemispheric regions and their networks in cognition suggests that their organizational foundations vary.

1.2 Structural Heterogeneity

While on the surface, the cortical surface may seem symmetric, closer inspection reveals many lateral peculiarities. For instance, the occipital petalia of the left hemisphere and the frontal petalia of the right hemisphere have larger protrusions in the coronal plane than their counterparts. And, their anticlockwise bend is a common feature across brains and is termed the Yakovlevian torque[15]. Moreover, cortical volume is known to differ between the hemispheres. Parts of the right hemispheric insular, cingulate, and striatal areas are larger than their homologs[16]. Of particular prominence is the leftward asymmetry of posterior language areas, like the planum temporale and the angular gyrus[16,17]. This asymmetry has been shown to be markedly larger in trained musicians[18].

Additionally, the properties of white matter are also subject to change. Numerical and volumetric leftward bias can be seen for the corticospinal tract and Broca-Wernicke segment of the arcuate fasciculus, whereas a similar rightward bias can be seen for the inferior frontooccipital fasciculus and frontoparietal segment of the arcuate fasciculus[19]. In terms of facilitating scattered communication, right hemispheric cortical nodes are substantially more interconnected, but left hemispheric nodes exhibit higher centrality[20], including the auditory system[21]. This finding lends credence to the idea that the left hemisphere serves a specialized role with focal representations, and the right hemisphere handles integrative tasks with diffuse representations[22]. Interestingly, this observation replicates itself at the scale of neuronal columns in the auditory cortex, with larger spacing among[23] and more afferents to the left cortical columns[24]. In this context, these structural differences have been linked to the observed differences in acoustic processing[6] and theorized to be the basis of speech-music lateralization[25].

The functional capabilities of the brain are, to a considerable extent, constrained by its structural architecture[26]. The coupling of structural and functional connectivities is robust, spanning multiple timescales[27], patterns, and developmental stages[28]. For the time being, however, the mechanisms tying together the hemispheric differences of structure and function remain largely elusive.

1.3 Tuning Emergence by Delay

While the structural connectome is known to reorganize with aging[29], it retains high stability in relatively short windows of observation. Yet, the interregional communication patterns vary on very fast timescales[30,31]. This dissonance between the two is a feature remarking on the metastable dynamics of the brain[32]. A prominent variable that tangibly affects brain network properties is the communication latency. Through computational network models, the impact of delays on synchronization[33], frequency slowing[34], and amplitude death[35] has been shown. Additionally, whole-brain network models have been used to predict that precise modulation of internodal delays specific to contexts underlies the higher cognitive processes[36,37].

Numerous possibilities can underscore a change in interregional signal transmission delay in the brain. Be it by differential conduction velocities[38], synaptic scaling[36], degenerate multi-hop pathways[39], oscillatory coherence[40], or other dynamic features of the recipient neural population[41]. The many differences in the white matter tract prominences and connectivities between the hemispheres particularly point towards a potential asymmetry of delays through altered conduction velocities and pathways. Indeed, it was recently shown that conduction velocities predicted through personalized whole-brain models lateralize across the hemispheres[42].

These collective observations can be approached with the perspective that through the course of development, a combined result of prescriptive and stochastic effects has driven the structural-functional lateralization of the brain. Heeding the asymmetric tract architecture, it is plausible that differential communication lags are the principal characters driving the emergence of unique hemispheric properties.

1.4 Goals

The following are the objectives of this work:

- Develop a method to accurately assess functional delays across temporal regimes.
- Delineate the relation of the delays with the structural connectome.
- Assess hemispheric differences in delays and tract properties.
- Establish if laterality of delays underlies functional specialization.

What to expect in the following chapters:

Chapter 2: Demonstration of the fitness of neuronal avalanches to measure delays.

Chapter 3: Interrelations of observed delays with tract lengths and widths.

Chapter 4: Hemispheric laterality analysis of structure and function.

Chapter 5: Summary of findings and possibilities for the future.

Chapter 2

Using Criticality to Decipher Time Delays

2.1 Introduction

Traditionally the conduction delays between the regions of the brain have been predicted through their underlying white matter connections[43]. Recent advancements have made possible the estimation of communication delays purely through noninvasive functional recordings[44]. This approach holistically captures the empirical distribution of delays mediated by their effectors. It does so by leveraging the approach of neuronal avalanches.

Avalanches are distributed motifs of communication in dynamical systems. They are characterized by bursts of activity distributed through space and time. In systems with large degrees of spatial freedom, such as the critical sandpile models[45], distributions of avalanche events follow the scale-invariant dynamics of the power law.

The power law is given by:

$$P(S) = kS^{-\alpha} \quad \Rightarrow \quad \log_{10} P(S) = \log_{10} k - \alpha \log_{10} S \tag{2.1}$$

Where $P(S)$ is the probability of observing an avalanche with event size S, α is the exponent giving the slope of the distribution in a log-log graph, and k is a proportionality constant.

With the brain being a large-scale dynamical system, neuronal avalanches were found to exist through electrophysiological recordings of cortical neuronal cultures[46]. Following this, they have been demonstrated to exist in vivo through invasive electrophysiological recordings in cats[47] and monkeys[48], and even noninvasively in human neurophysiology[49] and haemodynamics[50]. Moreover, properties of avalanches can be used to track changes in cognitive modulation[51,52].

Branching processes from probabilistic theory are phenomenological models widely used to explain the properties of neuronal avalanches[53]. This model posits that the distribution probabilities of avalanche events can be explained by the branching probabilities of its processing units. The branching parameter σ of an individual unit

x in a network is set by:

$$\sigma_x = \sum_{y=1}^{N} p_{xy} \tag{2.2}$$

Where σ_x is the predicted number of activated descendents of x, N is the number of units connected to x, and p_{xy} is the signal transmission probability from unit x to y. Turns out that when the aggregate branching of the model is tuned at criticality ($\sigma \approx 1$), the avalanche sizes of the computational network follow the power law. Additionally, since the transition probabilities of some node pairs is larger than others, the branching model captures recurrent metastable patterns of the network[54]. However, when branching is tuned moderately subcritical ($\sigma < 1$) or supercritical ($\sigma > 1$), these qualitative traits vanish.

In this chapter, we will see an empirical demonstration of the critical and causal nature of neuronal avalanches in a large data set of human resting-state recordings and arguments for why they serve as excellent candidates to extract functional delays from.

2.2 Methods

2.2.1 Data Description

This report utilizes data sourced from the Cambridge Centre for Aging and Neuroscience (Cam-CAN) project repository (available at http://www.mrc-cbu.cam.ac.uk/datasets/camcan/). In its stage 2, data were collected from approximately 700 cognitively healthy adults of age 18-87. Participants were selected uniformly from each age decile, with various other exclusion criteria having been implemented to remove confounds. See Shafto et al. [55] for details of the entire study protocol. From this highly multimodal neuroimaging data set, unprocessed structural and functional data were selectively employed—magnetic resonance images with T1- and diffusion-weighting and magnetoencephalogram recordings during eight minutes and forty seconds of eyes-closed rest. See Taylor et al. [56] for extensive acquisition details. Only participants with a lack of artifacts and the complete requisite data available locally were used for analysis ($N = 449$, $female = 50.11\%$, $mean\ age = 48.37 \pm 16.02$).

2.2.2 Volumetric Processing and Parcellation

High-resolution T1-weighted images for each subject were processed using Freesurfer's *recon-all* pipeline, which automatically segments and labels regions of the brain with high accuracy[57]. The Desikan-Killiany atlas was used to parcellate the cerebral cortex into 68 regions of interest (ROIs)[58]. Subsequently, these labels were used for both tractography-based connectome generation and MEG source reconstruction, ensuring a consistent spatial reference.

2.2.3 Tractography Processing and Connectome

A custom shell script was used to preprocess the DWI data. A detailed rationale of the pipeline can be found in Jain, Akhter, and Banerjee [59], but briefly, the corrections included denoising, Gibbs ringing removal, motion and distortion correction, bias field correction, which was followed by a brain mask estimation.

Following response function estimation for grey matter, white matter, and CSF, fiber orientation distributions were estimated using multi-shell multi-tissue constrained spherical deconvolution (MSMT–CSD)[60]. A global intensity normalization of FODs was then performed.

To implement anatomically constrained tractography (ACT), the T1 image was segmented into 5 tissue types, and registered to the diffusion image. Grey matter–white matter interface region was selected as the seed for probabilistic tractography. The generated 10 million streamlines were filtered with SIFT2 to mitigate reconstruction biases and produce biologically meaningful connection weights[61]. In reference to the Desikan-Killiany parcellation of the anatomy, symmetric matrices of mean edge distances and inverse-node-volume-scaled connection weights were computed using the *tck2connectome* command from MRtrix3[62].

Note: The resultant length and width connectomes are used for analysis in chapter 3.

2.2.4 rs-MEG Preprocessing and Source Reconstruction

Brainstorm package was used for preprocessing and source modeling of the resting-state MEG recordings[63]. For each participant, the anatomy and raw MEG files were imported. Automatically detected heartbeat artifacts from electrocardiogram recordings were removed with signal space projection, which was applied separately on the magnetometers and gradiometers. The recordings were then resampled from 1000 Hz to 200 Hz for computational efficiency. The DC offset and linear trends were then removed. A notch filter was applied at 50 Hz and 100 Hz, and the signal was bandpass filtered between 1 and 99 Hz.

The participants T1 images underwent linear affine transformation for normalization in the MNI space. Headpoints proximal to defaced regions were removed for refined registration. Source models were computed using overlapping-sphere head models, and noise covariance matrices were estimated using empty room recordings that underwent the same preprocessing steps. MEG sources were reconstructed using the minimum-norm estimate (MNE) approach, constrained to the cortical surface and regularized with $SNR = 3$ and depth weighting. Principal component source time series of 68 Desikan-Killiany parcels were exported.

2.2.5 Neuronal Avalanches

Prior to computing avalanches, the source time series for left hemispheric and right hemispheric regions were separated to investigate differential dynamics. The data were z-transformed and binarized with a threshold of |3.5| standard deviations. Suprathreshold excursions were termed events. The time series were divided in non-overlapping windows of 30 ms, and in every window, the number of events across regions is recorded.

When at least one event is identified in a window, an avalanche is considered to have begun. This encompasses all subsequent event-fostering windows and only stops when an empty window is encountered. For every avalanche, a matrix of variable size is generated to store the location and times of all its events.

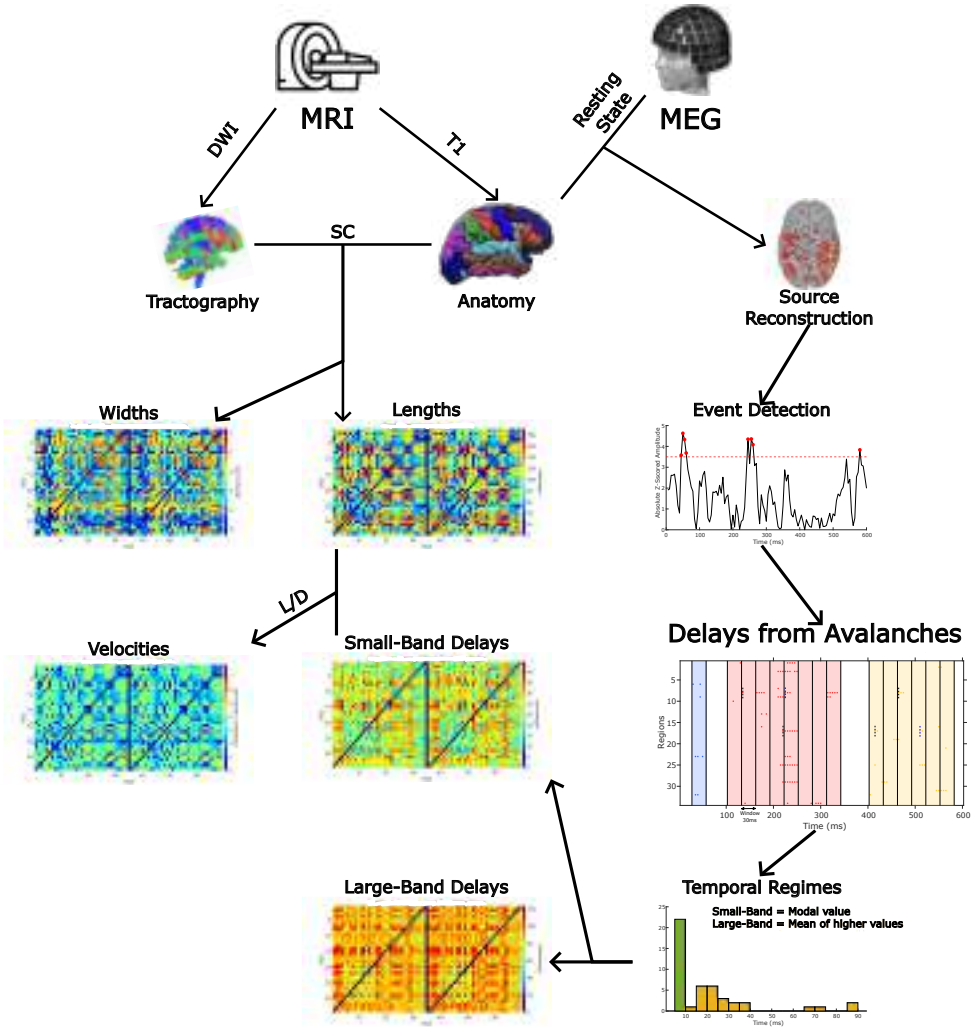

Figure 2.1: **Methodological pipeline for combined structural and functional analysis.**

2.2.6 Branching Parameter Estimation

To measure propagation dynamics empirically, the branching parameter σ_i was computed for each avalanche i by taking the geometric mean of branching values at each timepoint transition as such:

$$\sigma_i = \sqrt[n]{\prod_j \frac{E(j+1)}{E(j)}} \tag{2.3}$$

Where $E(j+1)$ and $E(j)$ are the descendent and ancestor number of events, respectively.

Then a participant specific branching parameter σ is estimated for each hemisphere by taking a geometric mean across their avalanches like this:

$$\sigma = \sqrt[n]{\prod_i \sigma_i} \tag{2.4}$$

Where σ is the participant specific branching estimate, obtained for each hemisphere.

2.2.7 Power Law Analysis

To assess the statistical properties of neuronal avalanches, we analyzed the distributions of their spatial (number of cortical regions), temporal (number of time windows), and spatiotemporal (number of events) spread. For each measure, values were collated across avalanches of all participants and binned using 50 logarithmically spaced intervals.

Probability distributions were plotted in log-log space, and linear regression was applied to estimate their scale invariance. The linear slope provided the exponent $-\alpha$, and the intercept corresponded to the normalization prefactor k of the power law relationship (Eq. 2.1).

For each measure, the null models were computed as probability mass functions of Poisson distributions, which were generated as such:

$$P(S) = \frac{\lambda^S e^{-\lambda}}{S!} \tag{2.5}$$

Where $P(S)$ is the probability of observing a measure of size S and λ is the mean of the empirical data. These surrogates represent uncorrelated random data, and were overlaid on top of the empirical distributions in the log-log space.

2.3 Results

Plotting the distributions of avalanche sources, bins, and events reveals a sharp early peak and a long rightward tail. When their probability distributions are plotted on log-log coordinates, they can be seen to fit well with a linearly decaying line. Moreover, in all three cases, the empirical probabilities of tail values are much higher relative to the Poisson probabilities computed for λ set at the respective empirical means (Fig. 2.2).

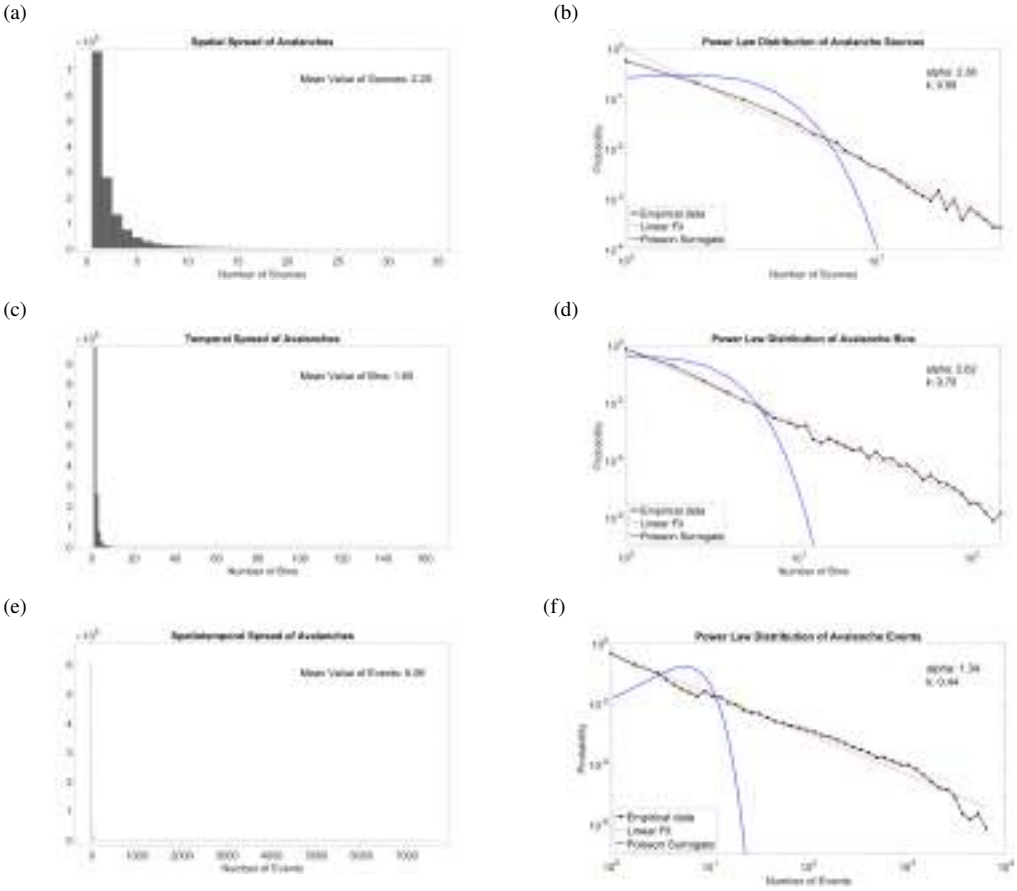

Figure 2.2: **Avalanche distributions follow the power law.** The empirical distributions of avalanche sources (a), bins (b), and events (c) exhibit significantly heavier tails than their respective null models, as signified by their linear slopes in log coordinates (d–f). This indicates that they follow the power law: $P(S) = k\,S^{-\alpha}$, suggesting the presence of criticality in the brain's avalanche dynamics.

In the logscaled probability plots, the highly shallow slope of the events (α_{events} = 1.34) heavily suggests critical organization of the system. The relative steepness of sources ($\alpha_{sources}$ = 2.38) and bins (α_{bins} = 2.62), however, suggests slight subcriticality. Although they still markedly differ from their null models. To validate the system dynamics, participant level branching distributions that were calculated over a large degree of data (Fig. 2.3), were found to cluster at the critical value ($\sigma = 1$).

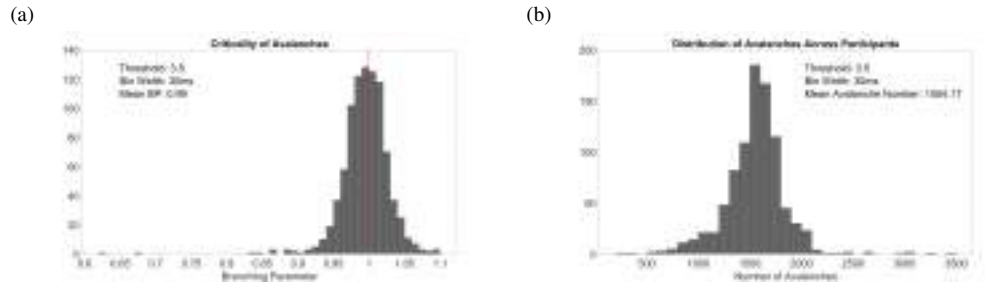

Figure 2.3: **Distributions of branching and avalanche quantity.** Most avalanches operate near criticality, as confirmed by the branching model (a) across a large number of avalanches (b).

Moreover, the analysis was replicated for varied threshold and window duration pa-

rameters of the avalanches. When the mean number of avalanches across participants when normalized across conditions were plotted, they expectedly reveal a variance with the initial avalanche parameter, however the mean branching parameter robustly indicates criticality (Fig. 2.4a,c). This strongly remarks on the scale-invariance of avalance dynamics.

The normalized mean (across avalanche then population) sizes of sources, bins, and events were also compared, to get a rough idea of their distribution trends with conditions (Fig. 2.4b,d), but in view of their power law nature, the mean does not hold too much meaning. Therefore, a more suitable analysis was further performed.

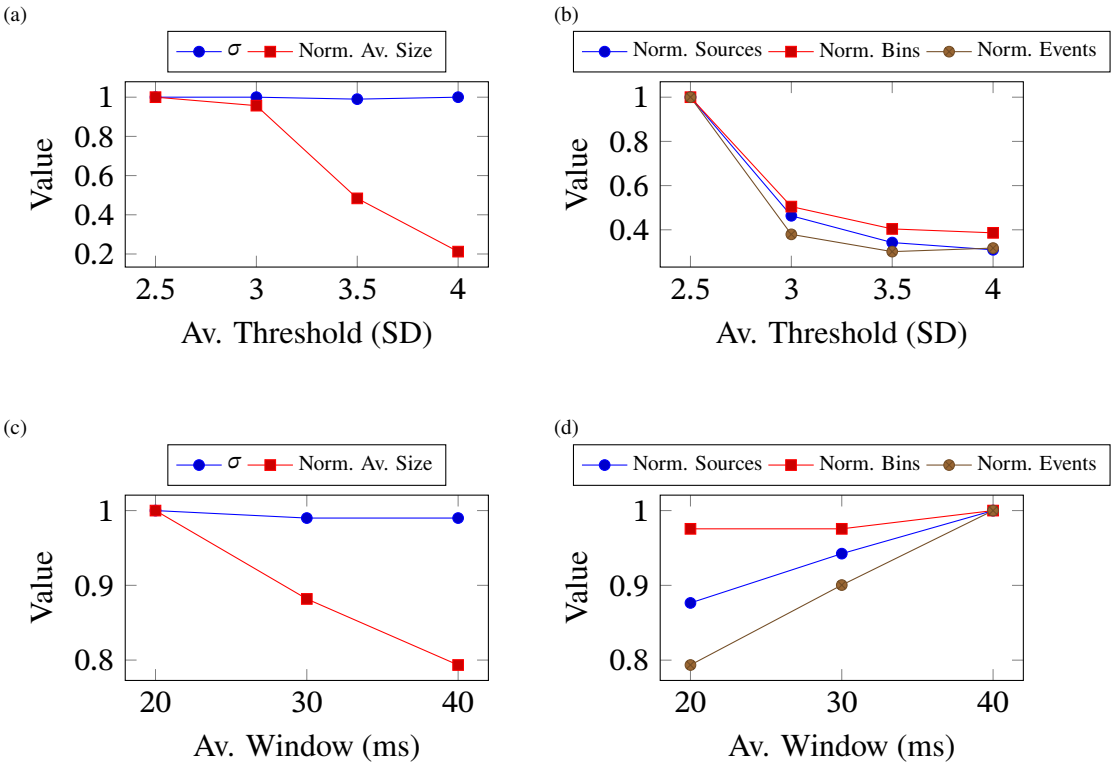

Figure 2.4: **Variance of averaged avalanche parameters across initial avalanche conditions.** Irrespective of the quantity of avalanches across threshold or window, the branching parameter (σ) remains close to 1 (a, c), indicating criticality. The mean spatiotemporal spread drops with the stringency of the threshold (b), but rises in avalanches of larger windows (d).

Power law fitted parameters of avalanche sources, bins, and events were compared across avalanche defining conditions (Fig. 2.5). Distribution parameters were notably indifferent to the choice of avalanche window durations. They did, however, vary for certain conditions across event thresholds.

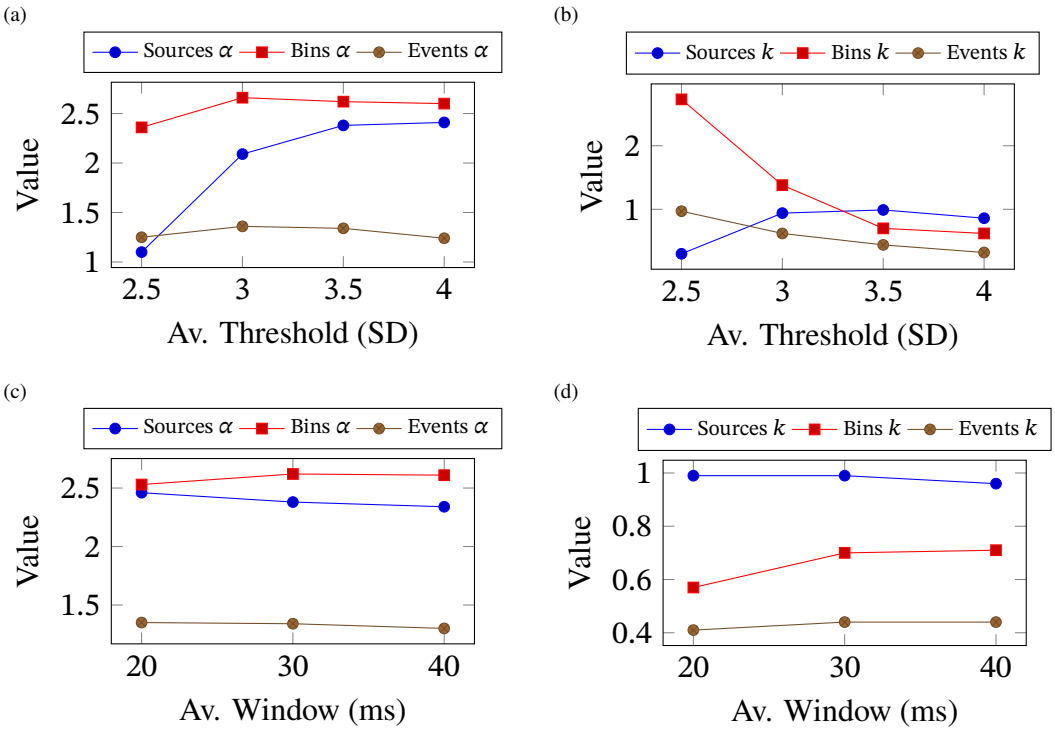

Figure 2.5: **Power law fitted parameters across initial avalanche conditions.** Exponent α and prefactor k remain fairly constant across windows for their respective distributions (c, d). With higher thresholds however, sources appear to shift towards subcriticality through their increased α (a), while bins appear to show more criticality with their decreased k (b).

It is important to note that although the power-law exponent for the source and bin distributions are relatively high, this does not necessarily indicate sub-critical dynamics. Coarse spatial and temporal resolution can limit the observational capacity for criticality. In this study, regions were parcellated using the Desikan-Killiany atlas, and avalanches were defined in $30ms$ windows, both of which line up with this possibility. Nonetheless, these discretization choices were deemed optimal for their compatibility for the analyses in chapter 3.

2.4 Discussion

In this chapter, we saw that defining neural activity into avalanches helps reveal its self-organized critical dynamics. The critical branching results and significantly different distributions of empirical data from the Poisson model (which represent unrelated activations) suggests that the events detected across regions are causally related to each other. It serves to reason that the causal communication among the regions mediated through bursts of activity, can be leveraged to extract communication latencies dynamically. Moreover, the scale-invariant nature of avalanche dynamics allow for extracting meaningful delays flexibly. The fact that patterns of communication in avalanches can change contextually opens the doors to the possibility of identifying lags across regimes of chatter.

Chapter 3

Structural Architecture Directs Functional Cascades

3.1 Introduction

Recently, an algorithm was devised by Sorrentino et al. [44] to estimate functional delays in vivo from cascades of neural activity. It iterates over many neuronal avalanches to extract the transition latencies of signals. They are able to estimate a pairwise delay chart by averaging the delay values across the avalanches. Here we enhance their approach, then put it through rigorous testing to delineate the extent of the dependence of the resultant delays on the properties of the white matter tracts that facilitate communication trends.

3.2 Methods

In this section, structural and functional metrics are defined and related to each other in two main conditions:

- **Population averaged:** Mean of all nonzero values pertaining to a metric.
- **Population pooled:** Collated values of a metric, only at indices with valid values across all metrics.

Note: The following analyses were performed primarily with delays derived from avalanches of threshold 3.5 *SD and window length* 30ms*, and then mostly replicated for varied conditions.*

3.2.1 Delay Estimation

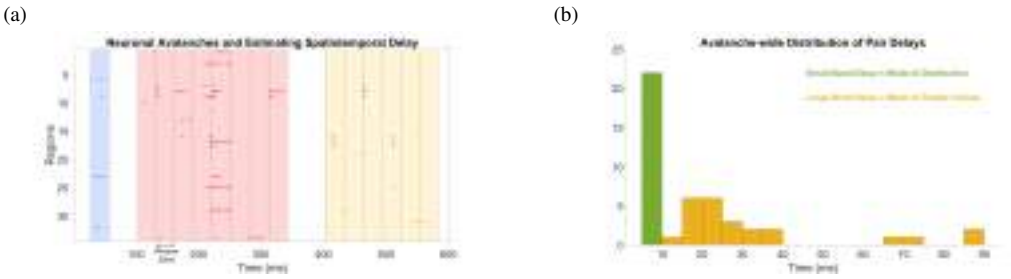

Figure 3.1: **Estimating delays in functional cascades.** (a) The temporal difference of subsequent initial regional activations are stored per avalanche. The resultant delay computation is directional in nature. (b) For a subject-level estimate, regional pairwise delays across avalanches are segregated into small-band delays and large-band delays.

For each hemispheric avalanche of a participant, as computed in chapter 2, the transition delays between pairs of regions were stored in a square ($ROI \times ROI$) delay matrix. For any two regions a and b, the delay from one to the other (τ_{ab}) may be different from its reciprocal (τ_{ba}), as they are quantified by measuring the temporal latency of the initial activation of one ***after*** the initial activation of the other (Fig. 3.1a). Following this, the left intra-hemispheric and right-intrahemispheric delay matrices were appended to form a (34×68) structure.

To characterize a participant-level estimate of the delays, we observed the delay distributions of region pairs across avalanches and observed that the delay distributions often demarcate into a sharp early peak and a broad right-skewed tail (Fig. 3.1b).

Here we define and calculate two regimes of delays:

- **Small-band delays:** Mode of delays across avalanches.
- **Large-band delays:** Mean of delays that are greater than the mode across avalanches.

For a further population level estimate, the participant matrices were averaged upon omitting the null values.

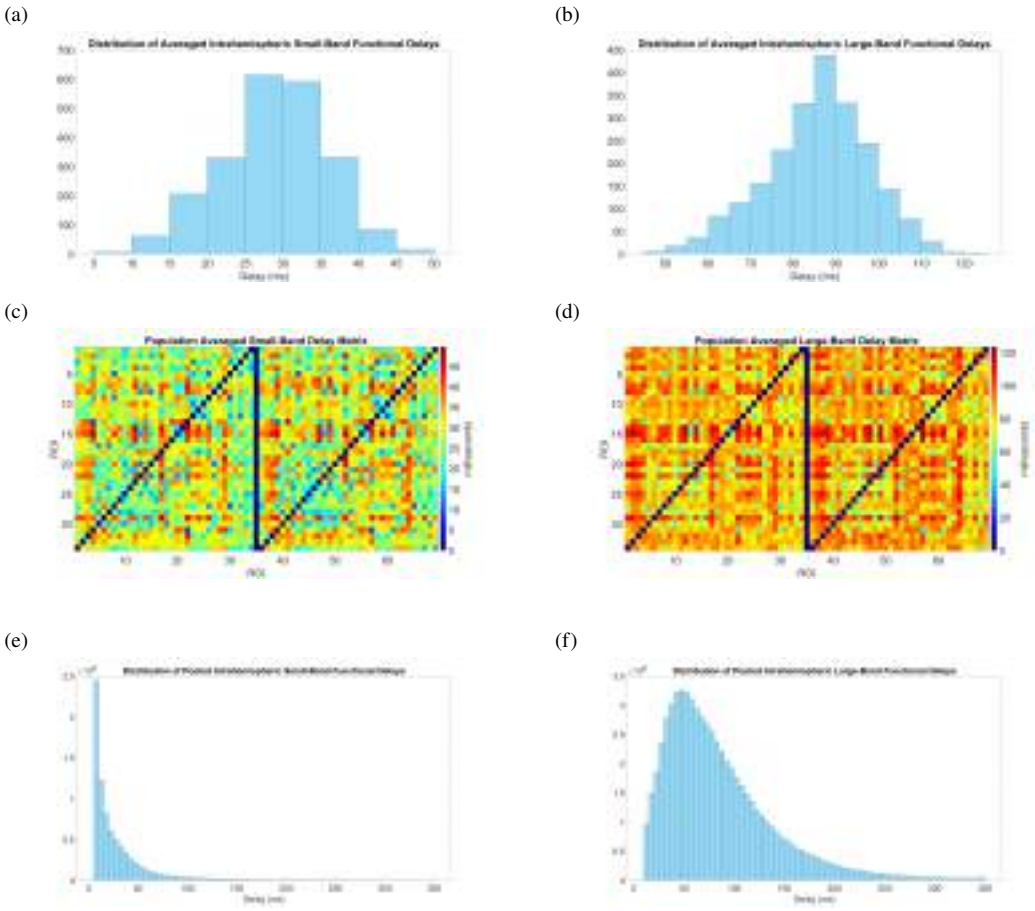

Figure 3.2: **Delay distributions.** Population averaged and collated distributions of small-band (a, e) and large-band (b, f) delays. Delays computed through modes across avalanches exist are almost non-overlapping with delays through mean of the rest. Delay matrices of small-band (c) and large-band (d) are averaged across subjects for subsequent analyses. The left and right intrahemishperic connections can be seen in respective halves of the matrices.

3.2.2 Connectome Rearrangement and Velocity Estimation

The length and width matrices, as obtained from chapter 2 were rearranged to be in the same reference frame as the delays, and pruned to only retain the intrahemispheric connections matrices (34×68). The participant matrices were then averaged to get a population estimate of the lengths and the widths.

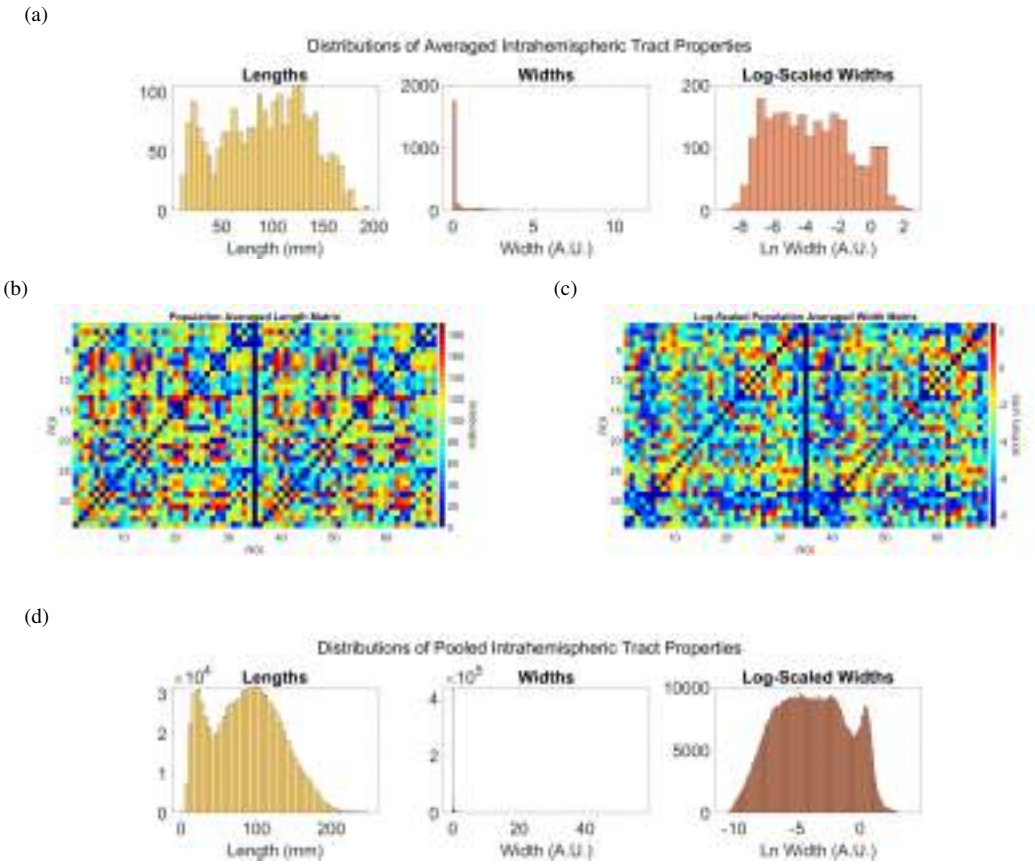

Figure 3.3: **Structural distributions.** Population averaged (a), and collated (d) distributions of tract lengths and widths. Connection weights are visualised on the log scale due to their skewed distribution. Structural connectivity matrices of lengths (b) and widths (c) are averaged across subjects for subsequent analyses. The left and right intrahemishperic connections can be seen in respective halves of the matrices.

For an estimation of the propagation properties, both at the level of population average and pool, the lengths were divided by the small-band and large-band delays to obtain the small-band and large-band velocities respectively.

It is important to note that the velocities obtained via this method simply serve as a proxy for the tract conduxtion velocities, and not a replacement. They do not account for latent factors that affect delays beyond conduction. Thus, if a set of delays are mediated by indirect communication for example, their velocities calculated from direct connection lengths would be spurious.

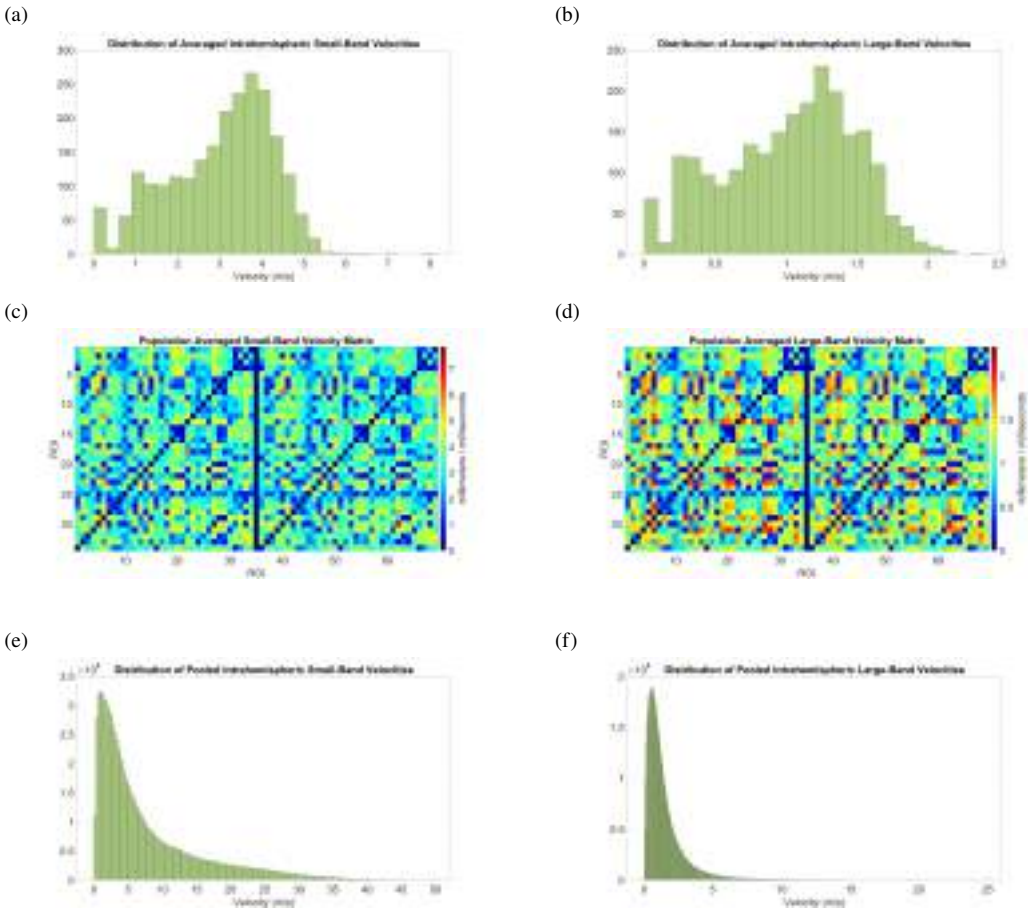

Figure 3.4: **Velocity distributions.** Population averaged and collated distributions of small-band (a, e) and large-band (b, f) functional velocities. Naturally as the empirical delays differ, their derived velocities differ reciprocally. Velocity matrices derived from small-band (c) and large-band (d) delays are averaged across subjects for subsequent analyses. The left and right intrahemishperic connections can be seen in respective halves of the matrices.

Note: The analysis pipeline in full is shown in Fig. 2.1.

3.2.3 Statistical Analysis

1. **Correlational analysis:** Both population averaged and pooled data were analyzed with parametric (using Pearson correlation) and nonparametric (using Spearman correlation) approaches to relate small-band and large-band delays with tract lengths and widths independently. The interrelations of tract lengths and widths were also assessed.

2. **Regressional analysis:** A linear model with tract lengths and widths as independent variables, was used to predict the functional small-band or large-band delays in the population averaged condition. In the pooled data, robust regression was applied with the same model structure to downweight the outliers.

3. **Representational similarity analysis:** Representational dissimilarity matrices (RDMs) are heterogenous patterns of any metric's variances across its conditions[64]. Population-level lengths, widths, small-band and large band delays

were extracted for each region-pair separately. RDMs were computed for each metric by computing the Kolmogorov-Smirnov distance among each of its region-pairs' distributions across subjects. KS was over the more commonly used Eucledian distance for its compatibility with unequal sample sizes of region-pairs. The RDMs of lengths and widths were independently related to those of small-band and large-band delays using the Spearman correlation.

3.3 Results

3.3.1 Correlational Analysis

A significant positive corelation was found among the lengths of white-matter tracts and the delays obtained through neuronal avalanches 3.5. The relationship held true for both small-band delays and large-band delays, but small-band delays showed a stronger relationship with tract lengths than the large-band delays across avalanche conditions (not shown).

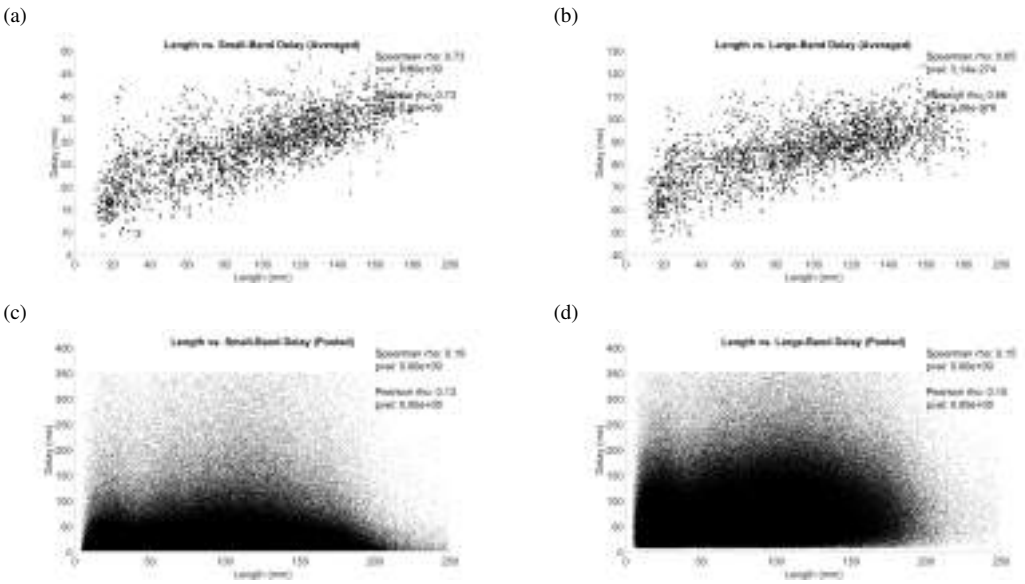

Figure 3.5: **Delays are related to tract lengths.**

Delays were also significantly correlated to log-transformed tract widths, in the negative direction (Fig. 3.6). It was again observed that despite both being significant, the small-band delays showed a stronger correlation to tract widths than the large-band delay did. And this trend was again consistent across avalanche conditions (not shown).

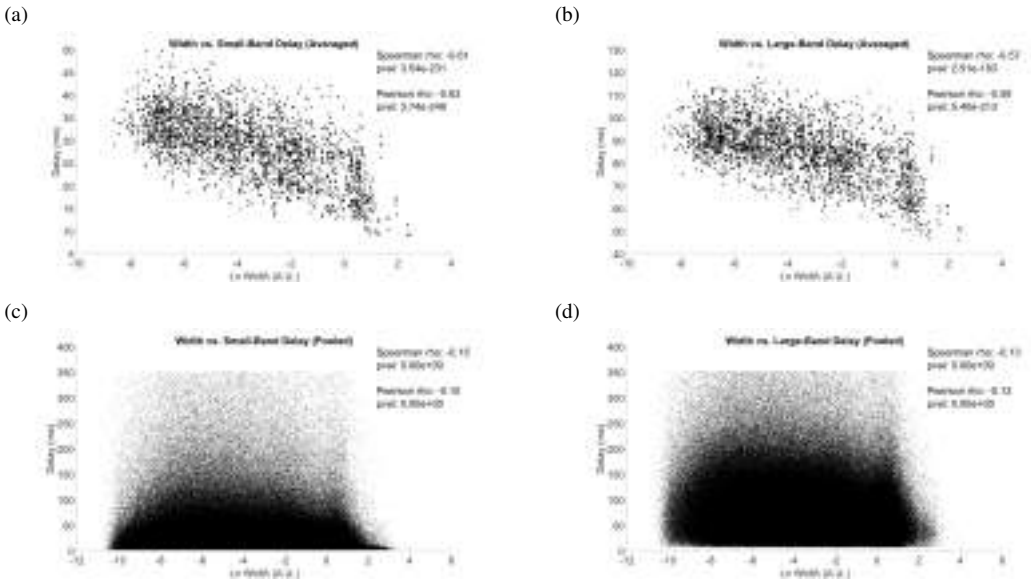

Figure 3.6: **Delays are related to tract widths.**

The independent effects of the tract lengths and widths on the delays could not yet be delineated, because a strongly negative logarithmic interrelation exists among them (Fig 3.7). This is a known property of the white-matter architecture, where nearby connections show the highest strength, and the connection weights decay exponentially with tract length.

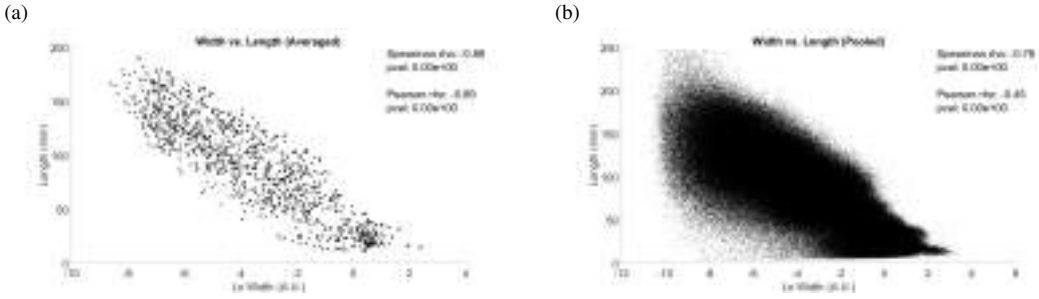

Figure 3.7: **However lengths and widths are interrelated.**

3.3.2 Regressional Analysis

To test the independent effects of tract lengths and widths on delays, linear regression models were implemented. In the case of population pooled data, robust regression was applied to downweight the effects of outliers that the traditional least squares approach is highly susceptible to.

The tract widths and delays were revealed to be sufficient and accurate predictors of functional delays 3.8. The population averaged and pooled models yielded large coefficients of determination for small-band delays ($Adj.\ R^2_{mean} = 0.549$, $Adj.\ R^2_{pool} = 0.34$). The population averaged model could also explain high variance in large-band delays ($Adj.\ R^2_{mean} = 0.458$), but the explaination capability of the pooled model

was drastically lower for large-band delays ($Adj.\ R^2_{pool} = 0.051$). This discrepant prediction ability was replicable for delays obtained across all avalanche conditions (Table A.1).

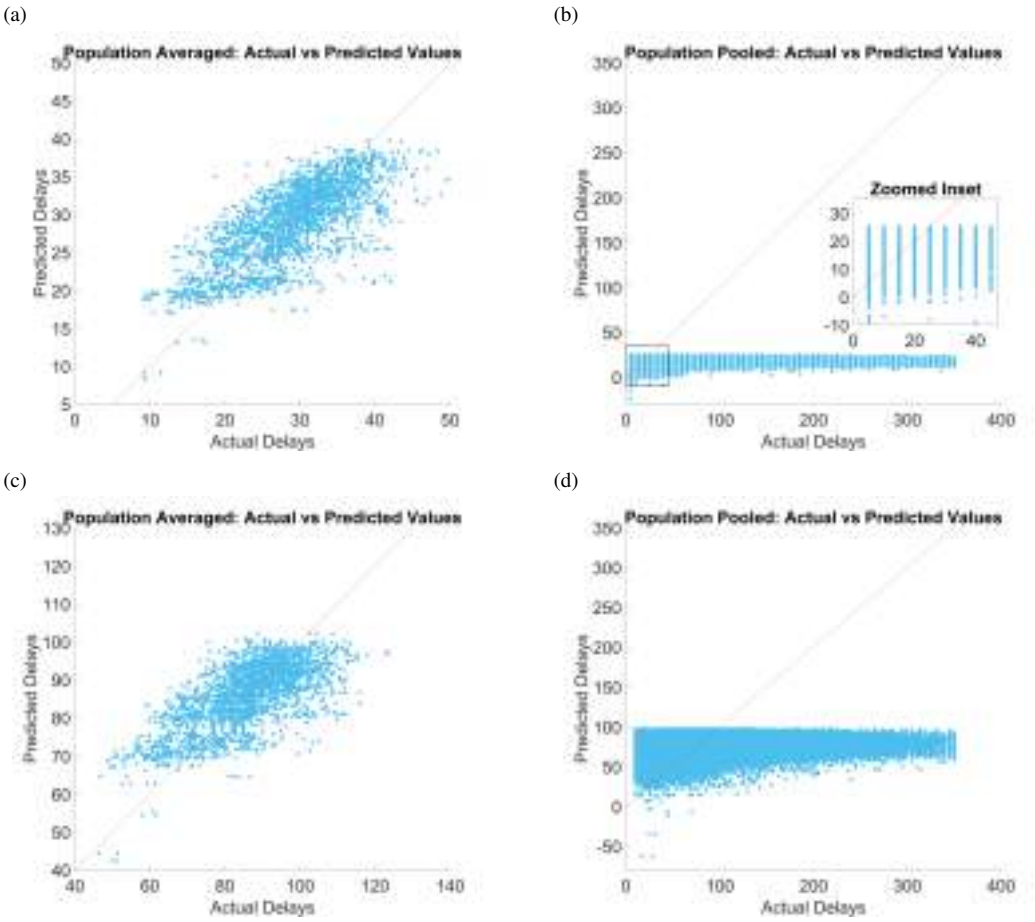

Figure 3.8: **Delays can be accurately predicted from structure.** Robust regression implemented pooled models downweigh outlier delay values in the data. For instance, the small inset region in (b) contains 80% of the empirical delays.

Significant effects of tract widths and tract lengths were independently present on the delays. Larger tract widths were tied to faster communication, and longer tract lengths associate with slower signal transfer. These results sit well with the underlying biophysical properties of axons that mediate these communications. Moreover, these independent relations were significantly present, and in the same directions, for large-band and small-band delays measured across various avalanche conditions (Table A.1).

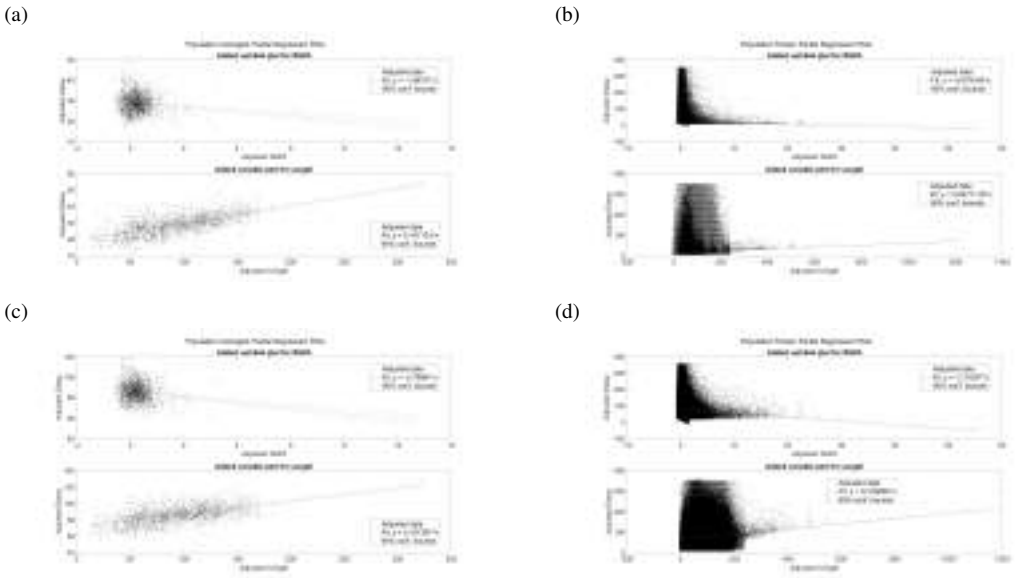

Figure 3.9: **Partial regression retains effects of widths and lengths on delays.**

3.3.3 Representational Similarity Analysis

Complementary to the predictive approach employed earlier, this method compares the second-order isomorphisms of tract properties and delays. That is just a sligtly complicated way to say that this approach compares if the clusters of region pairs that are similar to each other in one metric are also similar to each other in the other metric being compared. RDMs for lengths and widths of the tracts, and the small-band and large-band delays were computed as specified earlier.

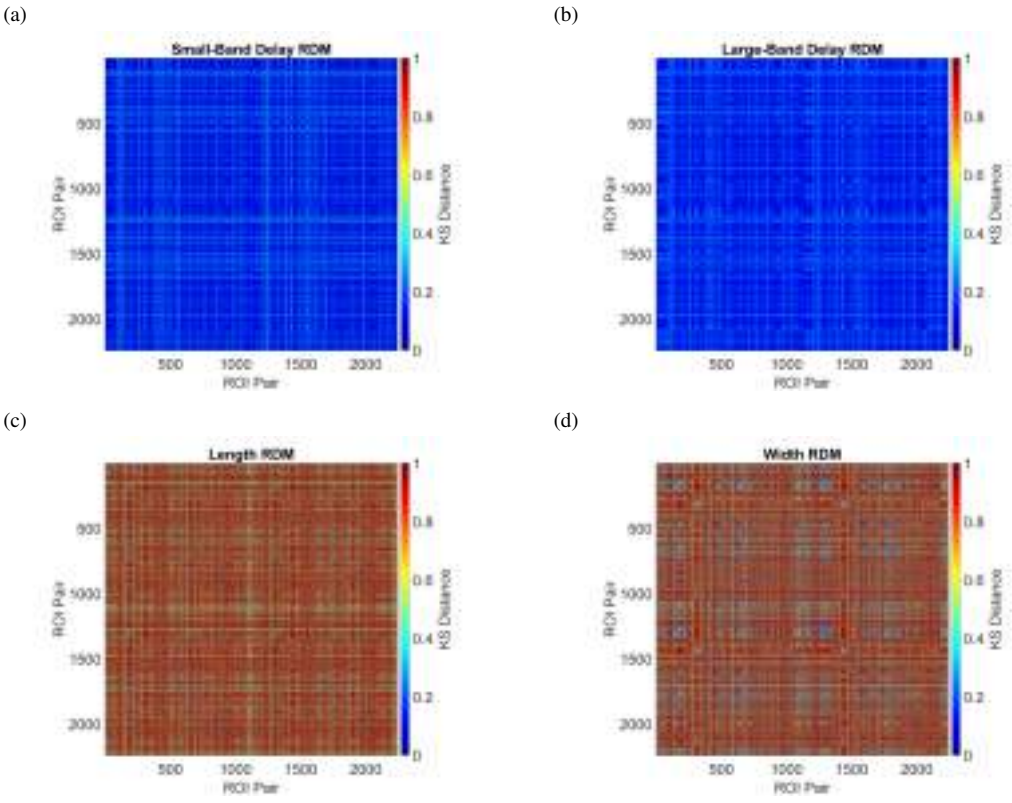

Figure 3.10: **Patterns of dissimilarity across pairs of regions.**

The representational structures of both, small-band and large-band delays, were significantly similar to those of tract lengths, and comparably with the tract widths as well. The representational patterns of large-band delays tracked significantly with tract lengths ($\rho_{large\ L} = 0.35$) and widths ($\rho_{large\ W} = 0.27$), yet less so than did small-band delays ($\rho_{small\ L} = 0.45,\ \rho_{small\ W} = 0.33$).

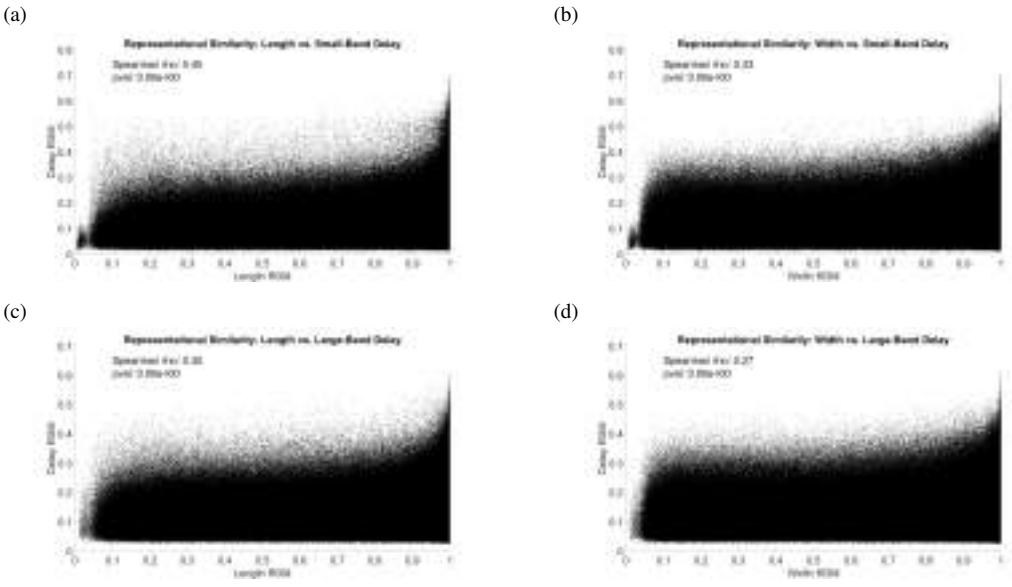

Figure 3.11: **Structural-functional similarity of pairwise dissimilarity.**

3.4 Discussion

In this chapter, we test an advanced method that extracts inter-regional functional delays with a two-pronged approach. Meticulous examination revealed that the empirically identified delays are significantly related to the white-matter geometry. Increasing values of tract lengths and widths independently extend and shorten communication lags, respectively. This observation lends credence to the arguments made in chapter 2 about the causal nature of avalanche dynamics, and it being mediated by the structural connectome. Additionally, another prediction from chapter 2 is confirmed, and it being that the scale-invariant avalanche dynamics allow for robust measurements of latencies, making the technique easily adaptable across experimental requirements.

The discord of small-band and large-band delays in their relational extent with the structure suggests that they are sensitively tuned to different communication regimes. To be precise, this suggests that despite the delays having been recorded among the same pair of regions, they are observed to drastically differ in few minutes of recordings because they stem from metastable brain dynamics. While the avalanches were obtained from resting-state recordings, the brain never truly rests. Rather it performs constant task switching. It is known that avalanche patterns can vary with task contexts, and thus it also stands to reason that delays derived from these qualitatively different avalanches could be the result of variable communication approaches.

Small-band delays may be better poised to identify highly myelinated efficient signal transfer of direct axonal connections. Large-band delays on the other hand may be tapping into communication delayed mediated by a constellation of latent factors, like differing conduction velocities, indirect communication pathways, and other local properties.

Chapter 4

Delays in Hemispheric Specialization

4.1 Introduction

The extent and directionality of laterality in the brain is subject to high variance when confounds are unaccounted for. Across demographic, patterns of structural and functional lateralization could found to be weaker or even inverted. Studies have found patterns to be demonstrably "atypical" on a higher extent with age[65], in left-handed individuals[66,67], and at times among females[68–70].

To find a mechanistic basis of "typical" hemispheric specialization, here we test delay and tract lateralities in a controlled set of participants, and assess their relationships with regional power differences.

4.2 Methods

Note: The following analyses were performed primarily with delays derived from avalanches of threshold 3.5 *SD and window length* 30ms*, and then replicated in full with varied conditions.*

4.2.1 Participant Selection and Metric Laterlization Assessment

Of the total 449 subjects, only male, right-handed (with Edinburgh Handedness Inventory scores > 40), and young (age < 35) participants were selected for further analysis ($N = 45,\ mean\ age = 28.98 \pm 4.93$).

Pairwise laterality matrices were derived from the population averaged data as such:

- Tract length and width laterality index:

$$LI_{pair\ tract} = \frac{RH_{tract} - LH_{tract}}{RH_{tract} + LH_{tract}} \tag{4.1}$$

  Where LH_{tract} and RH_{tract} are the tract lengths or widths of the left and right hemisphere, respectively.

- Small-band and large-band delay laterality index:

$$LI_{pair\ delay} = RH_{delay} - LH_{delay} \tag{4.2}$$

Where LH_{delay} and RH_{delay} are the small-band or large-band delays of the left and right hemisphere, respectively. The laterality indices for delays were not normalized with their summed values to get an interpretable magnitude difference between the small-band and large-band delays.

Regional metric laterality arrays were calculated as such:

$$LI_{region} = \frac{\sum_{k=1}^{N} LI_{aff,k}}{N} \tag{4.3}$$

Where N is the number of afferent connections to the region, k is the index of pairs, $LI_{aff,k}$ is the laterality at of either the structural or functional metrics at pair k.

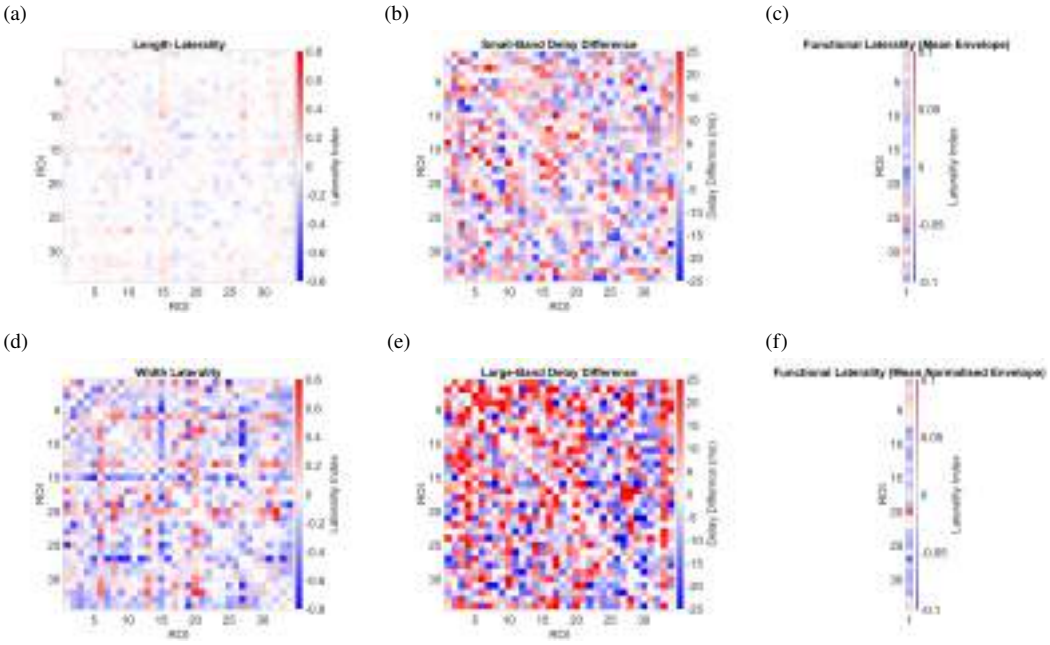

Figure 4.1: **Laterality maps of tract lengths, widths, functional delays, and amplitude envelopes.**

4.2.2 Computing amplitude envelopes and their laterality

Absolute source reconstructed regional time series of each participant were hilbert transformed. The magnitude of the hilbert transformed time series was averaged across time points for each region to get a mean envelope value. Parallely, the hilbert transformed time series was also percentage normalized and then averaged across time points to get a mean normalized envelope value.

A lateralization array of mean envelopes and normalized envelopes were computed as such:

$$LI_{envelope} = \frac{RH_{envelope} - LH_{envelope}}{RH_{envelope} + LH_{envelope}} \tag{4.4}$$

4.2.3 Statistical Analysis

In view of their non-normal distributions, hemispheric asymmetry of tract properties and functional delays across the hemispheres were assessed by the non-parametric Kolmogorov-Smirnov test. This analysis was performed for population averaged and pooled hemispheric distributions of the metrics. Additionally, each region pair was separately compared among the hemisphere, again with the Kolmogorov-Smirnov test.

Post the analysis of the raw metrics, their pairwise and regional laterality values were correlated amongst each other with the Spearman correlation. Additionally regional lateralities of all the metrics were Spearman correlated with the mean amplitude lateralities and the mean normalized amplitude lateralities.

All of the above delay related analyses were performed athwart delays obtained across multiple avalanche conditions.

4.3 Results

4.3.1 Distributional Analysis

Asymmetries of the left and right intrahemispheric tract lengths and connection weights were assessed by comparing their distributions with the Kolmogorov-Smirnov test. Both, population averaged and pooled set of length values showed an insignificant difference ($p - value > 0.05$). Population pooled width distributions were significantly different ($p - value \approx 0.001$), but averaged distributions were again insignificantly different ($p - value > 0.05$).

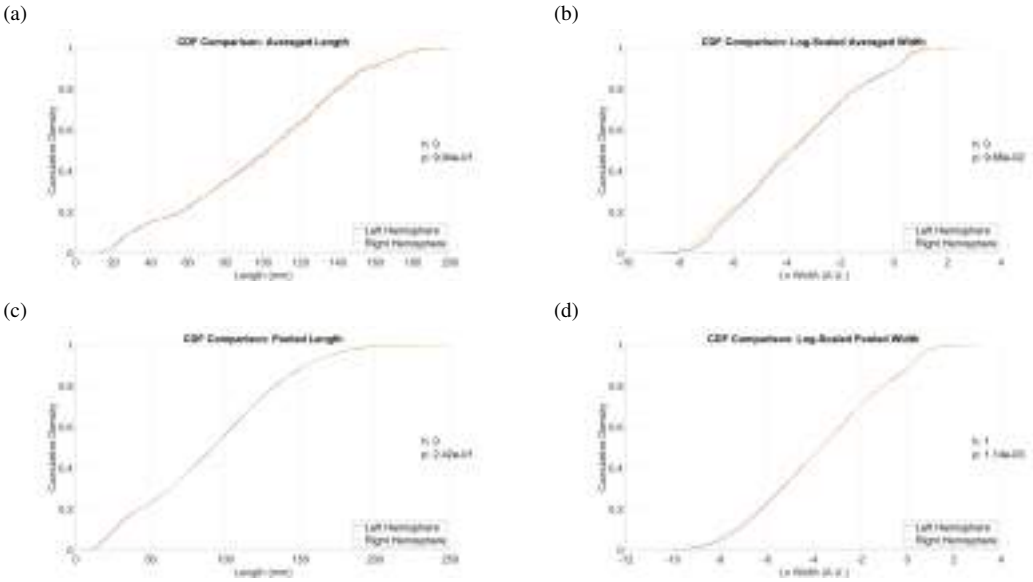

Figure 4.2: **Tract lengths and widths are mostly symmetric between the hemispheres.**

Delay differences among the hemispheres were assessed by the same approach. Small-band delays were symmetric in either cases ($p - value > 0.05$), but large-band delays showed a stark asymmetry in both population pooled ($p - value \approx e - 9$)

and averaged ($p - value \approx e - 5$) cases. The specificity of this difference was observable across most avalanches, but in avalaches with slightly lenient thresholds, small-band delays also turned asymmetric (not shown).

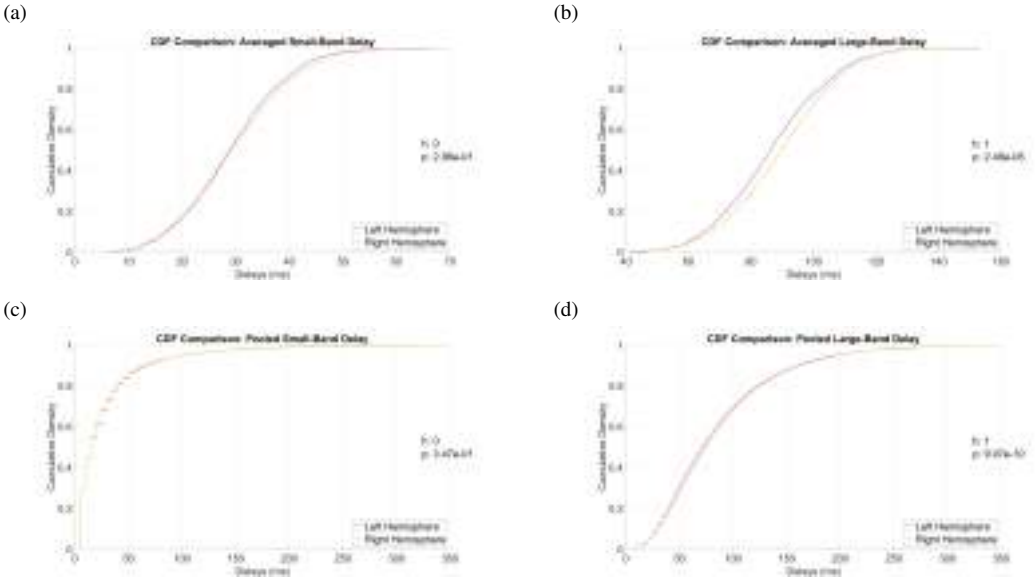

Figure 4.3: **Large-band delays, but not small-band delays, are hemispherically asymmetric.**

The delay differences were further observed on finer, region pair levels. This was done by grouping delay values for every ROI pair across participants, and comparing the distributions for homologous left and right ROI pairs. The numerousity of asymmetric ROI pairs and the magnitude of asymmetry across those pairs, as marked by the KS distance metric, were much higher for the large-band delays than the small-band delays.

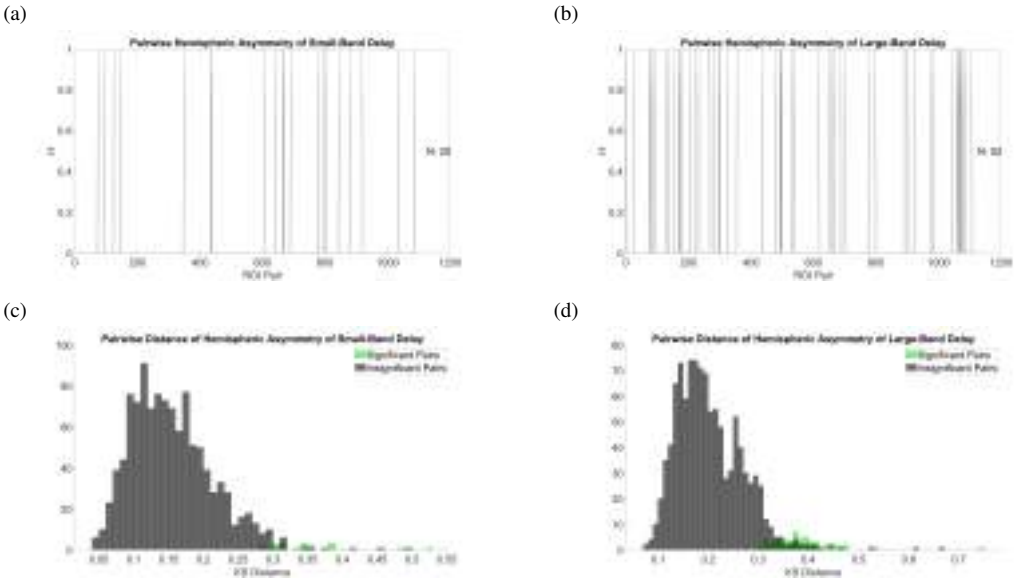

Figure 4.4: **Large-band delays show asymmetry across more pairs of regions.**

4.3.2 Laterality Analysis

To get a fine-grained estimate of structure-function relationships in the context of brain asymmetry, pairwise laterality matrices for tract lengths and widths, and for small-band and large-band delays were computed, as shown in Fig.4.1.

All the sets of lateralities of afferent connections to a region were aggregated to form a regional laterality value. The afferent connections in the matrices correspond to the columns. The primary reason of calculating this coarse laterality value is to allow comparison with laterality values of regional power.

Envelope lateralities and normalized envelope lateralities were two regional measures at the level of the population, that served as proxy for specialization of function. *Note: their computation method needs further rectification for sound analysis. The results obtained from them were included for the sake of a discussion.*

All possible combinations of pairwise and regionwise structural and functional laterality were tested by Spearman correlation. Most showed insignificant relations with each other.

The laterality of the large-band delays, however, showed a marked association with the normalized envelope laterality ($\rho = 0.49$ **). This was contrasted by the insignificant correlation of small-band delays with the normalized amplitude laterality($\rho = 0.26$ ^{ns}). This distinction was again replicable across delays obtained from varied avalanche conditions (not shown).

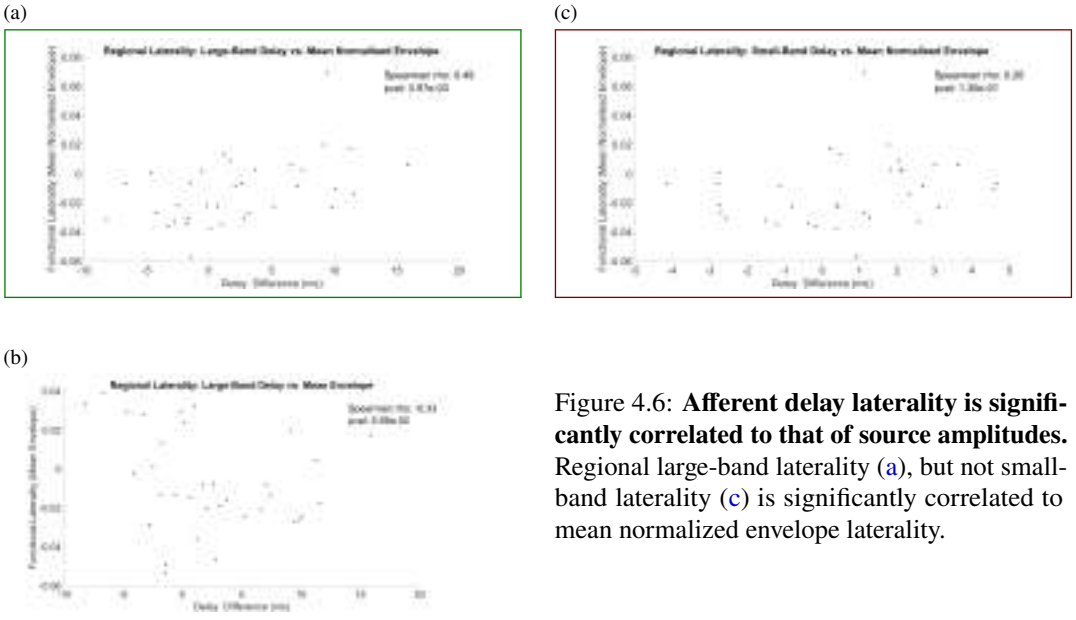

Figure 4.6: **Afferent delay laterality is significantly correlated to that of source amplitudes.** Regional large-band laterality (a), but not small-band laterality (c) is significantly correlated to mean normalized envelope laterality.

The significant positive correlation of large-band delays with the normalized envelope laterality, when inferred, posits that it is the larger afferent delay possesing homolog regions that have an increased activation power. This is counter-intuitive in regards to the traditional views stating that cerebral hemispheres that activate more strongly, have more prominent tracts and thus smaller delays. The negative correlations of large-band delays with envelope laterality (Fig. 4.5b), although insignificant, fits more so in that persepctive.

4.4 Discussion

In this chapter, we found that it's not the tract properties or the small-band delays (that closely link to structure), that are divided between the two sides of the brain, but rather the large-band delays that seem to be influenced by unknown factors along with the tracts that show significant differences between the hemispheres.

The possibility that large-band delays are mediated my indirect white-matter communication is strongly supported by the fact that right hemisphere has a higher regional interconnectivity that could facilitate longer latencies, and the fact that empirically right hemispheric large-band delays can be observed to be larger from their cummulative distributions. This idea is countered however by the fact that large-band delays are significantly relayted to direct tract lengths and widths, which suggests a modulation of conduction velocities rather than connectivities. Nonetheless, both or other factors could be the drivers of this trend, and more analyses are required to conclusively point in a direction.

Furthermore, the larger afferent large-band delays are associated with higher cortical activation. At face value, this suggests that specialization of functions across hemispheres is driven by deliberate slowing of signals, and this occurs primarily in the regimes of latent-factors driven large-band delays.

To normalize or not to normalize? That is the question:

Before solidifying inferences, it is necessary to redefine the methodological choices that yeilded the activation power LIs. Several improvements can be made to its definition. Firstly, Hilbert transform should be applied to zero-mean signals, not their absolute values as was done in this case. This distorts its spectral and phase structure. Secondly, especially in context of language lateralization studies, observability of maximal activation power laterality are typically associated with narrow-band signals, mostly the Beta band. Thirdly, choosing whether or not to normalize envelope amplitudes across time can have fundamentally different impacts on what they signify. While normalization of regional time series helps ameliorate signal aquisition differences that could falsely present laterality, they could also suppress actual lateralization of the activity. Choosing not to normalize has the reciprocal issues nonetheless. Lastly, aside from computing and relating population averaged regional metrics, more refined analysis without aggregating across subjects can be performed.

In view of the above observations, it would be interesting to test the relations of afferent delay lateralities with that of an improved metric for activation power differences, and see if it indeed is the presence of slowed signalling that are drives differential emergent properties.

Chapter 5

Conclusion

5.1 Summary

- Dynamics of the brain are tuned at the edge of phase transitions.
- Neuronal avalanches are representative of this critical organization, and they feature events caused by interregional communication.
- A method to extract empirical delays from neuronal avalanches was advanced to separate temporal regimes.
- Extracted delays can be predicted by, and have a similar representational structure as white matter tract lengths and widths.
- Small-band delays closely follow tract distributions, but large-band delays have show a weaker relation, signifying their sensitivity to higher-order differentiations.
- Large-band delays are signifianctly different between the hemispheres, but not the small-band delays and tract properties.
- Regional laterality of afferent large-band delays significantly relate to envelope laterality.
- Large-band delays, affected by mysterious substrates, seem to drive differential emergent properties that underlie hemispheric specialization.

5.2 Future Directions

Several further question and possibilities arise from current findings:

- **Testing the origins of large-band delays:** To delineate whether the large-band delay asymmetry is mediated by indirect connections, distributions of avalanche spatiotemporal spreads can be compared, since with indirect communications, higher spread is expected.
- **Testing demographic variance:** Patterns of hemispheric specialization are known to change with age, handednness, and sex. Laterality of delays can be tested to see if they too follow similar trends.

- **Did the delay laterality come first, or the emergent properties?:** Results presented here are suggestive of the idea that differential delays influence emergence of differential properties. To confirm the chronology, however, delay lateralities and functional power lateralities can be tested during the course of childhood development.
- **Contextual differences of small- and large-band delays:** The forked delay estimation method proposed here is excellently poised to compare communication dynamics across contexts of cognitive demand.

Appendix A

Statistical Table

Table A.1: **Statistical parameters of structural-functional regression models.**

Delay Band	Avalanche Condition	Population Type	Delay		Width			Length			R^2		F-Stat		
			Intercept	CI	β	CI	Sig	β	CI	Sig	Ord.	Adj.	F	(df1,df2)	Sig
Large	2.5SD, 30ms	mean	101.4	[100.6, 102.1]	−1.51	[-1.89, -1.14]	***	0.12	[0.12, 0.13]	***	0.489	0.489	1074.3	(2,2241)	***
		pooled	102.5	[102.4, 102.6]	−1.65	[-1.71, -1.60]	***	0.11	[0.10, 0.11]	***	0.063	0.063	30040.6	(2,920850)	***
	3SD, 30ms	mean	79.5	[78.8, 80.3]	−2.21	[-2.59, -1.84]	***	0.13	[0.13, 0.14]	***	0.546	0.546	1347.4	(2,2241)	***
		pooled	77.8	[77.6, 78.0]	−2.05	[-2.13, -1.97]	***	0.11	[0.11, 0.11]	***	0.048	0.048	17176.3	(2,916349)	***
	3.5SD, 20ms	mean	54.7	[53.5, 55.8]	−2.42	[-3.00, -1.83]	***	0.15	[0.14, 0.16]	***	0.373	0.372	666.5	(2,2241)	***
		pooled	48.8	[48.5, 49.0]	−2.07	[-2.17, -1.96]	***	0.10	[0.10, 0.10]	***	0.082	0.082	7040.5	(2,581233)	***
	3.5SD, 30ms	mean	72.1	[71.0, 73.2]	−2.80	[-3.33, -2.26]	***	0.16	[0.15, 0.17]	***	0.459	0.458	949.5	(2,2241)	***
		pooled	66.3	[66.0, 66.6]	−2.32	[-2.45, -2.19]	***	0.13	[0.12, 0.13]	***	0.051	0.051	7506.4	(2,644104)	***
	3.5SD, 40ms	mean	87.8	[86.8, 88.9]	−2.95	[-3.46, -2.44]	***	0.16	[0.15, 0.17]	***	0.493	0.493	1090.8	(2,2241)	***
		pooled	82.0	[81.7, 82.3]	−2.47	[-2.61, -2.33]	***	0.14	[0.14, 0.15]	***	0.039	0.039	7914.6	(2,686565)	***
	4SD, 30ms	mean	70.0	[68.4, 71.7]	−3.30	[-4.10, -2.50]	***	0.20	[0.19, 0.22]	***	0.379	0.378	682.7	(2,2241)	***
		pooled	61.1	[60.6, 61.5]	−2.81	[-3.01, -2.60]	***	0.18	[0.17, 0.18]	***	0.066	0.066	4685.4	(2,27424)	***
Small	2.5SD, 30ms	mean	14.3	[13.9, 14.7]	−0.93	[-1.12, -0.74]	***	0.07	[0.07, 0.07]	***	0.546	0.546	1347.2	(2,2241)	***
		pooled	11.8	[11.7, 11.8]	−0.72	[-0.75, -0.69]	***	0.05	[0.05, 0.05]	***	0.127	0.127	15852.7	(2,920914)	***
	3SD, 30ms	mean	15.3	[14.9, 15.7]	−1.04	[-1.22, -0.87]	***	0.07	[0.06, 0.07]	***	0.568	0.567	1471.6	(2,2241)	***
		pooled	12.0	[12.0, 12.1]	−0.69	[-0.72, -0.65]	***	0.04	[0.04, 0.04]	***	0.166	0.166	12353.3	(2,920406)	***
	3.5SD, 20ms	mean	15.4	[14.8, 15.9]	−0.78	[-1.03, -0.52]	***	0.09	[0.08, 0.09]	***	0.489	0.488	1071.7	(2,2241)	***
		pooled	11.0	[10.9, 11.1]	−0.52	[-0.55, -0.49]	***	0.03	[0.03, 0.03]	***	0.393	0.393	9668.4	(2,77259)	***
	3.5SD, 30ms	mean	19.3	[18.7, 19.8]	−1.09	[-1.37, -0.82]	***	0.11	[0.10, 0.11]	***	0.549	0.549	1364.8	(2,2241)	***
		pooled	13.3	[13.2, 13.4]	−0.68	[-0.72, -0.64]	***	0.05	[0.05, 0.05]	***	0.340	0.340	10460.3	(2,810698)	***
	3.5SD, 40ms	mean	22.8	[22.1, 23.4]	−1.26	[-1.58, -0.95]	***	0.12	[0.12, 0.13]	***	0.566	0.565	1459.5	(2,2241)	***
		pooled	15.5	[15.4, 15.6]	−0.84	[-0.89, -0.79]	***	0.06	[0.06, 0.06]	***	0.301	0.301	10820.0	(2,83860)	***
	4SD, 30ms	mean	25.9	[24.9, 26.8]	−1.64	[-2.10, -1.19]	***	0.15	[0.14, 0.16]	***	0.477	0.476	1021.2	(2,2241)	***
		pooled	15.6	[15.5, 15.7]	−0.86	[-0.93, -0.80]	***	0.06	[0.06, 0.06]	***	0.423	0.423	6484.7	(2,484508)	***

Appendix B

Parcellation Lookup Table

Table B.1: **Hemisphere aggregated parcellation scheme** (Desikan-Killiany atlas).

Index	Label	Region Name
1	bankssts	Banks of the Superior Temporal Sulcus
2	caudalanteriorcingulate	Caudal Anterior Cingulate
3	caudalmiddlefrontal	Caudal Middle Frontal Gyrus
4	cuneus	Cuneus
5	entorhinal	Entorhinal Cortex
6	frontalpole	Frontal Pole
7	fusiform	Fusiform Gyrus
8	inferiorparietal	Inferior Parietal Lobule
9	inferiortemporal	Inferior Temporal Gyrus
10	insula	Insular Cortex
11	isthmuscingulate	Isthmus of the Cingulate
12	lateraloccipital	Lateral Occipital Cortex
13	lateralorbitofrontal	Lateral Orbitofrontal Cortex
14	lingual	Lingual Gyrus
15	medialorbitofrontal	Medial Orbitofrontal Cortex
16	middletemporal	Middle Temporal Gyrus
17	paracentral	Paracentral Lobule
18	parahippocampal	Parahippocampal Gyrus
19	parsopercularis	Pars Opercularis
20	parsorbitalis	Pars Orbitalis
21	parstriangularis	Pars Triangularis
22	pericalcarine	Pericalcarine Cortex
23	postcentral	Postcentral Gyrus
24	posteriorcingulate	Posterior Cingulate Cortex
25	precentral	Precentral Gyrus
26	precuneus	Precuneus
27	rostralanteriorcingulate	Rostral Anterior Cingulate
28	rostralmiddlefrontal	Rostral Middle Frontal Gyrus
29	superiorfrontal	Superior Frontal Gyrus
30	superiorparietal	Superior Parietal Lobule
31	superiortemporal	Superior Temporal Gyrus
32	supramarginal	Supramarginal Gyrus
33	temporalpole	Temporal Pole
34	transversetemporal	Transverse Temporal Gyrus

Appendix C

Code Listings

This appendix contains the MATLAB scripts used to process the data and generate the figures in this dissertation.

C.1 MATLAB Script for Functional Data Processing

Details of volumetric and tractography data processing not included in this appendix. It was carried out through a pipeline developed in-house[71], which can be found at:
https://github.com/Pratikasiwatch/CBDL_DWI_script

```
% Author: Atharva Parolekar
% Email: atharva[dot]parolekar[at]gmail[dot]com
%% IMPORT, PRE-PROCESS, HEAD MODEL
% brainstorm nogui  % Local processing
brainstorm server local % Remote processing
% Brainstorm library is a dependency. Install the add-on in MATLAB, or download
    from https://neuroimage.usc.edu/brainstorm/Introduction
% Signal Processing Toolbox and Statistics and Machine Learning Toolbox are
    essential for some functions to perform well
% Internet connection required for MNI linear normalization
% Set path to the Globus directory with input data
GLOBUS_DIR = ('/path/to/dataset');
% Relative directories
RS_MEG = fullfile(GLOBUS_DIR, 'RS_MEG');
EMPTYROOM = fullfile(GLOBUS_DIR, 'EMPTY_ROOM');
ANAT = fullfile(GLOBUS_DIR, 'ANAT');
OUTPUT = fullfile(GLOBUS_DIR, 'OUTPUT');
diary(fullfile(OUTPUT, 'MATLAB_log.txt'));
REPORTS = fullfile(OUTPUT, 'REPORTS');
DATABASE = fullfile(OUTPUT, 'DATABASE');
bst_set('BrainstormDbDir', DATABASE);
gui_brainstorm('CreateProtocol', 'PROTOCOL', 0, 0);
SUBJECT = dir(fullfile(RS_MEG,'CC*'));
for iSub = 1:size(SUBJECT,1)
display(strcat('NOW PROCESSING>>>',SUBJECT(iSub).name),newline) % Progress
try
ExportDir = fullfile(REPORTS, SUBJECT(iSub).name);
if ~exist(ExportDir, 'dir')
    mkdir(ExportDir);
end
% Input files
sFiles = [];
SubjectNames = {...
    SUBJECT(iSub).name};
RawFiles = {...
    fullfile(ANAT,SUBJECT(iSub).name) ...
    fullfile(RS_MEG,SUBJECT(iSub).name,'transdef_mf2pt2_rest_raw.fif')};
% Start a new report
bst_report('Start', sFiles);
% Process: Import anatomy folder
sFiles = bst_process('CallProcess', 'process_import_anatomy', sFiles, [], ...
    'subjectname', SubjectNames{1}, ...
    'mrifile',     {RawFiles{1}, 'FreeSurfer+Thick'}, ...
    'nvertices',   15000, ...
```

```
    'nas',          [0, 0, 0], ...
    'lpa',          [0, 0, 0], ...
    'rpa',          [0, 0, 0], ...
    'ac',           [0, 0, 0], ...
    'pc',           [0, 0, 0], ...
    'ih',           [0, 0, 0]);
% Process: MNI normalization
sFiles = bst_process('CallProcess', 'process_mni_normalize', sFiles, [], ...
    'subjectname', SubjectNames{1}, ...
    'method',      'maff8', ...  % maff8:Affine registration using SPM mutual
        information algorithm.Estimates a simple 4x4 linear transformation to the
        MNI space.Included in Brainstorm.
    'uset2',       0);
% Process: Create link to raw file
sFiles = bst_process('CallProcess', 'process_import_data_raw', sFiles, [], ...
    'subjectname',    SubjectNames{1}, ...
    'datafile',       {RawFiles{2}, 'FIF'}, ...
    'channelreplace', 1, ...
    'channelalign',   1, ...
    'evtmode',        'value');
% Process: Remove head points
sFiles = bst_process('CallProcess', 'process_headpoints_remove', sFiles, [], ...
    'zlimit', 0);
% Process: Refine registration
sFiles = bst_process('CallProcess', 'process_headpoints_refine', sFiles, [], ...
    'tolerance', 0);
% Process: Detect heartbeats
sFiles = bst_process('CallProcess', 'process_evt_detect_ecg', sFiles, [], ...
    'channelname', 'ECG063', ...
    'timewindow',  [], ...
    'eventname',   'cardiac');
% Process: SSP ECG: cardiac
sFiles = bst_process('CallProcess', 'process_ssp_ecg', sFiles, [], ...
    'eventname',   'cardiac', ...
    'sensortypes', 'MEG MAG', ...
    'usessp',      1, ...
    'select',      1);
% Process: SSP ECG: cardiac
sFiles = bst_process('CallProcess', 'process_ssp_ecg', sFiles, [], ...
    'eventname',   'cardiac', ...
    'sensortypes', 'MEG GRAD', ...
    'usessp',      1, ...
    'select',      1);
% Process: Resample: 200Hz
sFiles = bst_process('CallProcess', 'process_resample', sFiles, [], ...
    'freq',     200, ...
    'read_all', 0);
% Process: DC offset correction: [All file]
sFiles = bst_process('CallProcess', 'process_baseline', sFiles, [], ...
    'baseline',    [], ...
    'sensortypes', 'MEG, EEG', ...
    'method',      'bl', ...  % DC offset correction:    x_std = x - &mu;
    'read_all',    0);
% Process: Remove linear trend: All file
sFiles = bst_process('CallProcess', 'process_detrend', sFiles, [], ...
    'timewindow',  [], ...
    'sensortypes', 'MEG, EEG', ...
    'read_all',    0);
% Process: Notch filter: 50Hz 100Hz
sFiles = bst_process('CallProcess', 'process_notch', sFiles, [], ...
    'sensortypes', 'MEG, EEG', ...
    'freqlist',    [50, 100], ...
    'cutoffW',     1, ...
    'useold',      0, ...
    'read_all',    0);
% Process: Band-pass:1Hz-99Hz
sFiles = bst_process('CallProcess', 'process_bandpass', sFiles, [], ...
    'sensortypes', 'MEG, EEG', ...
    'highpass',    1, ...
    'lowpass',     99, ...
    'tranband',    0, ...
    'attenuation', 'strict', ...  % 60dB
    'ver',         '2019', ...  % 2019
    'mirror',      0, ...
    'read_all',    0);
% Process: Compute head model
sFiles = bst_process('CallProcess', 'process_headmodel', sFiles, [], ...
    'Comment',     '', ...
    'sourcespace', 1, ...  % Cortex surface
    'meg',         3, ...  % Overlapping spheres
    'eeg',         3, ...  % OpenMEEG BEM
```

```
    'ecog',        2, ...  % OpenMEEG BEM
    'seeg',        2, ...  % OpenMEEG BEM
    'openmeeg',    struct(...
         'BemFiles',     {{}}, ...
         'BemNames',     {{'Scalp', 'Skull', 'Brain'}}, ...
         'BemCond',      [1, 0.0125, 1], ...
         'BemSelect',    [1, 1, 1], ...
         'isAdjoint',    0, ...
         'isAdaptative', 1, ...
         'isSplit',      0, ...
         'SplitLength',  4000), ...
    'channelfile', '');
% Save and display report
ReportFile = bst_report('Save', sFiles);
bst_report('Open', ReportFile);
bst_report('Export', ReportFile, ExportDir);
%% NOISE COVARIANCE USING EMPTY ROOM RECORDINGS
% Input files
sFiles = [];
RawFiles = {...
    fullfile(EMPTYROOM, SUBJECT(iSub).name, 'emptyroom', ['emptyroom_', SUBJECT(
        iSub).name, '.fif'])};
% Start a new report
bst_report('Start', sFiles);
% Process: Import MEG/EEG: Time
sFiles = bst_process('CallProcess', 'process_import_data_time', sFiles, [], ...
    'subjectname',   SubjectNames{1}, ...
    'condition',     'empty room', ...
    'datafile',      {{RawFiles{1}}, 'FIF'}, ...
    'timewindow',    [], ...
    'split',         0, ...
    'ignoreshort',   1, ...
    'channelalign',  1, ...
    'usectfcomp',    1, ...
    'usessp',        1, ...
    'freq',          200, ...
    'baseline',      'all', ...
    'blsensortypes', 'MEG, EEG');
% Process: Remove linear trend: All file
sFiles = bst_process('CallProcess', 'process_detrend', sFiles, [], ...
    'timewindow',  [], ...
    'sensortypes', 'MEG, EEG', ...
    'overwrite',   0);
% Process: Notch filter: 50Hz 100Hz
sFiles = bst_process('CallProcess', 'process_notch', sFiles, [], ...
    'sensortypes', 'MEG, EEG', ...
    'freqlist',    [50, 100], ...
    'cutoffW',     1, ...
    'useold',      0, ...
    'overwrite',   0);
% Process: Band-pass:1Hz-99Hz
sFiles = bst_process('CallProcess', 'process_bandpass', sFiles, [], ...
    'sensortypes', 'MEG, EEG', ...
    'highpass',    1, ...
    'lowpass',     99, ...
    'tranband',    0, ...
    'attenuation', 'strict', ...  % 60dB
    'ver',         '2019', ...  % 2019
    'mirror',      0, ...
    'overwrite',   0);
% Process: Compute covariance (noise or data)
sFiles = bst_process('CallProcess', 'process_noisecov', sFiles, [], ...
    'baseline',       [], ...
    'datatimewindow', [], ...
    'sensortypes',    'MEG, EEG, SEEG, ECOG', ...
    'target',         1, ...  % Noise covariance     (covariance over baseline
        time window)
    'dcoffset',       1, ...  % Block by block, to avoid effects of slow shifts in
         data
    'identity',       0, ...
    'copycond',       1, ...
    'copysubj',       0, ...
    'copymatch',      0, ...
    'replacefile',    1);  % Replace
% Save and display report
ReportFile = bst_report('Save', sFiles);
bst_report('Open', ReportFile);
bst_report('Export', ReportFile, ExportDir);
%% SOURCE RECONSTRUCTION
% Input files
sFiles = {...
```

```
    fullfile(DATABASE,'PROTOCOL','data',SubjectNames{1},'
        @rawtransdef_mf2pt2_rest_raw_resample_bl_detrend_notch_band','
        data_0raw_transdef_mf2pt2_rest_raw_resample_bl_detrend_notch_band.mat')};
% Start a new report
bst_report('Start', sFiles);
% Process: Compute sources [2018]
sFiles = bst_process('CallProcess', 'process_inverse_2018', sFiles, [], ...
    'output',  1, ...  % Kernel only: shared
    'inverse', struct(...
         'Comment',        'MN: MEG ALL', ...
         'InverseMethod',  'minnorm', ...
         'InverseMeasure', 'amplitude', ...
         'SourceOrient',   {{'fixed'}}, ...
         'Loose',          0.2, ...
         'UseDepth',       1, ...
         'WeightExp',      0.5, ...
         'WeightLimit',    10, ...
         'NoiseMethod',    'reg', ...
         'NoiseReg',       0.1, ...
         'SnrMethod',      'fixed', ...
         'SnrRms',         1e-06, ...
         'SnrFixed',       3, ...
         'ComputeKernel',  1, ...
         'DataTypes',      {{'MEG GRAD', 'MEG MAG'}}));
% Process: Scout time series: [68 scouts]
sFiles = bst_process('CallProcess', 'process_extract_scout', sFiles, [], ...
    'timewindow',     [], ...
    'scouts',         {'Desikan-Killiany', {'bankssts L', 'bankssts R', '
        caudalanteriorcingulate L', 'caudalanteriorcingulate R', '
        caudalmiddlefrontal L', 'caudalmiddlefrontal R', 'cuneus L', 'cuneus R', '
        entorhinal L', 'entorhinal R', 'frontalpole L', 'frontalpole R', 'fusiform
         L', 'fusiform R', 'inferiorparietal L', 'inferiorparietal R', '
        inferiortemporal L', 'inferiortemporal R', 'insula L', 'insula R', '
        isthmuscingulate L', 'isthmuscingulate R', 'lateraloccipital L', '
        lateraloccipital R', 'lateralorbitofrontal L', 'lateralorbitofrontal R', '
        lingual L', 'lingual R', 'medialorbitofrontal L', 'medialorbitofrontal R',
         'middletemporal L', 'middletemporal R', 'paracentral L', 'paracentral R',
         'parahippocampal L', 'parahippocampal R', 'parsopercularis L', '
        parsopercularis R', 'parsorbitalis L', 'parsorbitalis R', '
        parstriangularis L', 'parstriangularis R', 'pericalcarine L', '
        pericalcarine R', 'postcentral L', 'postcentral R', 'posteriorcingulate L'
        , 'posteriorcingulate R', 'precentral L', 'precentral R', 'precuneus L', '
        precuneus R', 'rostralanteriorcingulate L', 'rostralanteriorcingulate R',
        'rostralmiddlefrontal L', 'rostralmiddlefrontal R', 'superiorfrontal L', '
        superiorfrontal R', 'superiorparietal L', 'superiorparietal R', '
        superiortemporal L', 'superiortemporal R', 'supramarginal L', '
        supramarginal R', 'temporalpole L', 'temporalpole R', 'transversetemporal
        L', 'transversetemporal R'}}, ...   % Seed sequence alternates between L
        and R
    'flatten',        1, ...
    'scoutfunc',      'pca', ...  % PCA of values across seed vertices to optimize
         SNR
    'pcaedit',        struct(...
         'Method',         'pca', ...
         'Baseline',       [-0.1, 0], ...
         'DataTimeWindow', [0, 1], ...
         'RemoveDcOffset', 'file'), ...
    'isflip',         1, ...
    'isnorm',         0, ...
    'concatenate',    1, ...
    'save',           1, ...
    'addrowcomment',  1, ...
    'addfilecomment', []);
% Save and display report
ReportFile = bst_report('Save', sFiles);
bst_report('Open', ReportFile);
bst_report('Export', ReportFile, ExportDir);
catch ME
    disp(['Error processing subject ' SUBJECT(iSub).name ': ' getReport(ME)]);
    continue
end
end
gui_brainstorm('EmptyTempFolder');
brainstorm stop

%% CHARACTERIZING AVALANCHES SEPARATELY FOR BOTH HEMISPHERES
GLOBUS_DIR = ('/path/to/dataset');
% Relative directories
OUTPUT = fullfile(GLOBUS_DIR, 'OUTPUT_BROADBAND_pca');
DATABASE = fullfile(OUTPUT, 'DATABASE');
diary(fullfile(OUTPUT, 'MATLAB_log.txt'));
AVALANCHE = fullfile(OUTPUT, 'AVALANCHE_thresholded_3pt5_30');
```

```
fs = 200; % sampling rate
P = 3.5; % z-score threshold, change as required
bin = 6; % avalanche bin size ~30ms at 200Hz sampling, change as required
SUBJECT = dir(fullfile(DATABASE,'PROTOCOL','data','CC*'));
for iSub = 1:size(SUBJECT,1)
display(strcat('NOW PROCESSING>>>',SUBJECT(iSub).name),newline) % Progress
try
AvalancheDir = fullfile(AVALANCHE, SUBJECT(iSub).name);
LHAvalancheMatrix = [];
RHAvalancheMatrix = [];
LHAvalancheFrames = {};
RHAvalancheFrames = {};
LHAvalancheBinSize = [];
RHAvalancheBinSize = [];
LHAvalancheSourceSize = [];
RHAvalancheSourceSize = [];
LHAvalancheEventSize = [];
RHAvalancheEventSize = [];
LHNumEvents = [];
RHNumEvents = [];
LHEventMatrix = [];
RHEventMatrix = [];
LHBP = [];
RHBP = [];
filename = dir(fullfile(DATABASE, 'PROTOCOL', 'data', SUBJECT(iSub).name, '
    @rawtransdef_mf2pt2_rest_raw_resample_bl_detrend_notch_band', 'matrix_scout_*')
    );
load(fullfile(filename.folder, filename.name), 'Value');
r = 1:2:67;
LHValue = Value(r, 1:end);
RHValue = Value(r+1, 1:end);
LHdata = zscore(LHValue');
RHdata = zscore(RHValue');
LHBinary = zeros(size(LHdata));
RHBinary = zeros(size(RHdata));
for ii = 1:size(LHdata,1)
    for jj = 1:size(LHdata,2)
        if abs(LHdata(ii,jj)) >= P
            LHBinary(ii,jj) = 1;
        end
    end
end
for ii = 1:size(RHdata,1)
    for jj = 1:size(RHdata,2)
        if abs(RHdata(ii,jj)) >= P
            RHBinary(ii,jj) = 1;
        end
    end
end
LHwindows = 1:bin:size(LHBinary,1);
RHwindows = 1:bin:size(RHBinary,1);
LHnum_windows = length(LHwindows)-1;
RHnum_windows = length(RHwindows)-1;
% avalanche counter
LHCount = 1;
RHCount = 1;
c = 0; % flag
l = 1; % bin number within an avalanche
for ii = 1:LHnum_windows
    LHtemp = LHBinary(LHwindows(ii) : LHwindows(ii)+bin-1, :);
    LHnum_events = numel(nonzeros(sum(LHtemp,1)));
    if LHnum_events > 0
        LHNumEvents(l) = LHnum_events;
        LHEventMatrix(:,:,l) = LHtemp';
        l = l+1;
        c = 1;
    else
        if c == 1 % avalanche termination
            LHBP(LHCount) = BranchingParameterGM(LHNumEvents);
            LHAvalancheFrames{LHCount} = reshape(LHEventMatrix, [34 bin*(l-1)]);
                    % event patterns across left hemispheric avalanches
            LHAvalancheMatrix(LHCount,:,:) =  TransitionMatrix(reshape(
                LHEventMatrix, [34 bin*(l-1)]));
            LHAvalancheBinSize(LHCount) = l-1;
            LHCount = LHCount+1;
            l = 1;
            c = 0;
            LHNumEvents = [];
            LHEventMatrix = [];
        end
    end
```

```
end
c = 0;
l = 1;
for ii = 1:RHnum_windows
    RHtemp = RHBinary(RHwindows(ii) : RHwindows(ii)+bin-1, :);
    RHnum_events = numel(nonzeros(sum(RHtemp,1)));
    if RHnum_events > 0
        RHNumEvents(l) = RHnum_events;
        RHEventMatrix(:,:,l) = RHtemp';
        l = l+1;
        c = 1;
    else
        if c == 1 % avalanche termination
            RHBP(RHCount) = BranchingParameterGM(RHNumEvents);
            RHAvalancheFrames{RHCount} = reshape(RHEventMatrix, [34 bin*(l-1)]);
                  % event patterns across right hemispheric avalanches
            RHAvalancheMatrix(RHCount,:,:) =  TransitionMatrix(reshape(
                RHEventMatrix, [34 bin*(l-1)]));
            RHAvalancheBinSize(RHCount) = l-1;
            RHCount = RHCount+1;
            l = 1;
            c = 0;
            RHNumEvents = [];
            RHEventMatrix = [];
        end
    end
end
for  i = 1:length(LHAvalancheFrames)
    LHAvalancheSourceSize(i) = sum(any(LHAvalancheFrames{i}, 2));   % LH spatial
        spread
    LHAvalancheEventSize(i) = nnz(LHAvalancheFrames{i});    % LH termporal spread
end
for  i = 1:length(RHAvalancheFrames)
    RHAvalancheSourceSize(i) = sum(any(RHAvalancheFrames{i}, 2));   % RH spatial
        spread
    RHAvalancheEventSize(i) = nnz(RHAvalancheFrames{i});    % RH termporal spread
end
for i = 1:length(LHAvalancheFrames)
    for j = 1:34
        SeedTemp(i,j) = length(nonzeros(LHAvalancheFrames{i}(j,:)));
        LHSeedRecurrence(j) = mean(nonzeros(SeedTemp(:,j)));
    end
end
for i = 1:length(RHAvalancheFrames)
    for j = 1:34
        SeedTemp(i,j) = length(nonzeros(RHAvalancheFrames{i}(j,:)));
        RHSeedRecurrence(j) = mean(nonzeros(SeedTemp(:,j)));
    end
end
LHDirDelayMatrix = zeros(34);
RHDirDelayMatrix = zeros(34);
LHIndirDelayMatrix = zeros(34);
RHIndirDelayMatrix = zeros(34);
LHDirDelayMatrix = (1000/fs)*NonZeroModeHemiThresholded(LHAvalancheMatrix);
RHDirDelayMatrix = (1000/fs)*NonZeroModeHemiThresholded(RHAvalancheMatrix);
LHIndirDelayMatrix = (1000/fs)*NonZeroIndirMeanHemiThresholded(LHAvalancheMatrix);
RHIndirDelayMatrix = (1000/fs)*NonZeroIndirMeanHemiThresholded(RHAvalancheMatrix);
LHBranchingParameter = geomean(nonzeros(LHBP));
RHBranchingParameter = geomean(nonzeros(RHBP));
LHNumberOfAvalanches = LHCount-1;
RHNumberOfAvalanches = RHCount-1;
save(AvalancheDir,'LHBranchingParameter','RHBranchingParameter','LHSeedRecurrence'
    ,'RHSeedRecurrence','LHDirDelayMatrix','RHDirDelayMatrix','LHIndirDelayMatrix'
    ,'RHIndirDelayMatrix','LHNumberOfAvalanches','RHNumberOfAvalanches','
    LHAvalancheFrames','RHAvalancheFrames','LHAvalancheBinSize','
    RHAvalancheBinSize','LHAvalancheSourceSize','RHAvalancheSourceSize','
    LHAvalancheEventSize','RHAvalancheEventSize');
catch ME
    disp(['Error processing subject ' SUBJECT(iSub).name ': ' getReport(ME)]);
    continue
end
end
run_time = toc %#ok<NOPTS>
diary off;

%% PREREQUISITE FUNCTIONS
% Branching Parameter estimation
function S = BranchingParameterGM(x)
S = 0;
if length(x) >= 2
    for ii = 1:numel(x)-1
        y(ii) = (x(ii+1)/x(ii));
```

```
    end
    S = geomean(y);
end
end
% Estimate inter-regional delays for every avalanche
function x = TransitionMatrix(y) % y is avalanche (roi_x_t)
num_rois = size(y,1);
act_rois = find(sum(y,2)); % activated rois
act_times = zeros(numel(act_rois),1); % time of first activation

for ii= 1:numel(act_rois)
    act_times(ii) = find(y(act_rois(ii),:),1,'first');
end
[sorted_act_times, idx] = sort(act_times); % sort activation times in ascending order
sorted_act_rois = act_rois(idx);% sort rois based on activation times
P = numel(sorted_act_rois);
x = zeros(num_rois);
for ii = 1:P
    for jj = ii:P
        x(sorted_act_rois(ii),sorted_act_rois(jj)) =  sorted_act_times(jj) - sorted_act_times(ii);
    end
end
end
% Small-band delay across avalanches
function x = NonZeroModeHemiThresholded(TM)
x = zeros(34);
for ii = 1:34
    for jj = 1:34
        temp = nonzeros(TM(:,ii,jj));   % zeros omitted
        thresholded = temp(temp <= 70); % hard-cut at 350ms
        if ~isempty(thresholded)
            x(ii,jj) = mode(thresholded);   % mode of values
        end
    end
end
end
% Large-band delay across avalanches
function x = NonZeroIndirMeanHemiThresholded(TM)
x = zeros(34);
for ii = 1:34
    for jj = 1:34
        temp = nonzeros(TM(:,ii,jj));   % zeros omitted
        thresholded = temp(temp <= 70); % hard-cut at 350ms
        if ~isempty(thresholded)
            mode_val = mode(thresholded);
            indir = thresholded(thresholded > mode_val);
            x(ii,jj) = (sum(indir))./(numel(indir));    % mean of values larger than mode
        end
    end
end
end

%% ENVELOPE LATERALITY
% Set path to the Globus directory with input data
GLOBUS_DIR = ('/path/to/data');
% Relative directories
OUTPUT = fullfile(GLOBUS_DIR, 'OUTPUT_BROADBAND_pca');
DATABASE = fullfile(OUTPUT, 'DATABASE');
diary(fullfile(OUTPUT, 'MATLAB_log.txt'));
AMP_LI = fullfile(OUTPUT, 'AMPLITUDE_LI');
SUBJECT = dir(fullfile(DATABASE,'PROTOCOL','data','CC_*'));
for iSub = 1:size(SUBJECT,1)
display(strcat('NOW PROCESSING>>>',SUBJECT(iSub).name),newline) % Progress
try
AmpLIDir = fullfile(AMP_LI, SUBJECT(iSub).name);
filename = dir(fullfile(DATABASE, 'PROTOCOL', 'data', SUBJECT(iSub).name, '@rawtransdef_mf2pt2_rest_raw_resample_bl_detrend_notch_band', 'matrix_scout_*') );
load(fullfile(filename.folder, filename.name), 'Value');
r = 1:2:67;
LHValue = abs(Value(r, 1:end));
RHValue = abs(Value(r+1, 1:end));
LHEnv = abs(hilbert(LHValue));
RHEnv = abs(hilbert(RHValue));
LHMeanEnv = mean(LHEnv, 2);
RHMeanEnv = mean(RHEnv, 2);
EnvLI = (RHMeanEnv - LHMeanEnv) ./ (RHMeanEnv + LHMeanEnv);
LHNormEnv = LHEnv ./ max(LHEnv, [], 2);
```

```
RHNormEnv = RHEnv ./ max(RHEnv, [], 2);
LHMeanNormEnv = mean(LHNormEnv, 2);
RHMeanNormEnv = mean(RHNormEnv, 2);
NormEnvLI = (RHMeanNormEnv - LHMeanNormEnv) ./ (RHMeanNormEnv + LHMeanNormEnv);
save(AmpLIDir, 'LHMeanEnv', 'RHMeanEnv', 'EnvLI', 'LHMeanNormEnv', 'RHMeanNormEnv'
    , 'NormEnvLI');
catch ME
    disp(['Error processing subject ' SUBJECT(iSub).name ': ' getReport(ME)]);
    continue
end
end
```

C.2 MATLAB Script for Statistical Analysis and Figures

```
% Author: Atharva Parolekar
% Email: atharva[dot]parolekar[at]gmail[dot]com
%% CHAPTER 2 RESULTS: AVALANCHE PROPERTIES
% Analysis across all participants, n = 449
% Some results from chapter 2 were generated with pgfplots in LaTeX; not included
    here
%% IMPORT & INITIALIZE
AV_DIR = fullfile('path','to','avalanches');
Av_matfiles = dir(fullfile(AV_DIR, 'CC*.mat'));
for i = 1:length(Av_matfiles)
    SubjAv = load(fullfile(Av_matfiles(i).folder, Av_matfiles(i).name));
    LHBins = SubjAv.LHAvalancheBinSize;
    RHBins = SubjAv.RHAvalancheBinSize;
    Bins{i, :} = [LHBins, RHBins];
    LHSources = SubjAv.LHAvalancheSourceSize;
    RHSources = SubjAv.RHAvalancheSourceSize;
    Sources{i, :} = [LHSources, RHSources];
    LHEvents = SubjAv.LHAvalancheEventSize;
    RHEvents = SubjAv.RHAvalancheEventSize;
    Events{i, :} = [LHEvents, RHEvents];
    BP(i, :) = [SubjAv.LHBranchingParameter, SubjAv.RHBranchingParameter];
    LHRecurrence = SubjAv.LHSeedRecurrence;
    RHRecurrence = SubjAv.RHSeedRecurrence;
    Recurrence(i, :) = [LHRecurrence, RHRecurrence];
    LHAvalanches = SubjAv.LHNumberOfAvalanches;
    RHAvalanches = SubjAv.RHNumberOfAvalanches;
    Avalanches(i, :) = [LHAvalanches, RHAvalanches];
end
BinsCollated = horzcat(Bins{:});
SourcesCollated = horzcat(Sources{:});
EventsCollated = horzcat(Events{:});
BPCollated = horzcat(BP(:));
RecurrenceCollated = horzcat(Recurrence(:));
NumAvalanches = horzcat(Avalanches(:));
figure;
histogram(BinsCollated, 'BinEdges', [0,1:164], 'FaceColor', 'k'); xlabel('Number
    of Bins'); title('Temporal Spread of Avalanches');
text(0.6, 0.85, sprintf('Mean Value of Bins: %.2f', mean(BinsCollated)), 'Units',
    'normalized');
figure;
histogram(SourcesCollated, 'FaceColor', 'k'); xlabel('Number of Sources'); title('
    Spatial Spread of Avalanches');
text(0.6, 0.85, sprintf('Mean Value of Sources: %.2f', mean(SourcesCollated)), '
    Units', 'normalized');
figure;
histogram(EventsCollated, 'FaceColor', 'k'); xlabel('Number of Events'); title('
    Spatiotemporal Spread of Avalanches');
text(0.6, 0.85, sprintf('Mean Value of Events: %.2f', mean(EventsCollated)), '
    Units', 'normalized');
figure;
histogram(BPCollated, 'FaceColor', 'k'); xline(1, 'color', 'r', 'LineWidth', 2.5);
     xlabel('Branching Parameter'); title('Criticality of Avalanches');
text(0.1, 0.85, sprintf('Threshold: 3.5\nBin Width: 30ms\nMean BP: %.2f', mean(
    BPCollated)), 'Units', 'normalized');
figure;
histogram(RecurrenceCollated, 'FaceColor', 'k'); xlabel('Mean Recurrence'); title(
    'Collated Recurrability of Regions in Avalanches');
text(0.6, 0.85, sprintf('Mean Recurrence: %.2f', mean(RecurrenceCollated)), 'Units
    ', 'normalized');
```

```
figure;
histogram(NumAvalanches, 'FaceColor', 'k'); xlabel('Number of Avalanches'); title('Distribution of Avalanches Across Participants')
text(0.55, 0.85, sprintf('Threshold: 3.5\nBin Width: 30ms\nMean Avalanche Number: %.2f', mean(NumAvalanches)), 'Units', 'normalized');
%% POWER LAW
% Bins
edges = logspace(log10(min(BinsCollated)), log10(max(BinsCollated)), 50);
[countsBins, binsBins] = histcounts(BinsCollated, edges);
countsBins = countsBins/sum(countsBins);
log_bins = log10(binsBins(1:end-1));
log_probs = log10(countsBins);
valid_idx = ~isinf(log_probs) & ~isnan(log_probs);
log_bins_fit = log_bins(valid_idx);
log_probs_fit = log_probs(valid_idx);
coeffs = polyfit(log_bins_fit, log_probs_fit, 1);
alpha = -coeffs(1);
k = 10^(coeffs(2));
fitted_probs = 10.^(polyval(coeffs, log_bins_fit));
meanBins = mean(BinsCollated);
poisson_sizes = 1:max(floor(BinsCollated));
poisson_probs = poisspdf(poisson_sizes, meanBins);
poisson_probs = poisson_probs/sum(poisson_probs);
figure;
loglog(binsBins(valid_idx), countsBins(valid_idx), 'ok-', 'LineWidth', 2.5)
hold on
loglog(10.^log_bins_fit, fitted_probs, 'r:', 'LineWidth', 2);
hold on
loglog(poisson_sizes, poisson_probs, 'b-', 'LineWidth', 2.5)
ylim([1e-7 1e0]);
xlabel('Number of Bins')
ylabel('Probability')
legend({'Empirical data', 'Linear Fit', 'Poisson Surrogate'}, 'Location', 'southwest')
text(0.8, 0.85, sprintf('alpha: %.2f\nk: %.2f', alpha, k), 'Units', 'normalized');
title('Power Law Distribution of Avalanche Bins')
% Sources
edges = logspace(log10(min(SourcesCollated)), log10(max(SourcesCollated)), 50);
[countsSources, binsSources] = histcounts(SourcesCollated, edges);
countsSources = countsSources/sum(countsSources);
log_bins = log10(binsSources(1:end-1));
log_probs = log10(countsSources);
valid_idx = ~isinf(log_probs) & ~isnan(log_probs);
log_bins_fit = log_bins(valid_idx);
log_probs_fit = log_probs(valid_idx);
coeffs = polyfit(log_bins_fit, log_probs_fit, 1);
alpha = -coeffs(1);
k = 10^(coeffs(2));
fitted_probs = 10.^(polyval(coeffs, log_bins_fit));
meanSources = mean(SourcesCollated);
poisson_sizes = 1:max(floor(SourcesCollated));
poisson_probs = poisspdf(poisson_sizes, meanSources);
poisson_probs = poisson_probs/sum(poisson_probs);
figure;
loglog(binsSources(valid_idx), countsSources(valid_idx), 'ok-', 'LineWidth', 2.5)
hold on
loglog(10.^log_bins_fit, fitted_probs, 'r:', 'LineWidth', 2);
hold on
loglog(poisson_sizes, poisson_probs, 'b-', 'LineWidth', 2.5)
ylim([1e-4 1e0]);
xlabel('Number of Sources')
ylabel('Probability')
legend({'Empirical data', 'Linear Fit', 'Poisson Surrogate'}, 'Location', 'southwest')
text(0.8, 0.85, sprintf('alpha: %.2f\nk: %.2f', alpha, k), 'Units', 'normalized');
title('Power Law Distribution of Avalanche Sources')
% Events
edges = logspace(log10(min(EventsCollated)), log10(max(EventsCollated)), 50);
[countsEvents, binsEvents] = histcounts(EventsCollated, edges);
countsEvents = countsEvents/sum(countsEvents);
log_bins = log10(binsEvents(1:end-1));
log_probs = log10(countsEvents);
valid_idx = ~isinf(log_probs) & ~isnan(log_probs);
log_bins_fit = log_bins(valid_idx);
log_probs_fit = log_probs(valid_idx);
coeffs = polyfit(log_bins_fit, log_probs_fit, 1);
alpha = -coeffs(1);
k = 10^(coeffs(2));
fitted_probs = 10.^(polyval(coeffs, log_bins_fit));
```

```
meanEvents = mean(EventsCollated);
poisson_sizes = 1:max(floor(EventsCollated));
poisson_probs = poisspdf(poisson_sizes, meanEvents);
poisson_probs = poisson_probs/sum(poisson_probs);
figure;
loglog(binsEvents(valid_idx), countsEvents(valid_idx), 'ok-', 'LineWidth', 2.5)
hold on
loglog(10.^log_bins_fit, fitted_probs, 'r:', 'LineWidth', 2);
hold on
loglog(poisson_sizes, poisson_probs, 'b-', 'LineWidth', 2.5)
ylim([1e-7 1e0]);
xlabel('Number of Events')
ylabel('Probability')
legend({'Empirical data', 'Linear Fit', 'Poisson Surrogate'}, 'Location', '
    southwest')
text(0.8, 0.85, sprintf('alpha: %.2f\nk: %.2f', alpha, k), 'Units', 'normalized');
title('Power Law Distribution of Avalanche Events')

%% CHAPTER 3 RESULTS: RELATING DELAYS AND TRACT PROPERTIES
% Analysis across all participants, n = 449
% This script corresponds to small-band delays
% For large-band delays, LH.../RHIndirDelayMatrix used and all labels modified
    accordingly
%% IMPORT & INITIALIZE
DELAY_DIR = fullfile('C:','Atharva','Data','Cam-CAN_449','AVALANCHE','BROAD-
    BAND_pca_split','thresh_3pt5_30','all');
Delay_matfiles = dir(fullfile(DELAY_DIR, 'CC*.mat'));
WIDTH_DIR = fullfile('c:','Atharva','Data','Cam-CAN_449','WIDTH','all');
Width_csvfiles = dir(fullfile(WIDTH_DIR,'CC*.csv'));
LENGTH_DIR = fullfile('c:','Atharva','Data','Cam-CAN_449','LENGTH','all');
Length_csvfiles = dir(fullfile(LENGTH_DIR,'CC*.csv'));
Delay_group = [];
Length_group = [];
Width_group = [];
for i = 1:length(Delay_matfiles)
    Delay_data = load(fullfile(Delay_matfiles(i).folder, Delay_matfiles(i).name));
    Delay_intraLH = Delay_data.LHDirDelayMatrix;
    Delay_intraRH = Delay_data.RHDirDelayMatrix;
    Delay_group(:, :, i) = [Delay_intraLH, Delay_intraRH];

    Width_temp = readmatrix(fullfile(Width_csvfiles(i).folder, Width_csvfiles(i).
        name));
    Width_intraLH = Width_temp(1:2:67, 1:2:67);
    Width_intraRH = Width_temp(2:2:68, 2:2:68);
    Width_group(:, :, i) = [Width_intraLH, Width_intraRH];

    Length_temp = readmatrix(fullfile(Length_csvfiles(i).folder, Length_csvfiles(i
        ).name));
    Length_intraLH = Length_temp(1:2:67, 1:2:67);
    Length_intraRH = Length_temp(2:2:68, 2:2:68);
    Length_group(:, :, i) = [Length_intraLH, Length_intraRH];
end
Delay_group(isnan(Delay_group)) = 0;
% Pooled valid values across subjects for each ROI pair
Delay_flat = reshape(Delay_group, [], length(Delay_matfiles));
Width_flat = reshape(Width_group, [], length(Delay_matfiles));
Length_flat = reshape(Length_group, [], length(Delay_matfiles));
Delay_extracted = cell(2244, 1);
Width_extracted = cell(2244, 1);
Length_extracted = cell(2244, 1);
Velocity = cell(2244, 1);
n = 1;
for row = 1:2312
    valid_Delay = find(Delay_flat(row, :) ~= 0 & ~isnan(Delay_flat(row, :)));
    valid_Width = find(Width_flat(row, :) ~= 0 & ~isnan(Width_flat(row, :)));
    valid_Length = find(Length_flat(row, :) ~= 0 & ~isnan(Length_flat(row, :)));
    common_idx = intersect(intersect(valid_Length, valid_Width), valid_Delay);
    if isempty(Delay_flat(row, common_idx))
        continue
    else
        Delay_extracted{n} = Delay_flat(row, common_idx);
        Width_extracted{n} = Width_flat(row, common_idx);
        Length_extracted{n} = Length_flat(row, common_idx);
        Velocity{n} = Length_extracted{n} ./ Delay_extracted{n};
        n = n+1;
    end
end
CollatedDelay = horzcat(Delay_extracted{:});
CollatedWidth = horzcat(Width_extracted{:});
CollatedLength = horzcat(Length_extracted{:});
```

```
CollatedVelocity = horzcat(Velocity{:});
figure; histogram(CollatedDelay(:), 'BinWidth', 5, 'FaceColor', [0.3010, 0.7450, 0.9330]), xlabel('Delay (ms)'); title('Distribution of Pooled Intrahemispheric Small-Band Functional Delays')
figure; histogram(CollatedVelocity(:), 'FaceColor', [0.4660, 0.6740, 0.1880]), xlabel('Velocity (m/s)'); title('Distribution of Pooled Intrahemispheric Small-Band Velocities')
figure;
subplot(1,3,1); histogram(CollatedLength(:), 'BinWidth', 5, 'FaceColor', [0.9290, 0.6940, 0.1250]), xlabel('Length (mm)'); title('Lengths')
subplot(1,3,2); histogram(CollatedWidth(:), 'FaceColor', [0.8500, 0.3250, 0.0980]), xlabel('Width (A.U.)'); title('Widths')
subplot(1,3,3); histogram(log(CollatedWidth(:) + 0.00001), 'FaceColor', [0.8500, 0.3250, 0.0980]), xlabel('Ln Width (A.U.)'); title('Log-Scaled Widths')
sgtitle('Distributions of Pooled Intrahemispheric Tract Properties')
% Averaged valid values across subjects for each ROI pair
MeanDelay = NonZeroMeanIntra(Delay_group);
MeanLength = NonZeroMeanIntra(Length_group);
MeanWidth = NonZeroMeanIntra(Width_group);
MeanVelocity = MeanLength ./ MeanDelay;
MeanVelocity(isnan(MeanVelocity)) = 0;
figure; histogram(MeanDelay(:), 'BinWidth', 5, 'FaceColor', [0.3010, 0.7450, 0.9330]), xlabel('Delay (ms)'); title('Distribution of Averaged Intrahemispheric Small-Band Functional Delays')
figure; histogram(MeanVelocity(:), 'FaceColor', [0.4660, 0.6740, 0.1880]), xlabel('Velocity (m/s)'); title('Distribution of Averaged Intrahemispheric Small-Band Velocities')
figure;
subplot(1,3,1); histogram(MeanLength(:), 'BinWidth', 5, 'FaceColor', [0.9290, 0.6940, 0.1250]), xlabel('Length (mm)'); title('Lengths')
subplot(1,3,2); histogram(MeanWidth(:), 'FaceColor', [0.8500, 0.3250, 0.0980]), xlabel('Width (A.U.)'); title('Widths')
subplot(1,3,3); histogram(log(MeanWidth(:) + 0.00001), 'FaceColor', [0.8500, 0.3250, 0.0980]), xlabel('Ln Width (A.U.)'); title('Log-Scaled Widths')
sgtitle('Distributions of Averaged Intrahemispheric Tract Properties')
% Rearranging the matrices for aesthetic purposes *sparkles*
zero_col = zeros(34, 1);
NewMeanDelay = MeanDelay(end:-1:1, :); NewMeanDelay = [NewMeanDelay(:, 1:34), zero_col, NewMeanDelay(:, 35:68)];
NewMeanWidth = MeanWidth(end:-1:1, :); NewMeanWidth = [NewMeanWidth(:, 1:34), zero_col, NewMeanWidth(:, 35:68)];
NewMeanLength = MeanLength(end:-1:1, :); NewMeanLength = [NewMeanLength(:, 1:34), zero_col, NewMeanLength(:, 35:68)];
NewMeanVelocity = MeanVelocity(end:-1:1, :); NewMeanVelocity = [NewMeanVelocity(:, 1:34), zero_col, NewMeanVelocity(:, 35:68)];
figure; imagesc(NewMeanDelay); title('Population Averaged Small-Band Delay Matrix'); xlabel('ROI'); ylabel('ROI'); colormap(jet); cb = colorbar; cb.Label.String = 'milliseconds';
figure; imagesc(NewMeanVelocity); title('Population Averaged Velocity Matrix'); xlabel('ROI'); ylabel('ROI'); colormap(jet); cb = colorbar; cb.Label.String = 'millimeters / milliseconds';
figure; imagesc(log(NewMeanWidth) + 0.00001); title('Log-Scaled Population Averaged Width Matrix'); xlabel('ROI'); ylabel('ROI'); colormap(jet); cb = colorbar; cb.Label.String = 'abritrary units';
figure; imagesc(NewMeanLength); title('Population Averaged Length Matrix'); xlabel('ROI'); ylabel('ROI'); colormap(jet); cb = colorbar; cb.Label.String = 'millimeters';
%% POOLED RELATIONS
[rhos_ld, pvals_ld] = corr(CollatedLength', CollatedDelay', 'Type', 'Spearman');
[rhos_wd, pvals_wd] = corr(CollatedWidth', CollatedDelay', 'Type', 'Spearman');
[rhos_wl, pvals_wl] = corr(CollatedWidth', CollatedLength', 'Type', 'Spearman');
[rhop_ld, pvalp_ld] = corr(CollatedLength', CollatedDelay', 'Type', 'Pearson');
[rhop_wd, pvalp_wd] = corr(log(CollatedWidth + 0.00001)', CollatedDelay', 'Type', 'Pearson');
[rhop_wl, pvalp_wl] = corr(CollatedWidth', CollatedLength', 'Type', 'Pearson');
figure; scatter(CollatedLength, CollatedDelay, '.', 'k'); xlabel('Length (mm)'); ylabel('Delay (ms)'); text(0.8, 0.85, sprintf('Spearman rho: %.2f\npval: %.2e\n\nPearson rho: %.2f\npval: %.2e', rhos_ld, pvals_ld, rhop_ld, pvalp_ld), 'Units', 'normalized'); title('Length vs. Small-Band Delay (Pooled)')
figure; scatter(log(CollatedWidth + 0.00001), CollatedDelay, '.', 'k'); xlabel('Ln Width (A.U.)'); ylabel('Delay (ms)'); text(0.8, 0.85, sprintf('Spearman rho: %.2f\npval: %.2e\n\nPearson rho: %.2f\npval: %.2e', rhos_wd, pvals_wd, rhop_wd, pvalp_wd), 'Units', 'normalized'); title('Width vs. Small-Band Delay (Pooled)')
figure; scatter(log(CollatedWidth + 0.00001), CollatedLength, '.', 'k'); xlabel('Ln Width (A.U.)'); ylabel('Length (mm)'); text(0.8, 0.85, sprintf('Spearman rho: %.2f\npval: %.2e\n\nPearson rho: %.2f\npval: %.2e', rhos_wl, pvals_wl, rhop_wl, pvalp_wl), 'Units', 'normalized'); title('Width vs. Length (Pooled)')
jitter = -2.5 + (5) * rand(size(CollatedDelay));
```

```
CollatedDelayJitt = CollatedDelay + jitter;
figure; scatter(CollatedLength, CollatedDelayJitt, '.', 'k'); xlabel('Length (mm)'); ylabel('Delay (ms)'); text(0.8, 0.85, sprintf('Spearman rho: %.2f\npval: %.2e\n\nPearson rho: %.2f\npval: %.2e', rhos_ld, pvals_ld, rhop_ld, pvalp_ld), 'Units', 'normalized'); title('Length vs. Small-Band Delay (Pooled)')
figure; scatter(log(CollatedWidth + 0.00001), CollatedDelayJitt, '.', 'k'); xlabel('Ln Width (A.U.)'); ylabel('Delay (ms)'); text(0.8, 0.85, sprintf('Spearman rho: %.2f\npval: %.2e\n\nPearson rho: %.2f\npval: %.2e', rhos_wd, pvals_wd, rhop_wd, pvalp_wd), 'Units', 'normalized'); title('Width vs. Small-Band Delay (Pooled)')
% mdl_pooled = fitlm([CollatedWidth(:), CollatedLength(:)], CollatedDelay(:));  % prediction capability plummets without robust regression's outlier suppresion
mdl_pooled_robust = fitlm([CollatedWidth(:), CollatedLength(:)], CollatedDelay(:), 'RobustOpts', 'on');
% mdl_pooled_int = fitlm([CollatedWidth(:), CollatedLength(:), (CollatedWidth(:) .* CollatedLength(:))], CollatedDelay(:));
% mdl_pooled_int_robust = fitlm([CollatedWidth(:), CollatedLength(:), (CollatedWidth(:) .* CollatedLength(:))], CollatedDelay(:), 'RobustOpts', 'on');
% Adding interaction term does not improve the model performance significantly
figure;
subplot(2, 1, 1)
h = plotAdded(mdl_pooled_robust, 'x1');
set(h(1), 'Marker', '.', 'MarkerEdgeColor', 'k')
xlabel('Adjusted Width');
ylabel('Adjusted Delay');
title('Added variable plot for Width')
subplot(2, 1, 2)
h = plotAdded(mdl_pooled_robust, 'x2');
set(h(1), 'Marker', '.', 'MarkerEdgeColor', 'k')
xlabel('Adjusted Length');
ylabel('Adjusted Delay');
title('Added variable plot for Length')
sgtitle('Population Pooled: Partial Regression Plots')
y_pred = predict(mdl_pooled_robust, [CollatedWidth(:), CollatedLength(:)]);
figure;
scatter(CollatedDelay(:), y_pred, 36, [0.3010, 0.7450, 0.9330], 'filled');
xlabel('Actual Delays'); ylabel('Predicted Delays');
rectangle('Position', [0, -10, 45, 45], 'LineWidth', 1.2);
title('Population Pooled: Actual vs Predicted Values');
hold on;
refline(1, 0);
inset_axis = axes('Position', [0.6 0.3 0.3 0.3]);
hold(inset_axis, 'on');
box (inset_axis, 'on');
scatter(inset_axis, CollatedDelay(:), y_pred, 36, [0.3010, 0.7450, 0.9330], 'filled');
xlim(inset_axis, [0 47.5]); ylim(inset_axis, [-10 35]);
xref = [0 42.5]; yref = xref;
plot(inset_axis, xref, yref, '-', 'Color', [1 0 0]);
title('Zoomed Inset');
%% MEAN RELATIONS
valid_mean_idx = ~isnan(MeanDelay) & ~isnan(MeanLength) & ~isnan(MeanWidth);
[rhos_mean_ld, pvals_mean_ld] = corr(MeanLength(valid_mean_idx), MeanDelay(valid_mean_idx), 'Type', 'Spearman');
[rhos_mean_wd, pvals_mean_wd] = corr(MeanWidth(valid_mean_idx), MeanDelay(valid_mean_idx), 'Type', 'Spearman');
[rhos_mean_wl, pvals_mean_wl] = corr(MeanWidth(valid_mean_idx), MeanLength(valid_mean_idx), 'Type', 'Spearman');
[rhop_mean_ld, pvalp_mean_ld] = corr(MeanLength(valid_mean_idx), MeanDelay(valid_mean_idx), 'Type', 'Pearson');
[rhop_mean_wd, pvalp_mean_wd] = corr(log(MeanWidth(valid_mean_idx) + 0.00001), MeanDelay(valid_mean_idx), 'Type', 'Pearson');
[rhop_mean_wl, pvalp_mean_wl] = corr(log(MeanWidth(valid_mean_idx) + 0.00001), MeanLength(valid_mean_idx), 'Type', 'Pearson');
figure; scatter(MeanLength(:), MeanDelay(:), 'o', 'filled', 'k'); xlabel('Length (mm)'); ylabel('Delay (ms)'); text(0.8, 0.85, sprintf('Spearman rho: %.2f\npval: %.2e\n\nPearson rho: %.2f\npval: %.2e', rhos_mean_ld, pvals_mean_ld, rhop_mean_ld, pvalp_mean_ld), 'Units', 'normalized'); title('Length vs. Small-Band Delay (Averaged)')
figure; scatter(log(MeanWidth(:) + 0.00001), MeanDelay(:), 'o', 'filled', 'k'); xlabel('Ln Width (A.U.)'); ylabel('Delay (ms)'); text(0.8, 0.85, sprintf('Spearman rho: %.2f\npval: %.2e\n\nPearson rho: %.2f\npval: %.2e', rhos_mean_wd, pvals_mean_wd, rhop_mean_wd, pvalp_mean_wd), 'Units', 'normalized'); title('Width vs. Small-Band Delay (Averaged)')
figure; scatter(log(MeanWidth(:) + 0.00001), MeanLength(:), 'o', 'filled', 'k'); xlabel('Ln Width (A.U.)'); ylabel('Length (mm)'); text(0.8, 0.85, sprintf('Spearman rho: %.2f\npval: %.2e\n\nPearson rho: %.2f\npval: %.2e', rhos_mean_wl, pvals_mean_wl, rhop_mean_wl, pvalp_mean_wl), 'Units', 'normalized'); title('
```

```
    Width vs. Length (Averaged)')
mdl_mean = fitlm([MeanWidth(:), MeanLength(:)], MeanDelay(:));
% mdl_mean_robust = fitlm([MeanWidth(:), MeanLength(:)], MeanDelay(:), 'RobustOpts
    ', 'on'); % robust regression not necessary for popuilation averaged data
% mdl_mean_int = fitlm([MeanWidth(:), MeanLength(:), (MeanWidth(:) .* MeanLength
    (:))], MeanDelay(:));
% mdl_mean_int_robust = fitlm([MeanWidth(:), MeanLength(:), (MeanWidth(:) .*
    MeanLength(:))], MeanDelay(:), 'RobustOpts', 'on');
% Adding interaction term does not improve the model performance significantly
figure;
subplot(2, 1, 1)
h = plotAdded(mdl_mean, 'x1');
set(h(1), 'Marker', '.', 'MarkerEdgeColor', 'k')
xlabel('Adjusted Width');
ylabel('Adjusted Delay');
title('Added variable plot for Width')
subplot(2, 1, 2)
h = plotAdded(mdl_mean, 'x2');
set(h(1), 'Marker', '.', 'MarkerEdgeColor', 'k')
xlabel('Adjusted Length');
ylabel('Adjusted Delay');
title('Added variable plot for Length')
sgtitle('Population Averaged: Partial Regression Plots')
y_pred = predict(mdl_mean, [MeanWidth(:), MeanLength(:)]);
figure;
scatter(MeanDelay(:), y_pred, 36, [0.3010, 0.7450, 0.9330], 'filled');
xlabel('Actual Delays');
ylabel('Predicted Delays');
title('Population Averaged: Actual vs Predicted Values');
refline(1, 0);
%% REPRESENTATIONAL SIMILARITY ANALYSIS: KS DISTANCE
RDM_delay = zeros(numel(Delay_extracted),numel(Delay_extracted));
for i = 1:numel(Delay_extracted)
    vi = Delay_extracted{i};
    for j = 1:numel(Delay_extracted)
        vj = Delay_extracted{j};
        [~,~,d_z] = kstest2(vi, vj);
        RDM_delay(i,j) = d_z;
        RDM_delay(j,i) = d_z;
    end
end
figure; imagesc(RDM_delay); title('Small-Band Delay RDM'); xlabel('ROI Pair');
    ylabel('ROI Pair'); axis equal tight; clim([0 1]); colormap(jet); cb =
    colorbar; cb.Label.String = 'KS Distance';
RDM_length = zeros(numel(Length_extracted),numel(Length_extracted));
for i = 1:numel(Length_extracted)
    vi = Length_extracted{i};
    for j = 1:numel(Length_extracted)
        vj = Length_extracted{j};
        [~,~,d] = kstest2(vi, vj);
        RDM_length(i,j) = d;
        RDM_length(j,i) = d;
    end
end
figure; imagesc(RDM_length); title('Length RDM'); xlabel('ROI Pair'); ylabel('ROI
    Pair'); axis equal tight; clim([0 1]); colormap(jet); cb = colorbar; cb.Label.
    String = 'KS Distance';
RDM_width = zeros(numel(Width_extracted),numel(Width_extracted));
for i = 1:numel(Width_extracted)
    vi = Width_extracted{i};
    for j = 1:numel(Width_extracted)
        vj = Width_extracted{j};
        [~,~,d] = kstest2(vi, vj);
        RDM_width(i,j) = d;
        RDM_width(j,i) = d;
    end
end
figure; imagesc(RDM_width); title('Width RDM'); xlabel('ROI Pair'); ylabel('ROI
    Pair'); axis equal tight; clim([0 1]); colormap(jet); cb = colorbar; cb.Label.
    String = 'KS Distance';
DelayVec = squareform(RDM_delay);
LengthVec = squareform(RDM_length);
WidthVec = squareform(RDM_width);
[rho_RSA_ksd_ld, pval_RSA_ksd_ld] = corr(LengthVec(:), DelayVec(:), 'Type', '
    Spearman');
[rho_RSA_ksd_wd, pval_RSA_ksd_wd] = corr(WidthVec(:), DelayVec(:), 'Type', '
    Spearman');
figure; scatter(LengthVec, DelayVec, '.', 'k'); xlabel('Length RDM'); ylabel('
    Delay RDM'); text(0.1, 0.9, sprintf('Spearman rho: %.2f\npval: %.2e',
```

```
    rho_RSA_ksd_ld, pval_RSA_ksd_ld), 'Units', 'normalized'); title('
    Representational Similarity: Length vs. Small-Band Delay')
figure; scatter(WidthVec, DelayVec, '.', 'k'); xlabel('Width RDM'); ylabel('Delay
    RDM'); text(0.1, 0.9, sprintf('Spearman rho: %.2f\npval: %.2e', rho_RSA_ksd_wd
    , pval_RSA_ksd_wd), 'Units', 'normalized'); title('Representational Similarity
    : Width vs. Small-Band Delay')

%% CHAPTER 4 RESULTS: HEMISPHERIC ASYMMETRY OF DELAYS AND TRACTS, INTERRELATIONS
    OF TRACT, DELAY, and FUNCTIONAL LATERALITY
% Analysis across right-handed, young, male participants, n = 45
% This script corresponds to direct delays
% For indirect delays LH.../RHIndirDelayMatrix used and all labels modified
    accordingly
%% COLOR MAP
colors = [
    0.1000, 0.1000, 0.5000; % 1 Navy - Male
    0.9686, 0.5059, 0.7490; % 2 Pink - Female
    0.6000, 0.3000, 0.0000; % 3 Brown - L Hand
    0.0000, 0.6000, 0.6000; % 4 Teal - R Hand
    0.4940, 0.1840, 0.5560; % 5 Muted Purple - L Hemi
    0.9290, 0.6940, 0.1250; % 6 Soft Yellow - R Hemi / Length
    0.3010, 0.7450, 0.9330; % 7 Blue - Delay
    0.8500, 0.3250, 0.0980; % 8 Orange - Width
    0.4660, 0.6740, 0.1880; % 9 Soft Green - Velocity
    ];
%% IMPORT & INITIALIZE
DELAY_DIR = fullfile('C:','Atharva','Data','Cam-CAN_449','AVALANCHE','BROAD-
    BAND_pca_split','thresh_3pt5_30','control');
Delay_matfiles = dir(fullfile(DELAY_DIR, 'CC*.mat'));
SC_DIR = fullfile('c:','Atharva','Data','Cam-CAN_449','WIDTH','control');
SC_csvfiles = dir(fullfile(SC_DIR,'CC*.csv'));
LENGTH_DIR = fullfile('c:','Atharva','Data','Cam-CAN_449','LENGTH','control');
Length_csvfiles = dir(fullfile(LENGTH_DIR,'CC*.csv'));
LATERALITY_DIR = fullfile('C:','Atharva','Data','Cam-CAN_449','
    FUNCTIONAL_LATERALITY','bb_only','control');
Laterality_matfiles = dir(fullfile(LATERALITY_DIR, 'CC*.mat'));
LH_Delay_group = [];
RH_Delay_group = [];
LH_Length_group = [];
RH_Length_group = [];
LH_SC_group = [];
RH_SC_group = [];
Laterality_group = [];
for i = 1:length(Delay_matfiles)
    Delay_data = load(fullfile(Delay_matfiles(i).folder, Delay_matfiles(i).name));
    LH_Delay_group(:, :, i) = Delay_data.LHDirDelayMatrix;
    RH_Delay_group(:, :, i) = Delay_data.RHDirDelayMatrix;
    SC_temp = readmatrix(fullfile(SC_csvfiles(i).folder, SC_csvfiles(i).name));
    LH_SC_group(:, :, i) = SC_temp(1:2:67, 1:2:67);
    RH_SC_group(:, :, i) = SC_temp(2:2:68, 2:2:68);
    Length_temp = readmatrix(fullfile(Length_csvfiles(i).folder, Length_csvfiles(i
        ).name));
    LH_Length_group(:, :, i) = Length_temp(1:2:67, 1:2:67);
    RH_Length_group(:, :, i) = Length_temp(2:2:68, 2:2:68);
    Laterality_temp = load(fullfile(Laterality_matfiles(i).folder,
        Laterality_matfiles(i).name));
    EnvLI_group(:, i) = Laterality_temp.EnvLI;
    NormEnvLI_group(:, i) = Laterality_temp.NormEnvLI;
end
LH_Delay_group(isnan(LH_Delay_group)) = 0;
RH_Delay_group(isnan(RH_Delay_group)) = 0;
% Pooled valid values across subjects for each ROI pair
LHDelay_flat = reshape(LH_Delay_group, [], length(Delay_matfiles));
RHDelay_flat = reshape(RH_Delay_group, [], length(Delay_matfiles));
LHSC_flat = reshape(LH_SC_group, [], length(Delay_matfiles));
RHSC_flat = reshape(RH_SC_group, [], length(Delay_matfiles));
LHLength_flat = reshape(LH_Length_group, [], length(Delay_matfiles));
RHLength_flat = reshape(RH_Length_group, [], length(Delay_matfiles));
LHDelay_extracted = {};
RHDelay_extracted = {};
LHSC_extracted = {};
RHSC_extracted = {};
LHLength_extracted = {};
RHLength_extracted = {};
LHVelocity = {};
RHVelocity = {};
for row = 1:1156
    LHcommon_idx = LHDelay_flat(row,:) ~= 0 & LHSC_flat(row,:) ~= 0 &
        LHLength_flat(row,:) ~= 0;
```

```
    RHcommon_idx = RHDelay_flat(row,:) ~= 0 & RHSC_flat(row,:) ~= 0 &
        RHLength_flat(row,:) ~= 0;
    if any(LHcommon_idx)
        LHDelay_extracted{end+1} = LHDelay_flat(row, LHcommon_idx);
        LHSC_extracted{end+1} = LHSC_flat(row, LHcommon_idx);
        LHLength_extracted{end+1} = LHLength_flat(row, LHcommon_idx);
        LHVelocity{end+1} = LHLength_flat(row, LHcommon_idx) ./ LHDelay_flat(row,
            LHcommon_idx);
    end
    if any(RHcommon_idx)
        RHDelay_extracted{end+1} = RHDelay_flat(row, RHcommon_idx);
        RHSC_extracted{end+1} = RHSC_flat(row, RHcommon_idx);
        RHLength_extracted{end+1} = RHLength_flat(row, RHcommon_idx);
        RHVelocity{end+1} = RHLength_flat(row, RHcommon_idx) ./ RHDelay_flat(row,
            RHcommon_idx);
    end
end
LHCollatedDelay = horzcat(LHDelay_extracted{:});
RHCollatedDelay = horzcat(RHDelay_extracted{:});
LHCollatedSC = horzcat(LHSC_extracted{:});
RHCollatedSC = horzcat(RHSC_extracted{:});
LHCollatedLength = horzcat(LHLength_extracted{:});
RHCollatedLength = horzcat(RHLength_extracted{:});
LHCollatedVelocity = horzcat(LHVelocity{:});
RHCollatedVelocity = horzcat(RHVelocity{:});
% Averaged valid values across subjects for each ROI pair
LHMeanDelay = NonZeroMeanHemi(LH_Delay_group);
RHMeanDelay = NonZeroMeanHemi(RH_Delay_group);
LHMeanLength = NonZeroMeanHemi(LH_Length_group);
RHMeanLength = NonZeroMeanHemi(RH_Length_group);
LHMeanSC = NonZeroMeanHemi(LH_SC_group);
RHMeanSC = NonZeroMeanHemi(RH_SC_group);
LHMeanVelocity = LHMeanLength ./ LHMeanDelay;
LHMeanVelocity(isnan(LHMeanVelocity)) = 0;
RHMeanVelocity = RHMeanLength ./ RHMeanDelay;
RHMeanVelocity(isnan(RHMeanVelocity)) = 0;
MeanEnvLI = mean(EnvLI_group, 2);
MeanNormEnvLI = mean(NormEnvLI_group, 2);
%% POOLED DISTRIBUTION DIFFERENCES
[h_ks_d, p_ks_d] = kstest2(LHCollatedDelay(:), RHCollatedDelay(:));
[h_ks_l, p_ks_l] = kstest2(LHCollatedLength(:), RHCollatedLength(:));
[h_ks_sc, p_ks_sc] = kstest2(LHCollatedSC(:), RHCollatedSC(:));
[h_ks_v, p_ks_v] = kstest2(LHCollatedVelocity(:), RHCollatedVelocity(:));
[h_t_d, p_t_d] = ttest2(LHCollatedDelay(:), RHCollatedDelay(:));
[h_t_l, p_t_l] = ttest2(LHCollatedLength(:), RHCollatedLength(:));
[h_t_sc, p_t_sc] = ttest2(LHCollatedSC(:), RHCollatedSC(:));
[h_t_v, p_t_v] = ttest2(LHCollatedVelocity(:), RHCollatedVelocity(:));
figure;
hold on;
h(1) = cdfplot(LHCollatedDelay(:));
h(2) = cdfplot(RHCollatedDelay(:));
legend({'Left Hemisphere','Right Hemisphere'}, 'location', 'southeast');
xlabel('Delays (ms)');
ylabel('Cumulative Density');
text(0.925, 0.5, sprintf('h: %d\np: %.2e', h_ks_d, p_ks_d), 'Units', 'normalized')
    ;
title('CDF Comparison: Pooled Small-Band Delay')
set(h(1), 'LineWidth', 1.5, 'Color', colors(5, :));
set(h(2), 'LineWidth', 1.5, 'Color', colors(6, :));
figure;
hold on;
h(1) = cdfplot(LHCollatedLength(:));
h(2) = cdfplot(RHCollatedLength(:));
legend({'Left Hemisphere','Right Hemisphere'}, 'location', 'southeast');
xlabel('Length (mm)');
ylabel('Cumulative Density');
text(0.925, 0.5, sprintf('h: %d\np: %.2e', h_ks_l, p_ks_l), 'Units', 'normalized')
    ;
title('CDF Comparison: Pooled Length')
set(h(1), 'LineWidth', 1.5, 'Color', colors(5, :));
set(h(2), 'LineWidth', 1.5, 'Color', colors(6, :));
figure;
hold on;
h(1) = cdfplot(LHCollatedSC(:));
h(2) = cdfplot(RHCollatedSC(:));
legend({'Left Hemisphere','Right Hemisphere'}, 'location', 'southeast');
xlabel('Width (A.U.)');
ylabel('Cumulative Density');
```

```
text(0.925, 0.5, sprintf('h: %d\np: %.2e', h_ks_sc, p_ks_sc), 'Units', 'normalized');
title('CDF Comparison: Pooled Width')
set(h(1), 'LineWidth', 1.5, 'Color', colors(5, :));
set(h(2), 'LineWidth', 1.5, 'Color', colors(6, :));
figure;
hold on;
h(1) = cdfplot(log(LHCollatedSC(:) + 0.00001));
h(2) = cdfplot(log(RHCollatedSC(:) + 0.00001));
legend({'Left Hemisphere','Right Hemisphere'}, 'location', 'southeast');
xlabel('Ln Width (A.U.)');
ylabel('Cumulative Density');
text(0.925, 0.5, sprintf('h: %d\np: %.2e', h_ks_sc, p_ks_sc), 'Units', 'normalized');
title('CDF Comparison: Log-Scaled Pooled Width')
set(h(1), 'LineWidth', 1.5, 'Color', colors(5, :));
set(h(2), 'LineWidth', 1.5, 'Color', colors(6, :));
figure;
hold on;
h(1) = cdfplot(LHCollatedVelocity(:));
h(2) = cdfplot(RHCollatedVelocity(:));
legend({'Left Hemisphere','Right Hemisphere'}, 'location', 'southeast');
xlabel('Velocity (mm/ms)');
ylabel('Cumulative Density');
text(0.925, 0.5, sprintf('h: %d\np: %.2e', h_ks_v, p_ks_v), 'Units', 'normalized');
title('CDF Comparison: Pooled Small-Band Velocity')
set(h(1), 'LineWidth', 1.5, 'Color', colors(5, :));
set(h(2), 'LineWidth', 1.5, 'Color', colors(6, :));
% ROI Pair Level Analysis
roi_ks_delay = zeros(3, 1122);
roi_ks_length = zeros(3, 1122);
roi_ks_sc = zeros(3, 1122);
roi_ks_velocity = zeros(3, 1122);
for i = 1:1122
    dl = LHDelay_extracted{i}(:);
    ll = LHLength_extracted{i}(:);
    sl = LHSC_extracted{i}(:);
    vl = LHVelocity{i}(:);
    dr = RHDelay_extracted{i}(:);
    lr = RHLength_extracted{i}(:);
    sr = RHSC_extracted{i}(:);
    vr = RHVelocity{i}(:);
    [h_roi_ks_d, p_roi_ks_d, d_roi_ks_d] = kstest2(dl, dr);
    roi_ks_delay(1, i) = h_roi_ks_d; roi_ks_delay(2, i) = p_roi_ks_d; roi_ks_delay(3, i) = d_roi_ks_d;
    [h_roi_ks_l, p_roi_ks_l, d_roi_ks_l] = kstest2(ll, lr);
    roi_ks_length(1, i) = h_roi_ks_l; roi_ks_length(2, i) = p_roi_ks_l; roi_ks_length(3, i) = d_roi_ks_l;
    [h_roi_ks_sc, p_roi_ks_sc, d_roi_ks_sc] = kstest2(sl, sr);
    roi_ks_sc(1, i) = h_roi_ks_sc; roi_ks_sc(2, i) = p_roi_ks_sc; roi_ks_sc(3, i) = d_roi_ks_sc;
    [h_roi_ks_v, p_roi_ks_v, d_roi_ks_v] = kstest2(vl, vr);
    roi_ks_velocity(1, i) = h_roi_ks_v; roi_ks_velocity(2, i) = p_roi_ks_v; roi_ks_velocity(3, i) = d_roi_ks_v;
end
n_D = length(roi_ks_delay(roi_ks_delay(1,:) == 1));
n_V = length(roi_ks_velocity(roi_ks_velocity(1,:) == 1));
n_L = length(roi_ks_length(roi_ks_length(1,:) == 1));
n_W = length(roi_ks_sc(roi_ks_sc(1,:) == 1));
figure;
plot(roi_ks_delay(1, :), 'k')
title('Pairwise Hemispheric Asymmetry of Small-Band Delay')
xlabel('ROI Pair'); ylabel('H')
text(0.9375, 0.5, sprintf('N: %d', n_D), 'Units', 'normalized');
figure;
plot(roi_ks_velocity(1, :), 'k')
title('Pairwise Hemispheric Asymmetry of Small-Band Velocity')
xlabel('ROI Pair'); ylabel('H')
text(0.9375, 0.5, sprintf('N: %d', n_V), 'Units', 'normalized');
figure;
plot(roi_ks_length(1, :), 'k')
title('Pairwise Hemispheric Asymmetry of Length')
xlabel('ROI Pair'); ylabel('H')
text(0.9375, 0.5, sprintf('N: %d', n_L), 'Units', 'normalized');
figure;
plot(roi_ks_sc(1, :), 'k')
title('Pairwise Hemispheric Asymmetry of Width')
xlabel('ROI Pair'); ylabel('H')
```

```
text(0.9375, 0.5, sprintf('N: %d', n_W), 'Units', 'normalized');
sig_idx_d = find(roi_ks_delay(1, :) == 1);
Sig_ks_d_d = roi_ks_delay(3, sig_idx_d);
sig_idx_l = find(roi_ks_length(1, :) == 1);
Sig_ks_d_l = roi_ks_length(3, sig_idx_l);
sig_idx_s = find(roi_ks_sc(1, :) == 1);
Sig_ks_d_s = roi_ks_sc(3, sig_idx_s);
sig_idx_v = find(roi_ks_velocity(1, :) == 1);
Sig_ks_d_v = roi_ks_velocity(3, sig_idx_v);
insig_idx_d = find(roi_ks_delay(1, :) == 0);
inSig_ks_d_d = roi_ks_delay(3, insig_idx_d);
insig_idx_l = find(roi_ks_length(1, :) == 0);
inSig_ks_d_l = roi_ks_length(3, insig_idx_l);
insig_idx_s = find(roi_ks_sc(1, :) == 0);
inSig_ks_d_s = roi_ks_sc(3, insig_idx_s);
insig_idx_v = find(roi_ks_velocity(1, :) == 0);
inSig_ks_d_v = roi_ks_velocity(3, insig_idx_v);
figure;
hold on;
histogram(Sig_ks_d_d, 'FaceColor', 'g', 'BinWidth', 0.01)
histogram(inSig_ks_d_d, 'FaceColor', 'k', 'BinWidth', 0.01)
legend({'Significant Pairs', 'Insignificant Pairs'});
title('Pairwise Distance of Hemispheric Asymmetry of Small-Band Delay')
xlabel('KS Distance');
figure;
hold on;
histogram(Sig_ks_d_v, 'FaceColor', 'g', 'BinWidth', 0.01)
histogram(inSig_ks_d_v, 'FaceColor', 'k', 'BinWidth', 0.01)
legend({'Significant Pairs', 'Insignificant Pairs'});
title('Pairwise Distance of Hemispheric Asymmetry of Small-Band Velocity')
xlabel('KS Distance');
figure;
hold on;
histogram(Sig_ks_d_l, 'FaceColor', 'g', 'BinWidth', 0.01)
histogram(inSig_ks_d_l, 'FaceColor', 'k', 'BinWidth', 0.01)
legend({'Significant Pairs', 'Insignificant Pairs'});
title('Pairwise Distance of Hemispheric Asymmetry of Length')
xlabel('KS Distance');
figure;
hold on;
histogram(Sig_ks_d_s, 'FaceColor', 'g', 'BinWidth', 0.01)
histogram(inSig_ks_d_s, 'FaceColor', 'k', 'BinWidth', 0.01)
legend({'Significant Pairs', 'Insignificant Pairs'});
title('Pairwise Distance of Hemispheric Asymmetry of Width')
xlabel('KS Distance');
%% AVERAGED DISTRIBUTION DIFFERENCES
[h_ks_mean_d, p_ks_mean_d] = kstest2(LHMeanDelay(:), RHMeanDelay(:));
[h_ks_mean_l, p_ks_mean_l] = kstest2(LHMeanLength(:), RHMeanLength(:));
[h_ks_mean_sc, p_ks_mean_sc] = kstest2(LHMeanSC(:), RHMeanSC(:));
[h_ks_mean_v, p_ks_mean_v] = kstest2(LHMeanVelocity(:), RHMeanVelocity(:));
[h_t_mean_d, p_t_mean_d] = ttest2(LHMeanDelay(:), RHMeanDelay(:));
[h_t_mean_l, p_t_mean_l] = ttest2(LHMeanLength(:), RHMeanLength(:));
[h_t_mean_sc, p_t_mean_sc] = ttest2(LHMeanSC(:), RHMeanSC(:));
[h_t_mean_v, p_t_mean_v] = ttest2(LHMeanVelocity(:), RHMeanVelocity(:));
figure;
hold on;
h(1) = cdfplot(LHMeanDelay(:));
h(2) = cdfplot(RHMeanDelay(:));
legend({'Left Hemisphere','Right Hemisphere'}, 'location', 'southeast');
xlabel('Delays (ms)');
ylabel('Cumulative Density');
text(0.925, 0.5, sprintf('h: %d\np: %.2e', h_ks_mean_d, p_ks_mean_d), 'Units', '
    normalized');
title('CDF Comparison: Averaged Small-Band Delay')
set(h(1), 'LineWidth', 1.5, 'Color', colors(5, :));
set(h(2), 'LineWidth', 1.5, 'Color', colors(6, :));
figure;
hold on;
h(1) = cdfplot(LHMeanLength(:));
h(2) = cdfplot(RHMeanLength(:));
legend({'Left Hemisphere','Right Hemisphere'}, 'location', 'southeast');
xlabel('Length (mm)');
ylabel('Cumulative Density');
text(0.925, 0.5, sprintf('h: %d\np: %.2e', h_ks_mean_l, p_ks_mean_l), 'Units', '
    normalized');
title('CDF Comparison: Averaged Length')
set(h(1), 'LineWidth', 1.5, 'Color', colors(5, :));
set(h(2), 'LineWidth', 1.5, 'Color', colors(6, :));
figure;
```

```
hold on;
h(1) = cdfplot(LHMeanSC(:));
h(2) = cdfplot(RHMeanSC(:));
legend({'Left Hemisphere','Right Hemisphere'}, 'location', 'southeast');
xlabel('Width (A.U.)');
ylabel('Cumulative Density');
text(0.925, 0.5, sprintf('h: %d\np: %.2e', h_ks_mean_sc, p_ks_mean_sc), 'Units', '
    normalized');
title('CDF Comparison: Averaged Width')
set(h(1), 'LineWidth', 1.5, 'Color', colors(5, :));
set(h(2), 'LineWidth', 1.5, 'Color', colors(6, :));
figure;
hold on;
h(1) = cdfplot(log(LHMeanSC(:) + 0.00001));
h(2) = cdfplot(log(RHMeanSC(:) + 0.00001));
legend({'Left Hemisphere','Right Hemisphere'}, 'location', 'southeast');
xlabel('Ln Width (A.U.)');
ylabel('Cumulative Density');
text(0.925, 0.5, sprintf('h: %d\np: %.2e', h_ks_mean_sc, p_ks_mean_sc), 'Units', '
    normalized');
title('CDF Comparison: Log-Scaled Averaged Width')
set(h(1), 'LineWidth', 1.5, 'Color', colors(5, :));
set(h(2), 'LineWidth', 1.5, 'Color', colors(6, :));
figure;
hold on;
h(1) = cdfplot(LHMeanVelocity(:));
h(2) = cdfplot(RHMeanVelocity(:));
legend({'Left Hemisphere','Right Hemisphere'}, 'location', 'southeast');
xlabel('Velocity (mm/ms)');
ylabel('Cumulative Density');
text(0.925, 0.5, sprintf('h: %d\np: %.2e', h_ks_mean_v, p_ks_mean_v), 'Units', '
    normalized');
title('CDF Comparison: Averaged Small-Band Velocity')
set(h(1), 'LineWidth', 1.5, 'Color', colors(5, :));
set(h(2), 'LineWidth', 1.5, 'Color', colors(6, :));
%% AVERAGED DISTRIBUTION LATERALIZATION
DelayDiff = (RHMeanDelay - LHMeanDelay);
LengthLI = (RHMeanLength - LHMeanLength) ./ (RHMeanLength + LHMeanLength);
WidthLI = (RHMeanSC - LHMeanSC) ./ (RHMeanSC + LHMeanSC);
VelocityLI = (RHMeanVelocity - LHMeanVelocity) ./ (RHMeanVelocity + LHMeanVelocity
    );
DelayDiff(isnan(DelayDiff)) = 0;
LengthLI(isnan(LengthLI)) = 0;
WidthLI(isnan(WidthLI)) = 0;
VelocityLI(isnan(VelocityLI)) = 0;
LengthLI = reshape(LengthLI, 34, 34);
WidthLI = reshape(WidthLI, 34, 34);
VelocityLI = reshape(VelocityLI, 34, 34);
b2w = [linspace(0,1,128)', linspace(0,1,128)', ones(128, 1)];
w2r = [ones(128, 1),linspace(1,0,128)', linspace(1,0,128)'];
LateralityMap = [b2w;w2r];
figure;
imagesc(DelayDiff); title('Small-Band Delay Difference'); xlabel('ROI'); ylabel('
    ROI'); axis equal tight; clim([-25 25]); colormap(LateralityMap); cb =
    colorbar; cb.Label.String = 'Delay Differnce (ms)';
figure;
imagesc(LengthLI); title('Length Laterality'); xlabel('ROI'); ylabel('ROI'); axis
    equal tight; clim([-0.8 0.8]); colormap(LateralityMap); cb = colorbar; cb.
    Label.String = 'Laterality Index';
figure;
imagesc(WidthLI); title('Width Laterality'); xlabel('ROI'); ylabel('ROI'); axis
    equal tight; clim([-0.8 0.8]); colormap(LateralityMap); cb = colorbar; cb.
    Label.String = 'Laterality Index';
figure;
imagesc(VelocityLI); title('Small-Band Velocity Laterality'); xlabel('ROI');
    ylabel('ROI'); axis equal tight; clim([-0.8 0.8]); colormap(LateralityMap); cb
     = colorbar; cb.Label.String = 'Laterality Index';
figure;
imagesc(MeanEnvLI); title('Functional Laterality (Mean Envelope)'); ylabel('ROI');
     axis equal tight; clim([-0.1 0.1]); colormap(LateralityMap); cb = colorbar;
    cb.Label.String = 'Laterality Index';
figure;
imagesc(MeanNormEnvLI); title('Functional Laterality (Mean Normalised Envelope)');
     ylabel('ROI'); axis equal tight; clim([-0.1 0.1]); colormap(LateralityMap);
    cb = colorbar; cb.Label.String = 'Laterality Index';
[rho_LI_ld_pair, pval_LI_ld_pair] = corr(LengthLI(:), DelayDiff(:), 'Type', '
    Spearman');
[rho_LI_wd_pair, pval_LI_wd_pair] = corr(WidthLI(:), DelayDiff(:), 'Type', '
    Spearman');
```

```
figure; scatter(LengthLI(:), DelayDiff(:), 'o', 'filled', 'k'); xlabel('Length Laterality'); ylabel('Delay Laterality'); text(0.8, 0.85, sprintf('Spearman rho: %.2f\npval: %.2e\n', rho_LI_ld_pair, pval_LI_ld_pair), 'Units', 'normalized'); title('Pairwise Laterality: Length vs. Small-Band Delay')
figure; scatter(WidthLI(:), DelayDiff(:), 'o', 'filled', 'k'); xlabel('Width Laterality'); ylabel('Delay Laterality'); text(0.8, 0.85, sprintf('Spearman rho: %.2f\npval: %.2e\n', rho_LI_wd_pair, pval_LI_wd_pair), 'Units', 'normalized'); title('Pairwise Laterality: Width vs. Small-Band Delay')
% Regional Afferent Laterality Relations
AfferentDelayDiff = mean(DelayDiff, 1);
AfferentLengthLI = mean(LengthLI, 1);
AfferentWidthLI = mean(WidthLI, 1);
AfferentVelocityLI = mean(VelocityLI, 1);
[rho_LI_ld, pval_LI_ld] = corr(AfferentLengthLI(:), AfferentDelayDiff(:), 'Type', 'Spearman');
[rho_LI_wd, pval_LI_wd] = corr(AfferentWidthLI(:), AfferentDelayDiff(:), 'Type', 'Spearman');
[rho_LI_dEnv, pval_LI_dEnv] = corr(AfferentDelayDiff(:), MeanEnvLI(:), 'Type', 'Spearman');
[rho_LI_dNormEnv, pval_LI_dNormEnv] = corr(AfferentDelayDiff(:), MeanNormEnvLI(:), 'Type', 'Spearman');
[rho_LI_lEnv, pval_LI_lEnv] = corr(AfferentLengthLI(:), MeanEnvLI(:), 'Type', 'Spearman');
[rho_LI_lNormEnv, pval_LI_lNormEnv] = corr(AfferentLengthLI(:), MeanNormEnvLI(:), 'Type', 'Spearman');
[rho_LI_wEnv, pval_LI_wEnv] = corr(AfferentWidthLI(:), MeanEnvLI(:), 'Type', 'Spearman');
[rho_LI_wNormEnv, pval_LI_wNormEnv] = corr(AfferentWidthLI(:), MeanNormEnvLI(:), 'Type', 'Spearman');
figure; scatter(AfferentLengthLI(:), AfferentDelayDiff(:), 'o', 'filled', 'k'); xlabel('Length Laterality'); ylabel('Delay Difference (ms)'); text(0.8, 0.85, sprintf('Spearman rho: %.2f\npval: %.2e\n', rho_LI_ld, pval_LI_ld), 'Units', 'normalized'); title('Regional Laterality: Length vs. Small-Band Delay')
figure; scatter(AfferentWidthLI(:), AfferentDelayDiff(:), 'o', 'filled', 'k'); xlabel('Width Laterality'); ylabel('Delay  Difference (ms)'); text(0.8, 0.85, sprintf('Spearman rho: %.2f\npval: %.2e\n', rho_LI_wd, pval_LI_wd), 'Units', 'normalized'); title('Regional Laterality: Width vs. Small-Band Delay')
figure; scatter(AfferentDelayDiff(:), MeanEnvLI(:), 'o', 'filled', 'k'); xlabel('Delay  Difference (ms)'); ylabel('Functional Laterality (Mean Envelope)'); text(0.8, 0.85, sprintf('Spearman rho: %.2f\npval: %.2e\n', rho_LI_dEnv, pval_LI_dEnv), 'Units', 'normalized'); title('Regional Laterality: Small-Band Delay vs. Mean Envelope')
figure; scatter(AfferentDelayDiff(:), MeanNormEnvLI(:), 'o', 'filled', 'k'); xlabel('Delay  Difference (ms)'); ylabel('Functional Laterality (Mean Normalised Envelope)'); text(0.8, 0.85, sprintf('Spearman rho: %.2f\npval: %.2e\n', rho_LI_dNormEnv, pval_LI_dNormEnv), 'Units', 'normalized'); title('Regional Laterality: Small-Band Delay vs. Mean Normalised Envelope')
figure; scatter(AfferentLengthLI(:), MeanEnvLI(:), 'o', 'filled', 'k'); xlabel('Length Laterality'); ylabel('Functional Laterality (Mean Envelope)'); text(0.8, 0.85, sprintf('Spearman rho: %.2f\npval: %.2e\n', rho_LI_lEnv, pval_LI_lEnv), 'Units', 'normalized'); title('Regional Laterality: Length vs. Mean Envelope')
figure; scatter(AfferentLengthLI(:), MeanNormEnvLI(:), 'o', 'filled', 'k'); xlabel('Length Laterality'); ylabel('Functional Laterality (Mean Normalised Envelope)'); text(0.8, 0.85, sprintf('Spearman rho: %.2f\npval: %.2e\n', rho_LI_lNormEnv, pval_LI_lNormEnv), 'Units', 'normalized'); title('Regional Laterality: Length vs. Mean Normalised Envelope')
figure; scatter(AfferentWidthLI(:), MeanEnvLI(:), 'o', 'filled', 'k'); xlabel('Width Laterality'); ylabel('Functional Laterality (Mean Envelope)'); text(0.8, 0.85, sprintf('Spearman rho: %.2f\npval: %.2e\n', rho_LI_wEnv, pval_LI_wEnv), 'Units', 'normalized'); title('Regional Laterality: Width vs. Mean Envelope')
figure; scatter(AfferentWidthLI(:), MeanNormEnvLI(:), 'o', 'filled', 'k'); xlabel('Width Laterality'); ylabel('Functional Laterality (Mean Normalised Envelope)'); text(0.8, 0.85, sprintf('Spearman rho: %.2f\npval: %.2e\n', rho_LI_wNormEnv, pval_LI_wNormEnv), 'Units', 'normalized'); title('Regional Laterality: Width vs. Mean Normalised Envelope')
% Regional Afferent Absoulte Differences Relation
AbsAfferentDelayDiff = mean(abs(DelayDiff), 1);
AbsAfferentLengthLI = mean(abs(LengthLI), 1);
AbsAfferentWidthLI = mean(abs(WidthLI), 1);
AbsMeanEnvLI = abs(MeanEnvLI);
AbsMeanNormEnvLI = abs(MeanNormEnvLI);
[rho_LI_ld_abs, pval_LI_ld_abs] = corr(AbsAfferentLengthLI(:), AbsAfferentDelayDiff(:), 'Type', 'Spearman');
[rho_LI_wd_abs, pval_LI_wd_abs] = corr(AbsAfferentWidthLI(:), AbsAfferentDelayDiff(:), 'Type', 'Spearman');
[rho_LI_dEnv_abs, pval_LI_dEnv_abs] = corr(AbsAfferentDelayDiff(:), AbsMeanEnvLI(:), 'Type', 'Spearman');
```

```
[rho_LI_dNormEnv_abs, pval_LI_dNormEnv_abs] = corr(AbsAfferentDelayDiff(:), AbsMeanNormEnvLI(:), 'Type', 'Spearman');
[rho_LI_lEnv_abs, pval_LI_lEnv_abs] = corr(AbsAfferentLengthLI(:), AbsMeanEnvLI(:), 'Type', 'Spearman');
[rho_LI_lNormEnv_abs, pval_LI_lNormEnv_abs] = corr(AbsAfferentLengthLI(:), AbsMeanNormEnvLI(:), 'Type', 'Spearman');
[rho_LI_wEnv_abs, pval_LI_wEnv_abs] = corr(AbsAfferentWidthLI(:), AbsMeanEnvLI(:), 'Type', 'Spearman');
[rho_LI_wNormEnv_abs, pval_LI_wNormEnv_abs] = corr(AbsAfferentWidthLI(:), AbsMeanNormEnvLI(:), 'Type', 'Spearman');
figure; scatter(AbsAfferentLengthLI(:), AbsAfferentDelayDiff(:), 'o', 'filled', 'k'); xlabel('Length Laterality'); ylabel('Delay Difference (ms)'); text(0.8, 0.85, sprintf('Spearman rho: %.2f\npval: %.2e\n', rho_LI_ld_abs, pval_LI_ld_abs), 'Units', 'normalized'); title('Regional Absolute Laterality: Length vs. Small-Band Delay')
figure; scatter(AbsAfferentWidthLI(:), AbsAfferentDelayDiff(:), 'o', 'filled', 'k'); xlabel('Width Laterality'); ylabel('Delay Difference (ms)'); text(0.8, 0.85, sprintf('Spearman rho: %.2f\npval: %.2e\n', rho_LI_wd_abs, pval_LI_wd_abs), 'Units', 'normalized'); title('Regional Absolute Laterality: Width vs. Small-Band Delay')
figure; scatter(AbsAfferentDelayDiff(:), AbsMeanEnvLI(:), 'o', 'filled', 'k'); xlabel('Delay Difference (ms)'); ylabel('Functional Laterality (Mean Envelope)'); text(0.8, 0.85, sprintf('Spearman rho: %.2f\npval: %.2e\n', rho_LI_dEnv_abs, pval_LI_dEnv_abs), 'Units', 'normalized'); title('Regional Absolute Laterality: Small-Band Delay vs. Mean Envelope')
figure; scatter(AbsAfferentDelayDiff(:), AbsMeanNormEnvLI(:), 'o', 'filled', 'k'); xlabel('Delay Difference (ms)'); ylabel('Functional Laterality (Mean Normalised Envelope)'); text(0.8, 0.85, sprintf('Spearman rho: %.2f\npval: %.2e\n', rho_LI_dNormEnv_abs, pval_LI_dNormEnv_abs), 'Units', 'normalized'); title('Regional Absolute Laterality: Small-Band Delay vs. Mean Normalised Envelope')
figure; scatter(AbsAfferentLengthLI(:), AbsMeanEnvLI(:), 'o', 'filled', 'k'); xlabel('Length Laterality'); ylabel('Functional Laterality (Mean Envelope)'); text(0.8, 0.85, sprintf('Spearman rho: %.2f\npval: %.2e\n', rho_LI_lEnv_abs, pval_LI_lEnv_abs), 'Units', 'normalized'); title('Regional Absolute Laterality : Length vs. Mean Envelope')
figure; scatter(AbsAfferentLengthLI(:), AbsMeanNormEnvLI(:), 'o', 'filled', 'k'); xlabel('Length Laterality'); ylabel('Functional Laterality (Mean Normalised Envelope)'); text(0.8, 0.85, sprintf('Spearman rho: %.2f\npval: %.2e\n', rho_LI_lNormEnv_abs, pval_LI_lNormEnv_abs), 'Units', 'normalized'); title('Regional Absolute Laterality: Length vs. Mean Normalised Envelope')
figure; scatter(AbsAfferentWidthLI(:), AbsMeanEnvLI(:), 'o', 'filled', 'k'); xlabel('Width Laterality'); ylabel('Functional Laterality (Mean Envelope)'); text(0.8, 0.85, sprintf('Spearman rho: %.2f\npval: %.2e\n', rho_LI_wEnv_abs, pval_LI_wEnv_abs), 'Units', 'normalized'); title('Regional Absolute Laterality : Width vs. Mean Envelope')
figure; scatter(AbsAfferentWidthLI(:), AbsMeanNormEnvLI(:), 'o', 'filled', 'k'); xlabel('Width Laterality'); ylabel('Functional Laterality (Mean Normalised Envelope)'); text(0.8, 0.85, sprintf('Spearman rho: %.2f\npval: %.2e\n', rho_LI_wNormEnv_abs, pval_LI_wNormEnv_abs), 'Units', 'normalized'); title('Regional Absolute Laterality: Width vs. Mean Normalised Envelope')
```

References

[1] P. Broca. “Nouvelle observation d’aphémie produite par une lésion de la moitié postérieure des deuxième et troisième circonvolutions frontales. 36.” (), 1861.

[2] P. Broca. “Sur le siège de la faculté du langage articulé.” *Bulletins et Mémoires de la Société d’Anthropologie de Paris*, **6**(1), 1865, pp. 377–393.

[3] M. S. Gazzaniga and R. W. Sperry. “LANGUAGE AFTER SECTION OF THE CEREBRAL COMMISSURES.” *Brain*, **90**(1), 1967, pp. 131–148. ISSN: 0006-8950, 1460-2156. DOI: 10.1093/brain/90.1.131. URL: https://academic.oup.com/brain/article-lookup/doi/10.1093/brain/90.1.131 (visited on 06/10/2025).

[4] M. S. Gazzaniga, J. E. Bogen, and R. W. Sperry. “OBSERVATIONS ON VISUAL PERCEPTION AFTER DISCONNEXION OF THE CEREBRAL HEMISPHERES IN MAN.” *Brain*, **88**(2), 1965, pp. 221–236. ISSN: 0006-8950, 1460-2156. DOI: 10.1093/brain/88.2.221. URL: https://academic.oup.com/brain/article-lookup/doi/10.1093/brain/88.2.221 (visited on 06/10/2025).

[5] A. Seydell-Greenwald, C. E. Chambers, K. Ferrara, and E. L. Newport. “What you say versus how you say it: Comparing sentence comprehension and emotional prosody processing using fMRI.” *NeuroImage*, **209**(), Apr. 2020, p. 116509. ISSN: 10538119. DOI: 10.1016/j.neuroimage.2019.116509. URL: https://linkinghub.elsevier.com/retrieve/pii/S1053811919311000 (visited on 06/10/2025).

[6] R. J. Zatorre and P. Belin. “Spectral and Temporal Processing in Human Auditory Cortex.” *Cerebral Cortex*, **11**(10), Oct. 1, 2001, pp. 946–953. ISSN: 14602199. DOI: 10.1093/cercor/11.10.946. URL: https://academic.oup.com/cercor/article-lookup/doi/10.1093/cercor/11.10.946 (visited on 06/10/2025).

[7] S. G. Brederoo et al. “Towards a unified understanding of lateralized vision: A large-scale study investigating principles governing patterns of lateralization using a heterogeneous sample.” *Cortex*, **133**(), Dec. 2020, pp. 201–214. ISSN: 00109452. DOI: 10.1016/j.cortex.2020.08.029. URL: https://linkinghub.elsevier.com/retrieve/pii/S0010945220303543 (visited on 06/10/2025).

[8] J. P. Rauschecker and B. Tian. “Mechanisms and streams for processing of “what” and “where” in auditory cortex.” *Proceedings of the National Academy of Sciences*, **97**(22), Oct. 24, 2000, pp. 11800–11806. ISSN: 0027-8424, 1091-6490. DOI: 10.1073/pnas.97.22.11800. URL: https://pnas.org/doi/full/10.1073/pnas.97.22.11800 (visited on 06/15/2025).

[9] M. Corbetta and G. L. Shulman. “Control of goal-directed and stimulus-driven attention in the brain.” *Nature Reviews Neuroscience*, **3**(3), Mar. 1, 2002, pp. 201–215. ISSN: 1471-003X, 1471-0048. DOI: 10.1038/nrn755. URL: https://www.nature.com/articles/nrn755 (visited on 08/16/2024).

[10] Q. Cai, L. Van Der Haegen, and M. Brysbaert. "Complementary hemispheric specialization for language production and visuospatial attention." *Proceedings of the National Academy of Sciences*, **110**(4), Jan. 22, 2013. ISSN: 0027-8424, 1091-6490. DOI: 10.1073/pnas.1212956110. URL: https://pnas.org/doi/full/10.1073/pnas.1212956110 (visited on 06/15/2025).

[11] S. Dehaene, E. Spelke, P. Pinel, R. Stanescu, and S. Tsivkin. "Sources of Mathematical Thinking: Behavioral and Brain-Imaging Evidence." *Science*, **284**(5416), May 7, 1999, pp. 970–974. ISSN: 0036-8075, 1095-9203. DOI: 10.1126/science.284.5416.970. URL: https://www.science.org/doi/10.1126/science.284.5416.970 (visited on 06/10/2025).

[12] M. Wittmann, N. Von Steinbüchel, and E. Szelag. "Hemispheric specialisation for self-paced motor sequences." *Cognitive Brain Research*, **10**(3), Jan. 2001, pp. 341–344. ISSN: 09266410. DOI: 10.1016/S0926-6410(00)00052-5. URL: https://linkinghub.elsevier.com/retrieve/pii/S0926641000000525 (visited on 08/11/2024).

[13] S. Grafton, M. Arbib, L. Fadiga, and G. Rizzolatti. "Localization of grasp representations in humans by positron emission tomography: 2. Observation compared with imagination." *Experimental Brain Research*, **112**(1), Nov. 1996. ISSN: 0014-4819, 1432-1106. DOI: 10.1007/BF00227183. URL: http://link.springer.com/10.1007/BF00227183 (visited on 06/15/2025).

[14] K. Kocel, D. Galin, R. Ornstein, and E. L. Merrin. "Lateral eye movement and cognitive mode." *Psychonomic Science*, **27**(4), Oct. 1972, pp. 223–224. ISSN: 0033-3131. DOI: 10.3758/BF03328944. URL: http://link.springer.com/10.3758/BF03328944 (visited on 06/15/2025).

[15] R. M. Bilder. "Yakovlevian Torque: Something Old and Something New." *Biological Psychiatry*, **91**(8), Apr. 2022, pp. 697–698. ISSN: 00063223. DOI: 10.1016/j.biopsych.2022.01.013. URL: https://linkinghub.elsevier.com/retrieve/pii/S0006322322000555 (visited on 06/15/2025).

[16] K. Watkins et al. "Structural Asymmetries in the Human Brain: a Voxel-based Statistical Analysis of 142 MRI Scans." *Cerebral Cortex*, **11**(9), Sept. 1, 2001, pp. 868–877. ISSN: 14602199. DOI: 10.1093/cercor/11.9.868. URL: https://academic.oup.com/cercor/article-lookup/doi/10.1093/cercor/11.9.868 (visited on 06/15/2025).

[17] N. Geschwind and W. Levitsky. "Human Brain: Left-Right Asymmetries in Temporal Speech Region." *Science*, **161**(3837), July 12, 1968, pp. 186–187. ISSN: 0036-8075, 1095-9203. DOI: 10.1126/science.161.3837.186. URL: https://www.science.org/doi/10.1126/science.161.3837.186 (visited on 06/15/2025).

[18] G. Schlaug, L. Jäncke, Y. Huang, and H. Steinmetz. "In Vivo Evidence of Structural Brain Asymmetry in Musicians." *Science*, **267**(5198), Feb. 3, 1995, pp. 699–701. ISSN: 0036-8075, 1095-9203. DOI: 10.1126/science.7839149. URL: https://www.science.org/doi/10.1126/science.7839149 (visited on 06/15/2025).

[19] M. Thiebaut De Schotten et al. "Atlasing location, asymmetry and inter-subject variability of white matter tracts in the human brain with MR diffusion tractography." *NeuroImage*, **54**(1), Jan. 2011, pp. 49–59. ISSN: 10538119. DOI: 10.1016/j.neuroimage.2010.07.055. URL: https://linkinghub.elsevier.com/retrieve/pii/S1053811910010281 (visited on 06/16/2025).

[20] Y. Iturria-Medina et al. “Brain Hemispheric Structural Efficiency and Interconnectivity Rightward Asymmetry in Human and Nonhuman Primates.” *Cerebral Cortex*, **21**(1), Jan. 2011, pp. 56–67. ISSN: 1460-2199, 1047-3211. DOI: 10.1093/cercor/bhq058. URL: https://academic.oup.com/cercor/article-lookup/doi/10.1093/cercor/bhq058 (visited on 06/15/2025).

[21] B. Mišić et al. “Network-Based Asymmetry of the Human Auditory System.” *Cerebral Cortex*, **28**(7), July 1, 2018, pp. 2655–2664. ISSN: 1047-3211. DOI: 10.1093/cercor/bhy101. URL: https://doi.org/10.1093/cercor/bhy101 (visited on 06/20/2025).

[22] J. Semmes. “Hemispheric specialization: A possible clue to mechanism.” *Neuropsychologia*, **6**(1), Mar. 1968, pp. 11–26. ISSN: 00283932. DOI: 10.1016/0028-3932(68)90035-3. URL: https://linkinghub.elsevier.com/retrieve/pii/0028393268900353 (visited on 06/15/2025).

[23] R. A. W. Galuske, W. Schlote, H. Bratzke, and W. Singer. “Interhemispheric Asymmetries of the Modular Structure in Human Temporal Cortex.” *Science*, **289**(5486), Sept. 15, 2000, pp. 1946–1949. ISSN: 0036-8075, 1095-9203. DOI: 10.1126/science.289.5486.1946. URL: https://www.science.org/doi/10.1126/science.289.5486.1946 (visited on 06/16/2025).

[24] H. Seldon. “Structure of human auditory cortex. II. Axon distributions and morphological correlates of speech perception.” *Brain Research*, **229**(2), Dec. 1981, pp. 295–310. ISSN: 00068993. DOI: 10.1016/0006-8993(81)90995-1. URL: https://linkinghub.elsevier.com/retrieve/pii/0006899381909951 (visited on 06/16/2025).

[25] R. J. Zatorre, P. Belin, and V. B. Penhune. “Structure and function of auditory cortex: music and speech.” *Trends in Cognitive Sciences*, **6**(1), Jan. 2002, pp. 37–46. ISSN: 13646613. DOI: 10.1016/S1364-6613(00)01816-7. URL: https://linkinghub.elsevier.com/retrieve/pii/S1364661300018167 (visited on 06/16/2025).

[26] G. Deco, V. Jirsa, A. R. McIntosh, O. Sporns, and R. Kötter. “Key role of coupling, delay, and noise in resting brain fluctuations.” *Proceedings of the National Academy of Sciences*, **106**(25), June 23, 2009, pp. 10302–10307. ISSN: 0027-8424, 1091-6490. DOI: 10.1073/pnas.0901831106. URL: https://pnas.org/doi/full/10.1073/pnas.0901831106 (visited on 06/20/2025).

[27] C. J. Honey, R. Kötter, M. Breakspear, and O. Sporns. “Network structure of cerebral cortex shapes functional connectivity on multiple time scales.” *Proceedings of the National Academy of Sciences*, **104**(24), June 12, 2007. Publisher: Proceedings of the National Academy of Sciences, pp. 10240–10245. DOI: 10.1073/pnas.0701519104. URL: https://www.pnas.org/doi/full/10.1073/pnas.0701519104 (visited on 06/20/2025).

[28] Z. Wang, Z. Dai, G. Gong, C. Zhou, and Y. He. “Understanding Structural-Functional Relationships in the Human Brain: A Large-Scale Network Perspective.” *The Neuroscientist*, **21**(3), June 1, 2015. Publisher: SAGE Publications Inc STM, pp. 290–305. ISSN: 1073-8584. DOI: 10.1177/1073858414537560. URL: https://doi.org/10.1177/1073858414537560 (visited on 06/20/2025).

[29] A. Coelho et al. “Reorganization of brain structural networks in aging: A longitudinal study.” *Journal of Neuroscience Research*, **99**(5), 2021. _eprint: https://onlinelibrary.wiley.com/doi/pdf/10.1002/jnr.24795, pp. 1354–1376. ISSN: 1097-4547. DOI: 10.1002/jnr.24795. URL: https://onlinelibrary.wiley.com/doi/abs/10.1002/jnr.24795 (visited on 06/20/2025).

[30] B. Berger et al. "Dynamic regulation of interregional cortical communication by slow brain oscillations during working memory." *Nature Communications*, **10**(1), Sept. 18, 2019. Publisher: Nature Publishing Group, p. 4242. ISSN: 2041-1723. DOI: 10.1038/s41467-019-12057-0. URL: https://www.nature.com/articles/s41467-019-12057-0 (visited on 06/20/2025).

[31] A.-K. R. Bauer, S. Debener, and A. C. Nobre. "Synchronisation of Neural Oscillations and Cross-modal Influences." *Trends in Cognitive Sciences*, **24**(6), June 2020. Publisher: Elsevier Ltd, pp. 481–495. ISSN: 1364-6613. DOI: 10.1016/j.tics.2020.03.003. URL: https://pure.royalholloway.ac.uk/en/publications/synchronisation-of-neural-oscillations-and-cross-modal-influences (visited on 06/20/2025).

[32] E. Tognoli and J. A. S. Kelso. "The Metastable Brain." *Neuron*, **81**(1), Jan. 8, 2014, pp. 35–48. ISSN: 0896-6273. DOI: 10.1016/j.neuron.2013.12.022. URL: https://www.sciencedirect.com/science/article/pii/S0896627313011835 (visited on 06/21/2025).

[33] V. K. Jirsa. "Dispersion and time delay effects in synchronized spike–burst networks." *Cognitive Neurodynamics*, **2**(1), Mar. 1, 2008, pp. 29–38. ISSN: 1871-4099. DOI: 10.1007/s11571-007-9030-0. URL: https://doi.org/10.1007/s11571-007-9030-0 (visited on 08/29/2024).

[34] E. Niebur, H. G. Schuster, and D. M. Kammen. "Collective frequencies and metastability in networks of limit-cycle oscillators with time delay." *Physical Review Letters*, **67**(20), Nov. 11, 1991. Publisher: American Physical Society, pp. 2753–2756. DOI: 10.1103/PhysRevLett.67.2753. URL: https://link.aps.org/doi/10.1103/PhysRevLett.67.2753 (visited on 08/29/2024).

[35] D. V. Ramana Reddy, A. Sen, and G. L. Johnston. "Time Delay Induced Death in Coupled Limit Cycle Oscillators." *Physical Review Letters*, **80**(23), June 8, 1998. Publisher: American Physical Society, pp. 5109–5112. DOI: 10.1103/PhysRevLett.80.5109. URL: https://link.aps.org/doi/10.1103/PhysRevLett.80.5109 (visited on 06/20/2025).

[36] A. Pathak, D. Roy, and A. Banerjee. "Whole-Brain Network Models: From Physics to Bedside." *Frontiers in Computational Neuroscience*, **16**(), May 26, 2022. Publisher: Frontiers. ISSN: 1662-5188. DOI: 10.3389/fncom.2022.866517. URL: https://www.frontiersin.org/journals/computational-neuroscience/articles/10.3389/fncom.2022.866517/full (visited on 06/20/2025).

[37] S. Petkoski and V. K. Jirsa. "Transmission time delays organize the brain network synchronization." *Philosophical Transactions of the Royal Society A: Mathematical, Physical and Engineering Sciences*, **377**(2153), July 22, 2019. Publisher: Royal Society, p. 20180132. DOI: 10.1098/rsta.2018.0132. URL: https://royalsocietypublishing.org/doi/10.1098/rsta.2018.0132 (visited on 06/20/2025).

[38] R. Caminiti et al. "Diameter, Length, Speed, and Conduction Delay of Callosal Axons in Macaque Monkeys and Humans: Comparing Data from Histology and Magnetic Resonance Imaging Diffusion Tractography." *Journal of Neuroscience*, **33**(36), Sept. 4, 2013. Publisher: Society for Neuroscience Section: Articles, pp. 14501–14511. ISSN: 0270-6474, 1529-2401. DOI: 10.1523/JNEUROSCI.0761-13.2013. URL: https://www.jneurosci.org/content/33/36/14501 (visited on 06/20/2025).

[39] J. Goñi et al. "Resting-brain functional connectivity predicted by analytic measures of network communication." *Proceedings of the National Academy*

of Sciences, **111**(2), Jan. 14, 2014. Publisher: Proceedings of the National Academy of Sciences, pp. 833–838. DOI: 10.1073/pnas.1315529111. URL: https://www.pnas.org/doi/10.1073/pnas.1315529111 (visited on 06/20/2025).

[40] P. Fries. "A mechanism for cognitive dynamics: neuronal communication through neuronal coherence." *Trends in Cognitive Sciences*, **9**(10), Oct. 1, 2005, pp. 474–480. ISSN: 1364-6613. DOI: 10.1016/j.tics.2005.08.011. URL: https://www.sciencedirect.com/science/article/pii/S1364661305002421 (visited on 06/20/2025).

[41] X.-J. Wang. "Neurophysiological and Computational Principles of Cortical Rhythms in Cognition." *Physiological Reviews*, **90**(3), July 2010. Publisher: American Physiological Society, pp. 1195–1268. ISSN: 0031-9333. DOI: 10.1152/physrev.00035.2008. URL: https://journals.physiology.org/doi/full/10.1152/physrev.00035.2008 (visited on 06/20/2025).

[42] N. Kumar, D. Roy, and A. Banerjee. *Hemispheric specialization of functions are tuned by conduction velocities of neuronal propagation in large-scale brain networks*. Pages: 2024.05.02.592033 Section: New Results. May 5, 2024. DOI: 10.1101/2024.05.02.592033. URL: https://www.biorxiv.org/content/10.1101/2024.05.02.592033v1 (visited on 06/20/2025).

[43] M. Mancini, Q. Tian, Q. Fan, M. Cercignani, and S. Y. Huang. "Dissecting whole-brain conduction delays through MRI microstructural measures." *Brain Structure and Function*, **226**(8), Nov. 1, 2021, pp. 2651–2663. ISSN: 1863-2661. DOI: 10.1007/s00429-021-02358-w. URL: https://doi.org/10.1007/s00429-021-02358-w (visited on 06/21/2025).

[44] P. Sorrentino et al. "Whole-Brain Propagation Delays in Multiple Sclerosis, a Combined Tractography-Magnetoencephalography Study." *The Journal of Neuroscience: The Official Journal of the Society for Neuroscience*, **42**(47), Nov. 23, 2022, pp. 8807–8816. ISSN: 1529-2401. DOI: 10.1523/JNEUROSCI.0938-22.2022.

[45] P. Bak, C. Tang, and K. Wiesenfeld. "Self-organized criticality: An explanation of the 1/f noise." *Physical Review Letters*, **59**(4), July 27, 1987. Publisher: American Physical Society, pp. 381–384. DOI: 10.1103/PhysRevLett.59.381. URL: https://link.aps.org/doi/10.1103/PhysRevLett.59.381 (visited on 06/21/2025).

[46] J. M. Beggs and D. Plenz. "Neuronal avalanches in neocortical circuits." *The Journal of Neuroscience: The Official Journal of the Society for Neuroscience*, **23**(35), Dec. 3, 2003, pp. 11167–11177. ISSN: 1529-2401. DOI: 10.1523/JNEUROSCI.23-35-11167.2003.

[47] G. Hahn et al. "Neuronal Avalanches in Spontaneous Activity In Vivo." *Journal of Neurophysiology*, **104**(6), Dec. 2010. Publisher: American Physiological Society, pp. 3312–3322. ISSN: 0022-3077. DOI: 10.1152/jn.00953.2009. URL: https://journals.physiology.org/doi/full/10.1152/jn.00953.2009 (visited on 06/21/2025).

[48] T. Petermann et al. "Spontaneous cortical activity in awake monkeys composed of neuronal avalanches." *Proceedings of the National Academy of Sciences*, **106**(37), Sept. 15, 2009. Publisher: Proceedings of the National Academy of Sciences, pp. 15921–15926. DOI: 10.1073/pnas.0904089106. URL: https://www.pnas.org/doi/full/10.1073/pnas.0904089106 (visited on 06/21/2025).

[49] O. Shriki et al. "Neuronal Avalanches in the Resting MEG of the Human Brain." *Journal of Neuroscience*, **33**(16), Apr. 17, 2013. Publisher: Society for

Neuroscience Section: Articles, pp. 7079–7090. ISSN: 0270-6474, 1529-2401. DOI: 10.1523/JNEUROSCI.4286-12.2013. URL: https://www.jneurosci.org/content/33/16/7079 (visited on 06/21/2025).

[50] H. Bocaccio et al. "The avalanche-like behaviour of large-scale haemodynamic activity from wakefulness to deep sleep." *Journal of The Royal Society Interface*, **16**(158), Sept. 11, 2019. Publisher: Royal Society, p. 20190262. DOI: 10.1098/rsif.2019.0262. URL: https://royalsocietypublishing.org/doi/10.1098/rsif.2019.0262 (visited on 06/21/2025).

[51] O. Arviv, A. Goldstein, and O. Shriki. "Neuronal avalanches and time-frequency representations in stimulus-evoked activity." *Scientific Reports*, **9**(1), Sept. 16, 2019. Publisher: Nature Publishing Group, p. 13319. ISSN: 2045-2322. DOI: 10.1038/s41598-019-49788-5. URL: https://www.nature.com/articles/s41598-019-49788-5 (visited on 06/21/2025).

[52] S. Scarpetta et al. "Criticality of neuronal avalanches in human sleep and their relationship with sleep macro- and micro-architecture." *iScience*, **26**(10), Oct. 20, 2023, p. 107840. ISSN: 2589-0042. DOI: 10.1016/j.isci.2023.107840. URL: https://www.sciencedirect.com/science/article/pii/S258900422301917X (visited on 06/21/2025).

[53] T. E. Harris. *The Theory of Branching Process*. May 1, 1964. URL: https://www.rand.org/pubs/reports/R381.html (visited on 06/21/2025).

[54] C. Haldeman and J. M. Beggs. "Critical Branching Captures Activity in Living Neural Networks and Maximizes the Number of Metastable States." *Physical Review Letters*, **94**(5), Feb. 7, 2005. Publisher: American Physical Society, p. 058101. DOI: 10.1103/PhysRevLett.94.058101. URL: https://link.aps.org/doi/10.1103/PhysRevLett.94.058101 (visited on 06/18/2025).

[55] M. A. Shafto et al. "The Cambridge Centre for Ageing and Neuroscience (Cam-CAN) study protocol: a cross-sectional, lifespan, multidisciplinary examination of healthy cognitive ageing." *BMC Neurology*, **14**(), Oct. 14, 2014, p. 204. ISSN: 1471-2377. DOI: 10.1186/s12883-014-0204-1. URL: https://www.ncbi.nlm.nih.gov/pmc/articles/PMC4219118/ (visited on 06/18/2025).

[56] J. R. Taylor et al. "The Cambridge Centre for Ageing and Neuroscience (Cam-CAN) data repository: Structural and functional MRI, MEG, and cognitive data from a cross-sectional adult lifespan sample." *NeuroImage*. Data Sharing Part II, **144**(), Jan. 1, 2017, pp. 262–269. ISSN: 1053-8119. DOI: 10.1016/j.neuroimage.2015.09.018. URL: https://www.sciencedirect.com/science/article/pii/S1053811915008150 (visited on 06/18/2025).

[57] B. Fischl et al. "Automatically Parcellating the Human Cerebral Cortex." *Cerebral Cortex*, **14**(1), Jan. 1, 2004, pp. 11–22. ISSN: 1047-3211. DOI: 10.1093/cercor/bhg087. URL: https://doi.org/10.1093/cercor/bhg087 (visited on 06/22/2025).

[58] R. S. Desikan et al. "An automated labeling system for subdividing the human cerebral cortex on MRI scans into gyral based regions of interest." *NeuroImage*, **31**(3), July 1, 2006, pp. 968–980. ISSN: 1053-8119. DOI: 10.1016/j.neuroimage.2006.01.021. URL: https://www.sciencedirect.com/science/article/pii/S1053811906000437 (visited on 06/22/2025).

[59] P. Jain, A. Akhter, and A. Banerjee. *Frontal Vulnerability vs. Temporal Resilience: Neuro-compensatory mechanisms underline differential language aging trajectories*. Pages: 2025.04.29.651293 Section: New Results. May 2,

2025. DOI: 10.1101/2025.04.29.651293. URL: https://www.biorxiv.org/content/10.1101/2025.04.29.651293v1 (visited on 06/22/2025).

[60] B. Jeurissen, J.-D. Tournier, T. Dhollander, A. Connelly, and J. Sijbers. "Multi-tissue constrained spherical deconvolution for improved analysis of multi-shell diffusion MRI data." *NeuroImage*, **103**(), Dec. 1, 2014, pp. 411–426. ISSN: 1053-8119. DOI: 10.1016/j.neuroimage.2014.07.061. URL: https://www.sciencedirect.com/science/article/pii/S1053811914006442 (visited on 06/22/2025).

[61] R. E. Smith, D. Raffelt, J.-D. Tournier, and A. Connelly. "Quantitative streamlines tractography: methods and inter-subject normalisation." *Aperture Neuro*, **2**(), Apr. 7, 2022. Publisher: Organization for Human Brain Mapping, pp. 1–25. DOI: 10.52294/ApertureNeuro.2022.2.NEOD9565. URL: https://apertureneuro.org/article/81056-quantitative-streamlines-tractography-methods-and-inter-subject-normalisation (visited on 06/22/2025).

[62] J.-D. Tournier et al. "*MRtrix3*: A fast, flexible and open software framework for medical image processing and visualisation." *NeuroImage*, **202**(), Nov. 15, 2019, p. 116137. ISSN: 1053-8119. DOI: 10.1016/j.neuroimage.2019.116137. URL: https://www.sciencedirect.com/science/article/pii/S1053811919307281 (visited on 06/22/2025).

[63] G. Niso et al. "Brainstorm Pipeline Analysis of Resting-State Data From the Open MEG Archive." *Frontiers in Neuroscience*, **13**(), Apr. 5, 2019. Publisher: Frontiers. ISSN: 1662-453X. DOI: 10.3389/fnins.2019.00284. URL: https://www.frontiersin.org/journals/neuroscience/articles/10.3389/fnins.2019.00284/full (visited on 06/22/2025).

[64] N. Kriegeskorte, M. Mur, and P. A. Bandettini. "Representational similarity analysis - connecting the branches of systems neuroscience." *Frontiers in Systems Neuroscience*, **2**(), Nov. 24, 2008. Publisher: Frontiers. ISSN: 1662-5137. DOI: 10.3389/neuro.06.004.2008. URL: https://www.frontiersin.org/journals/systems-neuroscience/articles/10.3389/neuro.06.004.2008/full (visited on 06/23/2025).

[65] R. Cabeza. "Hemispheric asymmetry reduction in older adults: The HAROLD model." *Psychology and Aging*, **17**(1), 2002. Place: US Publisher: American Psychological Association, pp. 85–100. ISSN: 1939-1498. DOI: 10.1037/0882-7974.17.1.85.

[66] L. T. Johnstone, E. M. Karlsson, and D. P. Carey. "Left-Handers Are Less Lateralized Than Right-Handers for Both Left and Right Hemispheric Functions." *Cerebral Cortex*, **31**(8), Aug. 1, 2021, pp. 3780–3787. ISSN: 1047-3211. DOI: 10.1093/cercor/bhab048. URL: https://doi.org/10.1093/cercor/bhab048 (visited on 06/23/2025).

[67] M. Somers et al. "On the relationship between degree of hand-preference and degree of language lateralization." *Brain and Language*, **144**(), May 1, 2015, pp. 10–15. ISSN: 0093-934X. DOI: 10.1016/j.bandl.2015.03.006. URL: https://www.sciencedirect.com/science/article/pii/S0093934X15000668 (visited on 06/23/2025).

[68] K. M. Bishop and D. Wahlsten. "Sex Differences in the Human Corpus Callosum: Myth or Reality?" *Neuroscience & Biobehavioral Reviews*, **21**(5), Jan. 1, 1997, pp. 581–601. ISSN: 0149-7634. DOI: 10.1016/S0149-7634(96)00049-8. URL: https://www.sciencedirect.com/science/article/pii/S0149763496000498 (visited on 06/24/2025).

[69] N. Geschwind and A. M. Galaburda. "Cerebral lateralization: Biological mechanisms, associations, and pathology: I. A hypothesis and a program for research." *Archives of Neurology*, **42**(5), 1985. Place: US Publisher: American Medical Association, pp. 428–459. ISSN: 1538-3687. DOI: 10.1001/archneur.1985.04060050026008.

[70] M. Hiscock, R. Inch, C. Jacek, C. Hiscock-Kalil, and K. M. Kalil. "Is there a sex difference in human laterality? I. An exhaustive survey of auditory laterality studies from six neuropsychology journals." *Journal of Clinical and Experimental Neuropsychology*, **16**(3), 1994. Place: United Kingdom Publisher: Taylor & Francis, pp. 423–435. ISSN: 1744-411X. DOI: 10.1080/01688639408402653.

[71] P. Jain. *CBDL DWI Processing Script*. original-date: 2025-04-16T06:24:26Z. Apr. 16, 2025. URL: https://github.com/PartikaJain/CBDL_DWI_script (visited on 06/18/2025).